Study on Functionalization of DNA by Artificial Pseudo Base Pairs

(DNA を機能化する疑似塩基対の開発に関する研究)

DOI Tetsuya

土居　哲也

2016

TABLE OF CONTENTS

Chapter 1. General Introduction

1-1 Properties of native DNAs

Deoxyribonucleic acid, DNA, is one of the famous biological molecules with well-defined structure and properties. The function and the properties of DNAs have been investigated in details since J. Watson and F. Crick discovered its unique double-helical structure in 1953.[1] Canonical structure of double-stranded DNA is called B-form DNA (or B-DNA), which has right-handed double-helical structure with 2 nm of diameter, 3.4 Å long per each base pair, and 10.5 base pairs per helix-turn (Fig. 1-1a, b).

The construction units of DNAs could be largely divided in two parts. One is the backbone part which is composed of D-deoxyribose with phosphodiester bond linkage (Fig. 1-1c). This backbone mainly determines the whole structure of double-helix. The other is nucleobase, which contributes to the sequence selectivity on double-helix formation. DNAs are composed of four types of nucleobases, Adenine (A), Thymine (T), Guanine (G), and Cytosine (C). These nucleobases recognizes each other through complementary hydrogen bondings between A-T and G-C which is so called "Watson-Crick base pairing" (Fig.1-1d). Owing to the complementary hydrogen bondings, DNA forms a double-helical structure with excellent sequence selectivity.

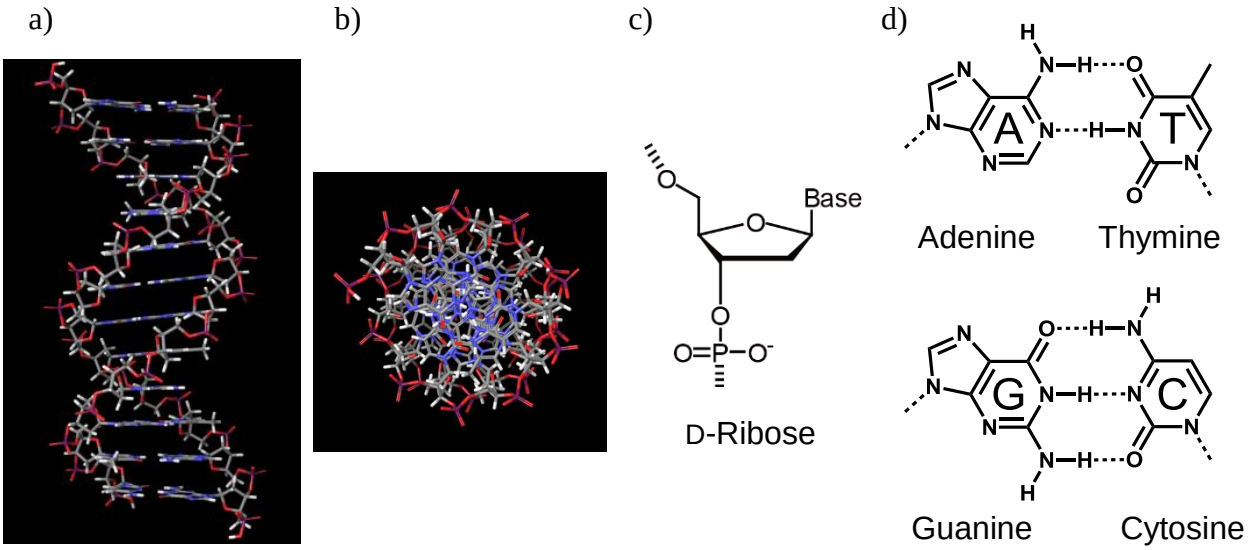

Figure 1-1. The structure of a) Side view and b) top view of B-DNA. Chemical structures of c) D-deoxiribose backbone and d) nucleobases with complementary hydrogen bondings.

High sequence selectivity on duplex formation of DNAs plays an important role in biological systems. It is well-known that DNA carries genetic information for almost all of the living things. In the living cells, DNAs are replicated (during cell devision), transcripted into RNAs, and RNAs are finally translated to proteins. During all these routines, the genetic information of DNA is preserved through the complementary hydrogen bonding of native nucleobases. Also, DNA analyses owe a great deal to the sequence selectivity. For example, DNA amplification (polymerase chain reaction[2] for famous), or many fluorescence signaling methods to detect target DNAs are achieved[3-5] depending on the sequence selective double-helix formation.

1-2 Application of DNA as a nanomaterial

Well-defined and sequence selective double-helix formation makes DNAs as very attractive molecules not only in the biology related field but also in the field of nanomaterial science. DNA nanotechnology has been of interest after pioneering work by Seeman.[6-8] For example, he reported a cube like DNA nanostructure formed by direct self-assembly of complementarily designed DNAs (Fig. 1-2). Also, in 2006, Rothemund reported an astonishing DNA nano-architecture so called "DNA-origami".[9] He used 7,249 nt long virus genome DNA as a scaffold and folded it into the desired shape by adding 200-250 kinds of complementary short DNAs (Fig. 1-3).

Today, numbers of DNA nanostructures or DNA nanomachines and their applications have been reported.[10-13] For example, direct observation of enzyme activity was

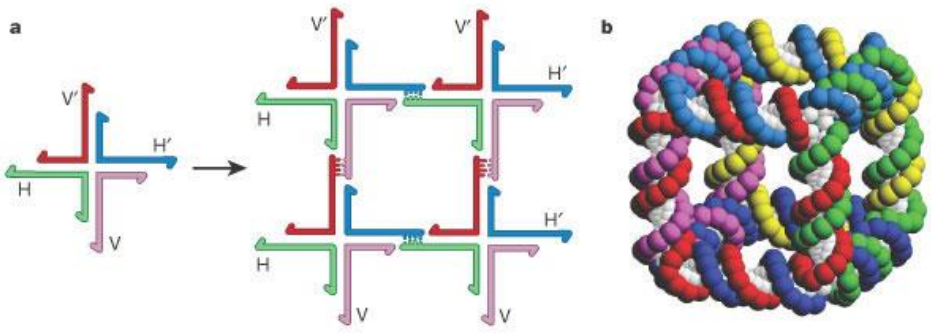

Figure 1-2. The schematic illustration of formation of Seeman's DNA cube. a) self-assembly of four-way junction DNA into two dimensional array. b) Structure of DNA cube. Reprinted from Ref. 7.

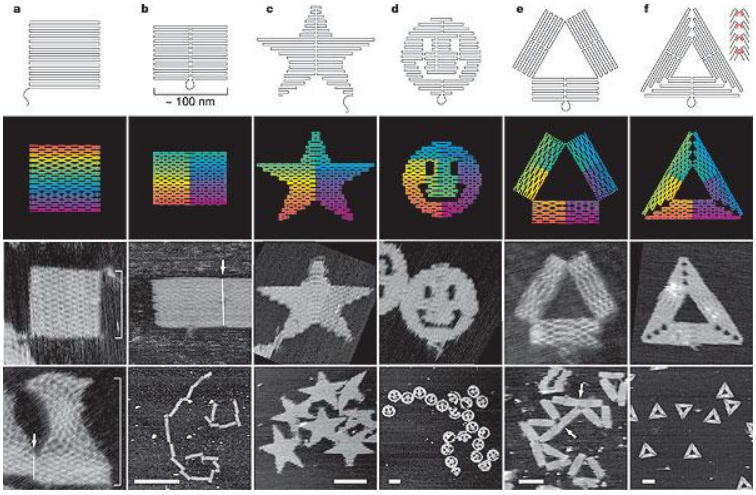

Figure 1-3. AFM image of DNA-origami structures. Reprinted from Ref. 9.

achieved using DNA nanostructure as a scaffold.[14,15] Also, DNA nanoarchitectures are promising tools in nanodelivery as drug delivery systems.[16,17]

1-3 Functionalization of DNA by non-native molecules

As described above, DNA is a highly useful material both in the fields of biotechnology and nanotechnology. As a material however, there are several drawbacks of native DNAs.

1) Thermal stability: DNA duplex is stabilized by hydrogen bonding, London dispersion force, and hydrophobic effect. These are all non-covalent interactions, and hence, the double-helix formation of DNA is just reversible. While DNAs form a double-helix at low temperatures, they dissociates into single-strands at high temperatures. This reversibility is very important in the enzymatic systems to read out

or copy the sequence. DNA dependent DNA polymerases or RNA polymerases could replicate or transcript single-stranded DNAs. Therefore, double-stranded DNAs have to be temporarily dissociated into single-strands during enzymatic recognitions (anyway thermally or enzymatically), and reversibly form double-helices. However, high reversibility could be restated as flexibility or instability. From the point of view of nanomaterial chemistry, such instability cause low yield of nano-architecting, and often requires fine temperature control or cause low yields. Accordingly, high thermal stability of the double-stranded structure is favorable for application of DNAs as a nanomaterial.

2) Sequence patterns: Each native nucleobases recognize the complemental nucleobase through hydrogen bondings which has a lot to do with the sequence selective duplex formation. However, there are only two complementary pairs in native DNAs, A-T and G-C, which strictly limits the sequence patterns. Hence, the long sequence is required for complicated systems, which might cause problems as misrecognition or secondary structure formations. Therefore, with more additional kinds of base pairs, the sequence designability should improve and more complicated nanostructures could be constructed

3) No functionality: Native nucleobases are chemically stable compounds and has no

special functionality other than base pairing. This chemical stability is an important property for the living things to preserve the genetic information precisely for a long while. On the other hand, this makes it difficult to functionalize the native nucleobases. For example, direct chemical labeling, introduction of functional groups, chemical crosslinking, and so on is difficult to perform as long as native nucleobases are used. Also, native nucleobases are non-fluorescent. Ultrafast deactivation of nucleobases after UV absorption contributes to the photostability of DNA. However, this non-fluorescent property requires fluorescence labeling or hybridization of fluorescently labelled complementary strands to observe the DNAs, which often affect the stability or structures of it. These properties, chemical stability and non-fluorescent, strictly limits the application of DNAs.

To overcome these drawbacks, chemists have been attempted to develop "artificial base pairs" which could improve the properties of DNA. For example, artificial base pairs with complementary hydrogen bonds have been reported.[18-23] Benner *et al.* reported an artificial base pair with complementary hydrogen bondings, while their hydrogen bonding patterns were different from native nucleobases (**1** in Fig. 1-4). Therefore, they had orthogonality with native nucleobases and expected to expand the sequence patterns. Also, some of the artificial base pairs with hydrogen bondings were

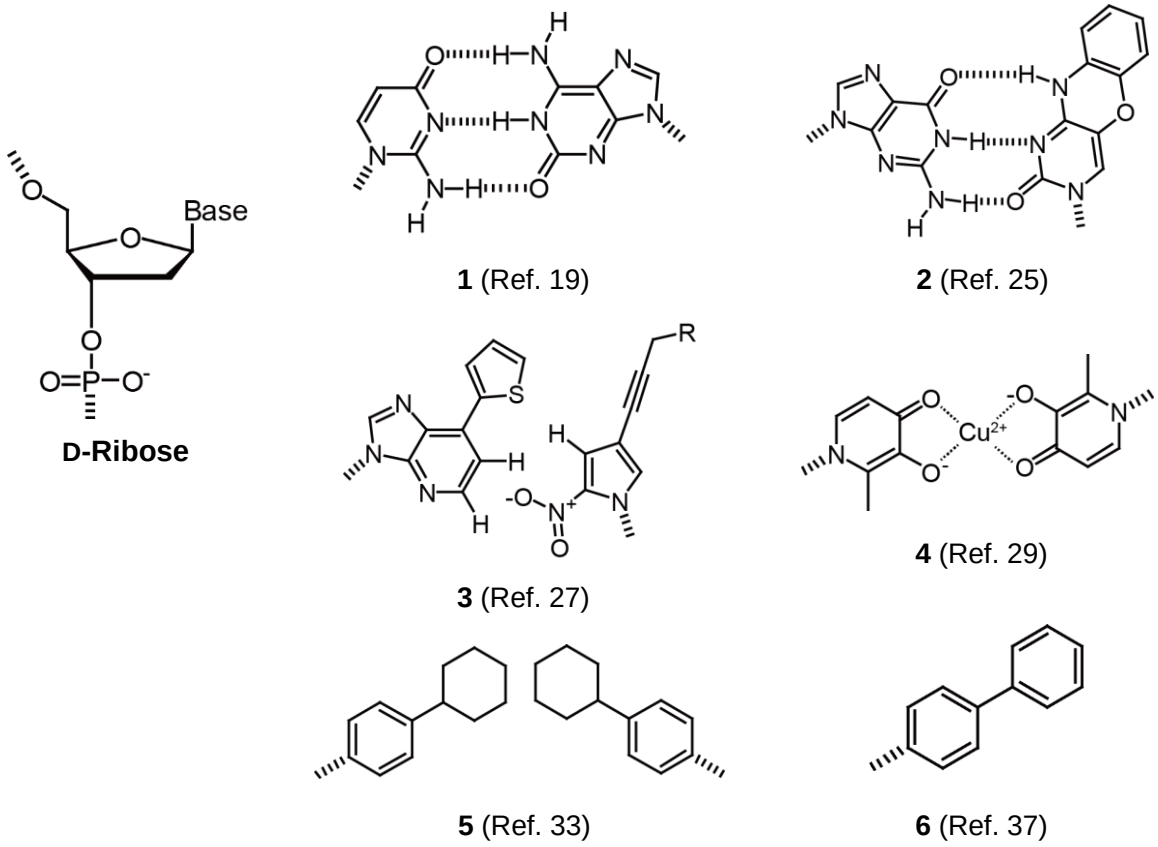

Figure 1-4. Examples of artificial base pairs tethered on D-ribose backbones.

reported to be fluorescent (**2**).[24,25] On the other hand, unique shape complementary artificial base pairs, without any hydrogen bondings, were reported after pioneering work by Kool *et al*.[26-28] Though they no longer have complementary hydrogen bondings, they selectively recognized the complementary bases through "shape fitting" of the molecules (**3**). Furthermore, shape complementary artificial base pairs were able to replicate using native enzymes, and hence, expected to expand the genetic alphabets. Besides the shape complementarity, artificial base pairs without hydrogen bondings stabilized by metal binding (**4**) [29-32] or hydrophobic effects (**5**) [33] were reported.

Interestingly, moreover, the base pairing of artificial base pairs are not limited to the planner manner. There are several artificial base pairs which forms a π-stacked conformation along the helix axis in the context of DNA duplex (**6**).[34-39] Though they do not form an edge-to-edge faced structure as native nucleobases, they were found to recognize each other and stabilized the DNA duplex. These artificial base pairs are often called as "pseudo base pairs".

Thus, various artificial base pairs were reported for stabilization, functionalization, or sequence expansion of the DNA duplexes. However, most of the artificial base pairs were tethered on native D-ribose backbones, which should cause difficulty in synthesis, and also it limits the available molecules. On the other hand, the backbones of the artificial base pairs could also be "artificial", and not limited to the native D-riboses. For example, native nucleobases tethered on non-native cyclic backbones are known to form a stable duplex, as well as native D-ribose backbones[40-42] (**7**-**9** in Fig. 1-5). Furthermore, the backbones are not only limited to the cyclic backbones. For example, native nucleobases with non-native acyclic backbones as peptides[43,44] (**10**), glycols[45] (**11**), threoninols[46,47] (**12**), and serinols[48,49] (**13**) are known to form stable duplexes, even though their structures were totally different from native backbones. Hence, all these non-native linkers are potentially available as the backbone of the artificial base pairs.

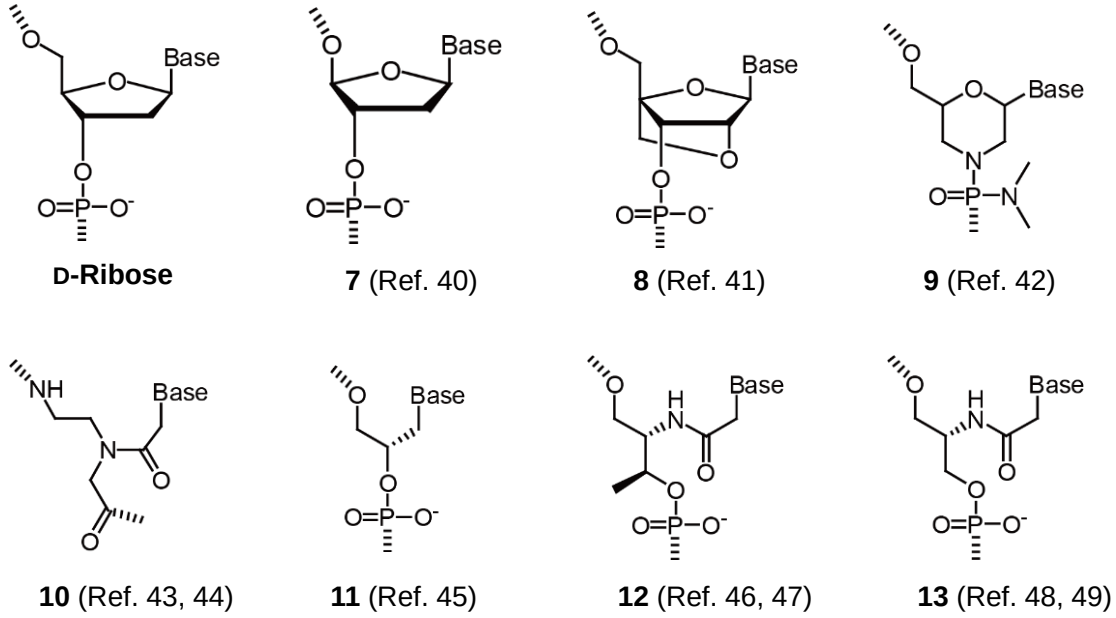

Figure 1-5. Examples of backbones of artificial nucleic acids.

According to these reports, our group has been developed several artificial base pairs using acyclic D-threoninol as backbones (Fig. 1-6). D-Threoninol backbones allow us to introduce various non-native molecules into DNA strands. And for example, we reported that azobenzene derivatives introduced at complementary positions of the DNA strands stabilize the DNA duplex through π-π interaction between the azobenzene molecules (**14** in Fig. 1-7).[50] Also, we reported cationic stilbazole derivative stabilizes the DNA duplex not only by π-π interaction but also by electrostatic interaction between positive charge of the dye and negative charge of phosphate anion of the backbone at the counter strand (**15**).[51] This cationic pseudo base pair was found stable enough to connect between the DNA duplexes when they were introduced at the 5' overhang

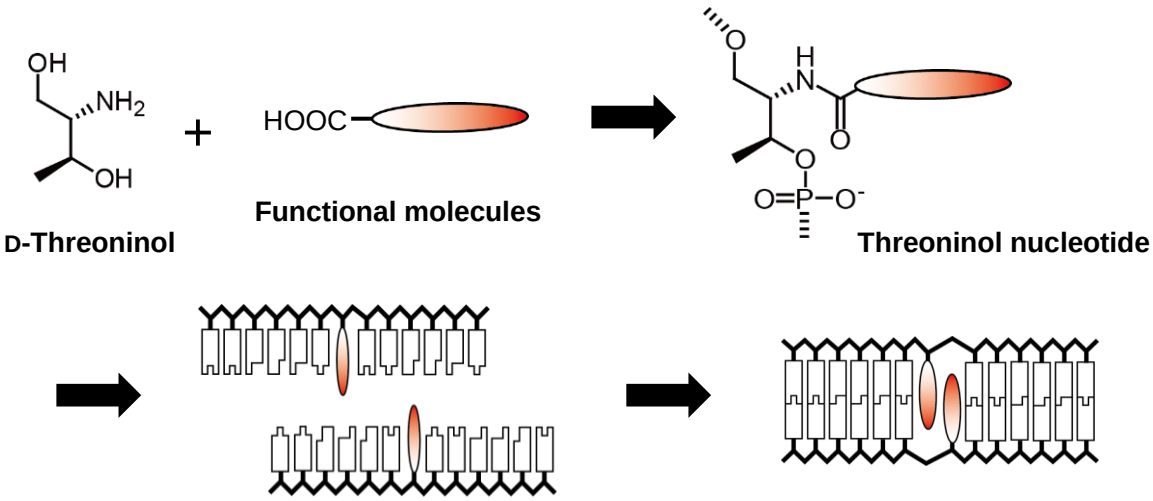

Figure 1-6. Schematic illustration of threoninol nucleotides.

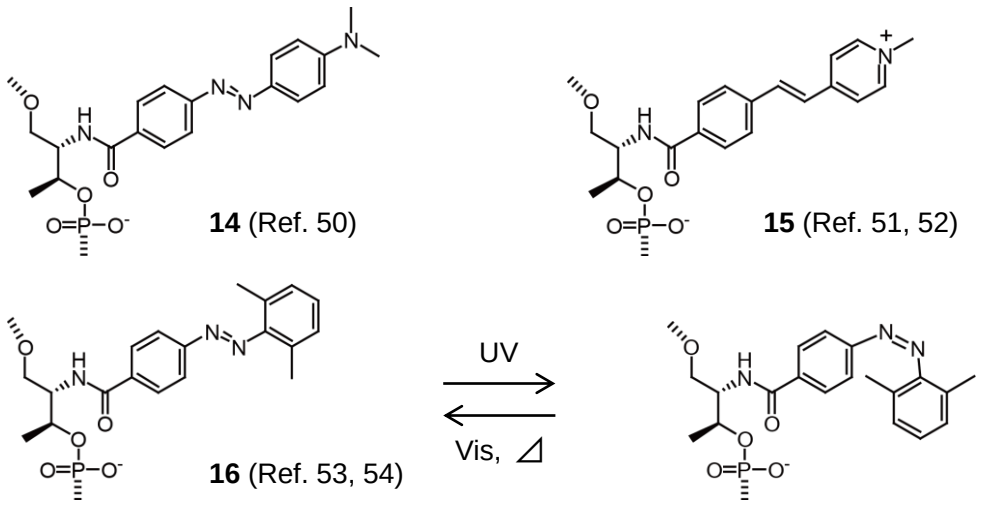

Figure 1-7. Examples of threoninol nucleotides.

positon of the DNA duplexes.[52] Note that, this cationic pseudo base pair was thermally far more stable than any native nucleobases. Furthermore, we reported photoreactive pseudo base pairs using azobenzene derivatives with photoisomerization reactivity.[53,54] Compound **16** were found to isomerize upon UV/Vis photo irradiation. Based on this *cis-trans* isomerization, **16** served as a photoreactive pseudo base pair which stabilize

the DNA duplex through π-π interaction at *trans*-form while the duplex was destabilized or dissociated at *cis*-form due to their nonplanar structures. This *cis*/*trans* isomerization of azobenzene successfully and reversibly controlled the hybridization/dissociation of DNA duplex through UV/visible light irradiation. Thus, sequence expansion, stabilization, and functionalization have been achieved by introducing various types of artificial pseudo base pairs into DNA strands.

1-4 Purpose of this study

In this study, we developed several novel pseudo base pairs with unique functionalities. These pseudo bases are expected to enlarge the application of DNA as a nanomaterial.

First, we demonstrate hetero selective pseudo base pairs with electrostatically complementary designs. Pseudo base pairs with high orthogonality with native nucleobases allow us to expand the sequence patterns, and hence, to construct more complicated hybridization based systems. To let them have high orthogonality with native base pairs, we focused on the electrostatic complementarity of aromatic molecules. We adopted electron-rich and electron-deficient aromatic molecules as pseudo bases, and expected them to recognize each other hetero-selectively through

electrostatic interaction between the donor and acceptor residues.

In chapter 2, donor-acceptor pseudo base pair using azobenzene derivatives is described. Their stability, selectivity, and the effect of chirality of the linkers were investigated. And in chapter 3, another series of donor-acceptor pseudo base pair using pyrene and anthraquinone is demonstrated. In this series, hetero-pairing of pseudo bases were able to monitor through fluorescent measurements. Moreover, a totally artificial hetero-duplex formation, that is, a hetero-duplex composed of pseudo base pairs only was investigated using this pseudo base pair.

Second, we demonstrate pseudo base pairs with photo-crosslinking abilities. We introduced two *p*-stilbazole moieties at complementary position of DNA duplex and expected them to crosslink the DNA duplex through [2+2] photocycloaddition. The reaction was investigated in details through UV-vis, HPLC, and NMR measurements, which are demonstrated in chapter 4.

Additionally, the reactivities of various stilbene derivatives were investigated by using DNA duplex as a scaffold in chapter 5. In chapter 4, [2+2] photodimerization of stilbazoles were used to crosslink the DNA duplex. On the other hand, it was found that this photo-crosslinking reaction could also be regarded as DNA scaffolded [2+2] photodimerization of stilbene derivatives. Therefore, reactivities of various stilbene

derivatives were investigated using this DNA scaffolded approach. Moreover, not only the reactivities of homo-photodimerizations (photodimerization between the same derivatives), but also the reactivities of hetero-photodimerizaitons (photodimerization between the different derivatives), which were almost impossible to examine in solution, were investigated.

1-5 References

(1) Watson, J. D.; Crick, F. H. C. *Nature* **1953**, *171*, 737.

(2) Mullis, K. B.; Faloona, F. A. In *Methods in Enzymology*; Academic Press: 1987; Vol. Volume 155, p 335.

(3) Tyagi, S.; Kramer, F. R. *Nat Biotech* **1996**, *14*, 303.

(4) Rosi, N. L.; Mirkin, C. A. *Chem. Rev.* **2005**, *105*, 1547.

(5) Sassolas, A.; Leca-Bouvier, B. D.; Blum, L. J. *Chem. Rev.* **2008**, *108*, 109.

(6) Winfree, E.; Liu, F.; Wenzler, L. A.; Seeman, N. C. *Nature* **1998**, *394*, 539.

(7) Seeman, N. C. *Nature* **2003**, *421*, 427.

(8) Seeman, N. C. *Nano Letters* **2001**, *1*, 22.

(9) Rothemund, P. W. K. *Nature* **2006**, *440*, 297.

(10) Han, D.; Pal, S.; Nangreave, J.; Deng, Z.; Liu, Y.; Yan, H. *Science* **2011**, *332*, 342.

(11) Shin, J.-S.; Pierce, N. A. *J. Am. Chem. Soc.* **2004**, *126*, 10834.

(12) Yurke, B.; Turberfield, A. J.; Mills, A. P.; Simmel, F. C.; Neumann, J. L. *Nature* **2000**, *406*, 605.

(13) Zhang, F.; Nangreave, J.; Liu, Y.; Yan, H. *J. Am. Chem. Soc.* **2014**, *136*, 11198.

(14) Endo, M.; Tatsumi, K.; Terushima, K.; Katsuda, Y.; Hidaka, K.; Harada, Y.; Sugiyama, H. *Angew. Chem. Int. Ed.* **2012**, *51*, 8778.

(15) Endo, M.; Katsuda, Y.; Hidaka, K.; Sugiyama, H. *J. Am. Chem. Soc.* **2010**, *132*, 1592.

(16) Andersen, E. S.; Dong, M.; Nielsen, M. M.; Jahn, K.; Subramani, R.; Mamdouh, W.; Golas, M. M.; Sander, B.; Stark, H.; Oliveira, C. L. P.; Pedersen, J. S.; Birkedal, V.; Besenbacher, F.; Gothelf, K. V.; Kjems, J. *Nature* **2009**, *459*, 73.

(17) Douglas, S. M.; Bachelet, I.; Church, G. M. *Science* **2012**, *335*, 831.

(18) Kool, E. T.; Morales, J. C.; Guckian, K. M. *Angew. Chem. Int. Ed.* **2000**, *39*, 990.

(19) Switzer, C.; Moroney, S. E.; Benner, S. A. *J. Am. Chem. Soc.* **1989**, *111*, 8322.

(20) Piccirilli, J. A.; Benner, S. A.; Krauch, T.; Moroney, S. E. *Nature* **1990**, *343*, 33.

(21) Minakawa, N.; Kojima, N.; Hikishima, S.; Sasaki, T.; Kiyosue, A.; Atsumi, N.; Ueno, Y.; Matsuda, A. *J. Am. Chem. Soc.* **2003**, *125*, 9970.

(22) Liu, H.; Gao, J.; Lynch, S. R.; Saito, Y. D.; Maynard, L.; Kool, E. T. *Science* **2003**, *302*, 868.

(23) Gao, J.; Liu, H.; Kool, E. T. *Angew. Chem. Int. Ed.* **2005**, *44*, 3118.

(24) Krueger, A. T.; Lu, H.; Lee, A. H. F.; Kool, E. T. *Acc. Chem. Res.* **2007**, *40*, 141.

(25) Börjesson, K.; Preus, S.; El-Sagheer, A. H.; Brown, T.; Albinsson, B.; Wilhelmsson, L. M. *J. Am. Chem. Soc.* **2009**, *131*, 4288.

(26) Schweitzer, B. A.; Kool, E. T. *J. Am. Chem. Soc.* **1995**, *117*, 1863.

(27) Kimoto, M.; Kawai, R.; Mitsui, T.; Yokoyama, S.; Hirao, I. *Nucleic Acids Res.* **2009**, *37*, e14.

(28) Malyshev, D. A.; Seo, Y. J.; Ordoukhanian, P.; Romesberg, F. E. *J. Am. Chem. Soc.* **2009**, *131*, 14620.

(29) Tanaka, K.; Tengeiji, A.; Kato, T.; Toyama, N.; Shiro, M.; Shionoya, M. *J. Am. Chem. Soc.* **2002**, *124*, 12494.

(30) Tanaka, K.; Tengeiji, A.; Kato, T.; Toyama, N.; Shionoya, M. *Science* **2003**, *299*, 1212.

(31) Clever, G. H.; Kaul, C.; Carell, T. *Angew. Chem. Int. Ed.* **2007**, *46*, 6226.

(32) Tanaka, K.; Clever, G. H.; Takezawa, Y.; Yamada, Y.; Kaul, C.; Shionoya, M.; Carell, T. *Nat Nano* **2006**, *1*, 190.

(33) Kaufmann, M.; Gisler, M.; Leumann, C. J. *Angew. Chem. Int. Ed.* **2009**, *48*, 3810.

(34) Schmucker, W.; Wagenknecht, H.-A. *Synlett* **2012**, *23*, 2435.

(35) Varghese, R.; Wagenknecht, H.-A. *Chem. Commun.* **2009**, 2615.

(36) Hainke, S.; Seitz, O. *Angew. Chem. Int. Ed.* **2009**, *48*, 8250.

(37) Brotschi, C.; Leumann, C. J. *Angew. Chem. Int. Ed.* **2003**, *42*, 1655.

(38) Guckian, K. M.; Schweitzer, B. A.; Ren, R. X. F.; Sheils, C. J.; Tahmassebi, D. C.; Kool, E. T. *J. Am. Chem. Soc.* **2000**, *122*, 2213.

(39) Häner, R.; Garo, F.; Wenger, D.; Malinovskii, V. L. *J. Am. Chem. Soc.* **2010**, *132*, 7466.

(40) Schöning, K. U.; Scholz, P.; Guntha, S.; Wu, X.; Krishnamurthy, R.; Eschenmoser, A. *Science* **2000**, *290*, 1347.

(41) K. Singh, S.; A. Koshkin, A.; Wengel, J.; Nielsen, P. *Chem. Commun.* **1998**, 455.

(42) Summerton, J.; Weller, D. *Antisense Nucleic Acid Drug Dev.* **1997**, *7*, 187.

(43) Nielsen, P. E.; Egholm, M.; Berg, R. H.; Buchardt, O. *Science* **1991**, *254*, 1497.

(44) Wittung, P.; Nielsen, P. E.; Buchardt, O.; Egholm, M.; Norden, B. *Nature* **1994**, *368*, 561.

(45) Zhang, L.; Peritz, A.; Meggers, E. *J. Am. Chem. Soc.* **2005**, *127*, 4174.

(46) Asanuma, H.; Toda, T.; Murayama, K.; Liang, X.; Kashida, H. *J. Am. Chem. Soc.* **2010**, *132*, 14702.

(47) Murayama, K.; Kashida, H.; Asanuma, H. *Chem. Commun.* **2015**, *51*, 6500.

(48) Kashida, H.; Murayama, K.; Toda, T.; Asanuma, H. *Angew. Chem. Int. Ed.* **2011**, *50*, 1285.

(49) Murayama, K.; Tanaka, Y.; Toda, T.; Kashida, H.; Asanuma, H. *Chem. Eur. J.* **2013**, *19*, 14151.

(50) Fujii, T.; Kashida, H.; Asanuma, H. *Chem. Eur. J.* **2009**, *15*, 10092.

(51) Kashida, H.; Ito, H.; Fujii, T.; Hayashi, T.; Asanuma, H. *J. Am. Chem. Soc.* **2009**, *131*, 9928.

(52) Kashida, H.; Hayashi, T.; Fujii, T.; Asanuma, H. *Chem. Eur. J.* **2011**, *17*, 2614.

(53) Asanuma, H.; Nishioka, H.; Ishikawa, T.; Liang, X. In *Current Protocols in Nucleic Acid Chemistry*; John Wiley & Sons, Inc.: 2011.

(54) Kamiya, Y.; Asanuma, H. *Acc. Chem. Res.* **2014**, *47*, 1663.

Chapter 2. Development of a hetero-selective pseudo base pair with electrostatically complementary design

2-1 Abstract

In chapter 2, we describe a novel pseudo base pair designed with electrostatic complementarity. We adopted nitro- and dimethylamino- modified azobenzene derivatives as an acceptor and a donor respectively. It was found that, acceptor/acceptor or donor/donor pairs sufficiently stabilized the DNA duplex when they were introduced at the complementary positions at the center of DNA duplexes. Also, they were able to form a pseudo base pair at the 5'-overhang positon of the duplexes, which indicates they served as a pseudo base pair without the cooperative assistance by native nucleobases. Moreover, azobenzene pseudo base pairs showed a significant stabilization with donor/acceptor pair, compared with donor/donor or acceptor/acceptor pairs. Introduction of nitro group to the donor azobenzene drastically decreased the stability of the hetero-pseudo base pair, which indicates that the donor/acceptor pair was certainly stabilized by interaction between the donor and acceptor residues. Furthermore, this hetero-pseudo base pair was found to recognize the chirality of the linkers and right-handed donor formed stable pair with right handed-acceptor and *vice versa*.

2-2 Introduction

DNA duplex is a molecular architecture with vast properties which allows them to serve as an ideal scaffold to align non-native aromatic molecules. Complementary hydrogen bondings and stacking interactions between native nucleobases, combined with hydrophobic effects, contribute to the formation of the DNA duplex with remarkable sequence specificity. And since native base pairs are stacked in well-defined ladder-like fashions, DNA duplex could be exploited as a scaffold to arrange aromatic residues in a precise manner. DNA duplex scaffold enables us to construct stacked aggregate of aromatic molecules with well-defined and predicted structures, which allows us to construct functional supramolecular aggregates with predicted structures, as well as to prepare ideal system for theoretical investigation.[1-3] Indebt to ladder-like stacked manner of DNA duplex scaffold, properties of aromatic non-native residues, such as electron transfer,[4-6] energy transfer,[7-9] or exciton coupling[3,10] has been investigated in the context of DNA duplex.

On the other hand, non-native molecules aligned in the DNA duplex have capability to serve as a "pseudo base pair", that is, a non-native residues which stabilize the DNA duplex as well as, or more than, the native nucleobases. For example, Leumann et al. reported non-native aromatic molecules tethered on D-ribose scaffold serve as a pseudo

base pair and stabilize the DNA duplex.[11-13] Also, our group reported that aromatic molecules tethered on D-threoninol scaffold serve as a pseudo base pair in the context of DNA duplex, and found that they have high orthogonality with native nucleobases.[14,15] These pseudo base pairs stabilize the DNA duplex through π-π interaction of the aromatic rings, and there are several reports on pseudo base pairs using this kind of interaction.

Previously, our group reported a stacked pseudo base pair with additional interaction than π-stacking. In the report, we adopted *p*-methylstilbazolium as a pseudo base pair and aligned them at the central position of the DNA duplex.[16] The *p*-methylstilbazolium pseudo base pairs were found to stabilize the duplex not only by π-stacking, but also by electrostatic interaction between the positive charge of the dye and the negative charge of the phosphate at the backbone of counter strand. This cationic base surrogate was found to stabilize the duplex more than the GC pairs, which is the most stable pair in nature. More interestingly, it was found that this cationic base pair was stable enough to connect the DNA duplexes with only 3 mer pairs.[17]

However, reported stacked-type pseudo base pairs were all homo-selective and hetero-selective recognition, the selective recognition and pairing between the different residues, was yet difficult to achieve by stacked base surrogates. Nevertheless,

hetero-selective pairing is just important recognition mode since it contributes to the expansion of the sequence patterning and subsequent designing of complicated hybridization-based systems. For example, only one pattern of pairing could be formed with homo-pairs (Fig. 2-1a). In contrast, hetero-pairing leads to two patterns of pairing on each pairs, and sequence pattern increases exponentially as the number of the pair increases (Fig. 2-1b). Thus, hetero-pairing is a promising recognition mode which may act as an additional base pair to diversify the sequence patterns.

In order to construct such hetero-recognition system, we focused on the electrostatic complementarity of aromatic molecules.[18-20] In this chapter, we adopted donor- and acceptor- modified azobenzene derivatives as a pseudo base pair and expected them to stabilize the DNA duplex hetero-selectively through the electrostatic complementarity.

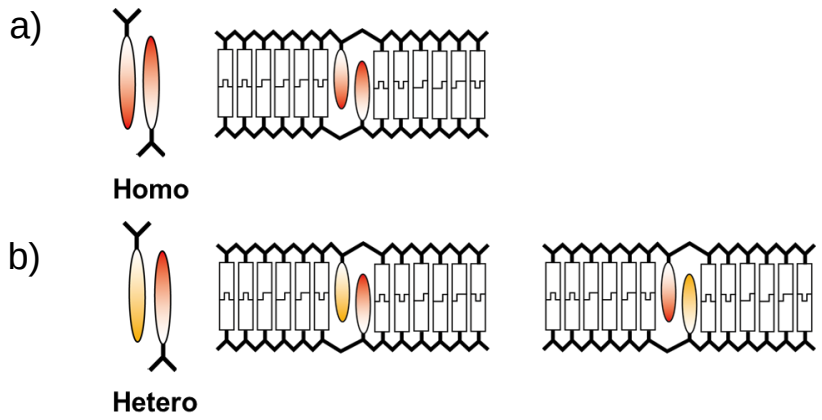

Figure 2-1. Illustration of pairing patterns of DNAs containing a) homo- or b) hetero-selective pseudo base pairs,

When the donor and acceptor residues were paired at the center of the DNA duplex, the thermal stability of the duplex drastically increased with donor/acceptor pair compared to donor/donor or acceptor/acceptor pairs. Moreover, this pseudo base pair showed an excellent selective hetero-complexation even when they were introduces at 5' overhang positions of the DNA duplex, where they are no longer forced to form a hetero-aggregates.

2-3 Results and discussions

2-3-1 Photophysical properties and thermal stabilities of donor/acceptor azobenzene pseudo base pairs

Here, *p*-nitroazobenzene (**N**) and Methyl Red (**M**) were used as an acceptor- and a donor-type azobenzenes and expected them to recognize each other through their electrostatic complementarity (Figs. S2-1a, b). Azobenzene residues were introduced into the DNA strands through D-threoninol linker using standard solid-phase DNA synthesis (Fig. 2-2). In this study, we investigated on two series of duplexes. First is center series, which the azobenzene residues were introduced at the complementary positions at the center of DNA duplexes (Scheme 2-1a). And second is overhang series, which azobenzenes were introduced at 5’ overhang positions of DNA duplexes (Scheme 2-1b). With the center series, we investigated the spectroscopic behavior and stability of

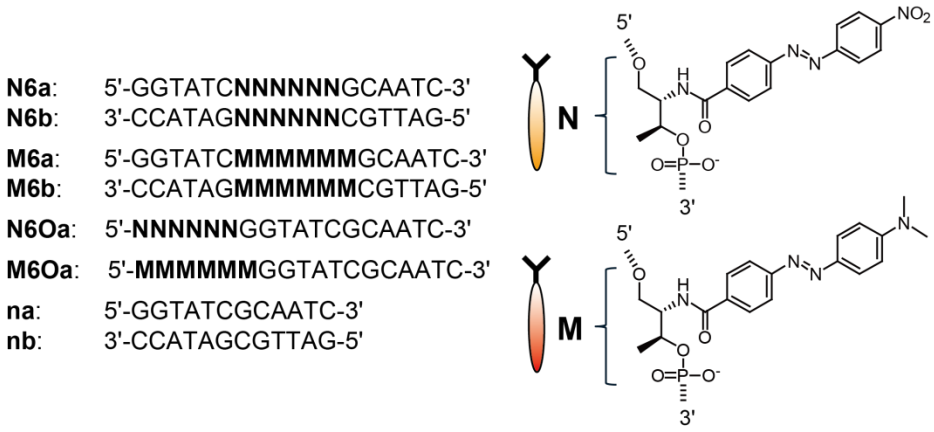

Figure 2-2. Sequences and chemical structures of oligomers containing **N** or **M** residues. A, G, C, and T represents 2'-deoxyribonucleotides.

Scheme 2-1. Schematic illustration of **N**/**M** hetero-pair formation in DNAs a) **M6a**/**N6b**, and b) **N6Oa**/**nb**+**M6Oa**/**nb**.

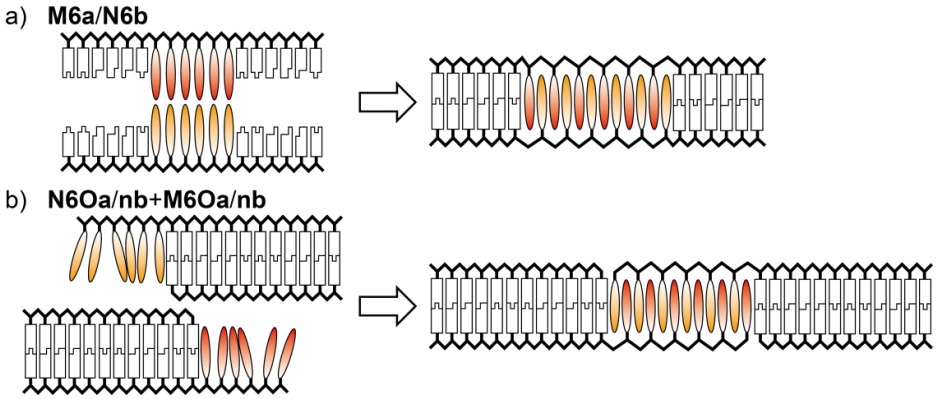

N/**M** hetero pair against **N**/**N** or **M**/**M** homo-pairs. And the selectivity of **N**/**M** hetero pseudo base pair itself was investigated using the overhang series.

First, the spectroscopic character of **N**/**M** hetero-pairing compared to **N**/**N** or **M**/**M** homo-pairs was investigated using center series sequences. The UV-vis spectra of **N6a**/**N6b** or **M6a**/**M6b** showed a hypsochromic shift of the band as the temperature was

lowered from 80 °C to 0 °C (Figs. 2-2a, b). Such hypsochromic shift is characteristic of H-type homo-aggregation of the dyes, and hence, it was indicated that **N** or **M** residues formed a cluster within DNA duplexes. Positive-negative cotton effect observed in CD spectra indicated that **N** or **M** residues formed a right-handed helical structure within DNA duplex (Figs. 2-3 c, d). This result is consistent with the previous report which also indicated that the dyes tethered on D-threoninol linkers prefer to form right-handed

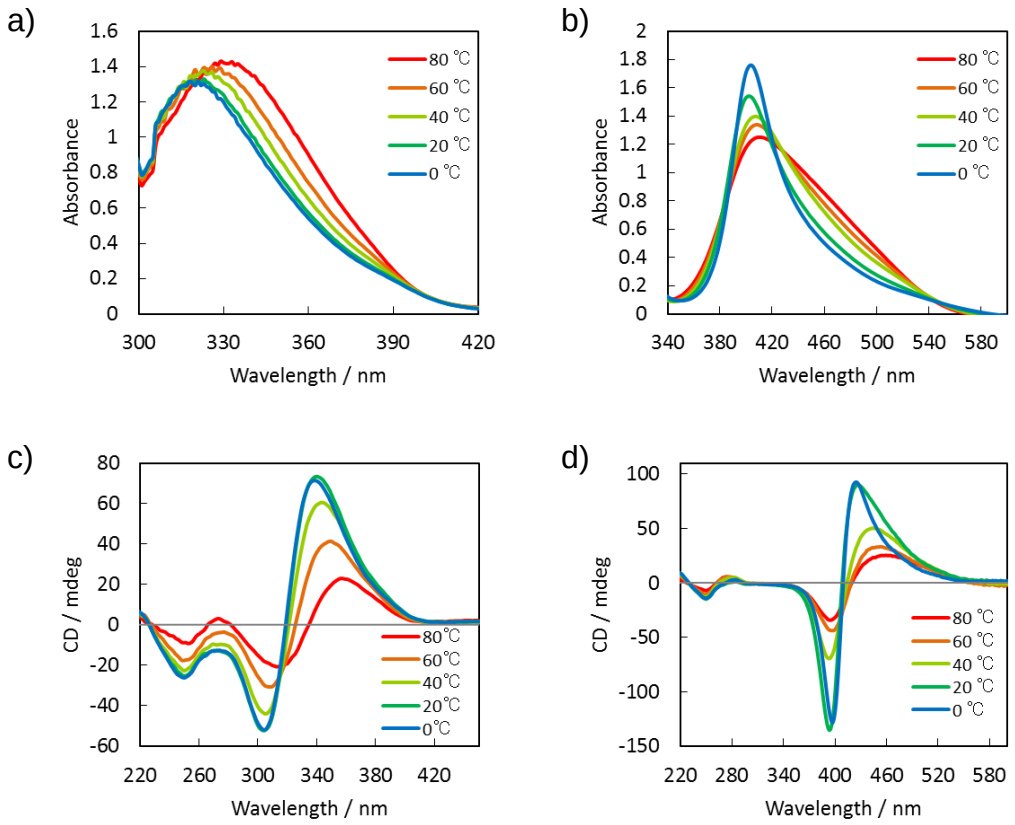

Figure 2-3. UV-vis and CD spectra of a), c) **N6a**/**N6b**, and b), d) **M6a**/**M6b** (5.0 μM each strand) at indicated temperatures. Conditions: 100 mM NaCl, 10 mM phosphate buffer (pH 7.0).

aggregates.

In contrast, **M6a**/**N6b** showed a distinct bathochromic shift of the band along the lowering temperature (Fig. 2-4a). Bathochromic shift of the band could be assigned to H-type hetero-aggregation of the dye molecules, suggesting that **N** and **M** residues formed a hetero-aggregate and interacted with each other in **M6a**/**N6b**. In order to

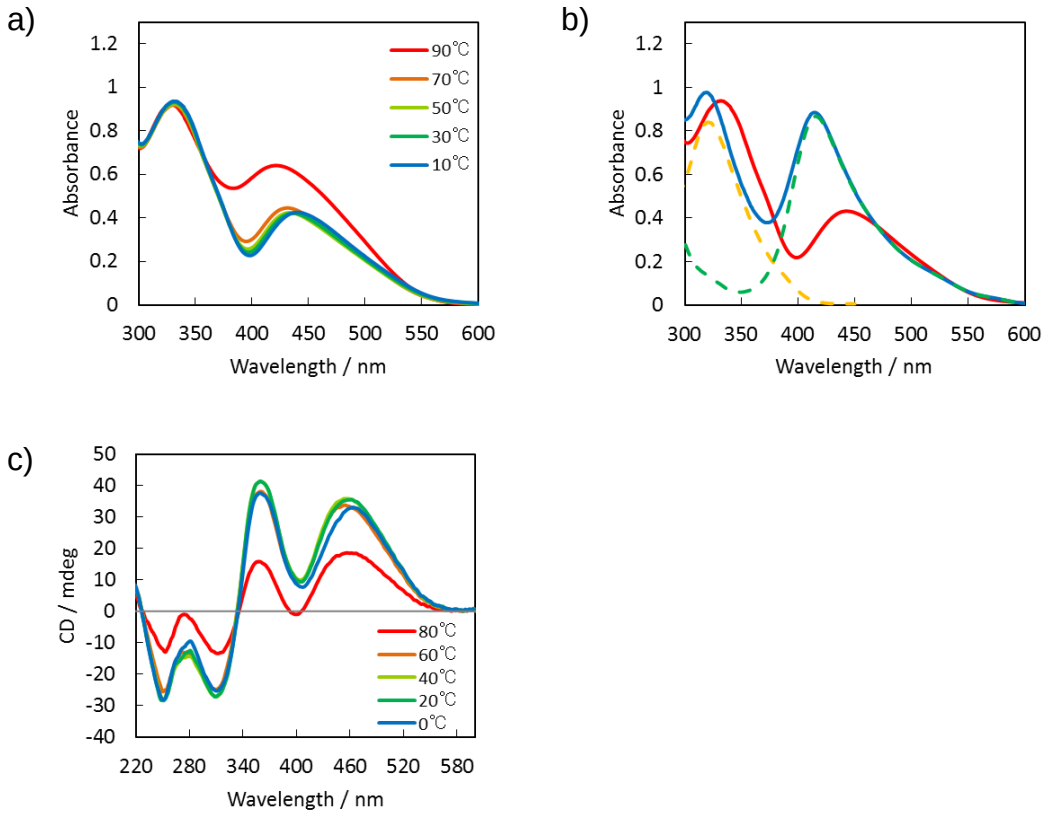

Figure 2-4. a) UV-vis spectra of **M6a**/**N6b** (5.0 μM each strand) at indicated temperatures. b) Comparison of UV-vis spectra of **M6a**/**N6b** (red line) with the mathematical sum (blue line) of single stranded **N6b** (orange broken line) and **M6a** (green broken line) at 0 ^{o}C; strand concentrations 5.0 μM. c) CD spectra of **M6a**/**N6b** (5.0 μM each strand) at indicated temperatures. Conditions: 100 mM NaCl, 10 mM phosphate buffer (pH 7.0).

confirm that the bathochromic shift was caused by the interaction between **N** and **M** residues, the spectrum of **M6a**/**N6b** was compared with a sum spectrum of each single strands. Blue line in Fig. 2-4b shows the sum spectrum of single stranded **M6a** and **N6b** at 0 ^{o}C. Compared to this spectrum, the spectrum of **M6a**/**N6b** showed a bathochromic shifted band around 340 and 450 nm respectively. From this result, it was confirmed that the observed red shift in **M6a**/**N6b** certainly caused by the interaction between **N** and **M** residues. Thus, it was indicated that **N**/**M** hetero-aggregate was formed in DNA duplex, and their spectroscopic character was identified. Though CD spectra of **M6a**/**N6b** were difficult to render, we believe they formed a right-handed aggregate as well as **N6a**/**N6b** or **M6a**/**N6b** (Fig. 2-4c).

Then, we measured the thermal stability of **N**/**M** hetero pair through melting measurements of the duplex. Two melting temperatures (T_ms) at different wavelength were determined for each samples; 260 nm for hybridization of native DNA part (T_m^{260}), and 350-450 nm for aggregation of dye part (T_m^{dye}). Table 2-1 shows the obtained T_ms for each sequence. Compared to T_m^{260} of native **na**/**nb** of 47.7 ^{o}C, all the three duplexes containing homo- or hetero-azobenzene pairs showed higher T_m^{260}s of 76.7, 66.4 and 65.9 ^{o}C for **N**/**M**, **N**/**N** and **M**/**M** pairs respectively, which indicates that azobenzenes served as a pseudo base pairs to stabilize the duplex. Noteworthy, **M6a**/**N6b** showed the

Table 2-1. Melting temperatures of duplexes containing **N** or **M** residues.[a]

Sequence	T_m^{260} [°C][b]	T_m^{dye} [°C][c]
M6a/N6b	76.7	81.3
N6a/N6b	66.4	66.3
M6a/M6b	65.9	67.5
na/nb	47.7	n.d.[d]

[a] Measurement conditions: 100 mM NaCl, 10 mM phosphate buffer (pH 7.0), 5.0 μM each oligomer strand. [b] Melting temperature determined from the absorbance at 260 nm. [c] Melting temperatures determined from the absorbance due to **N**/**M**, 420 nm; **N**/**N,** 350 nm; **M**/**M,** 450 nm; these wavelengths were those of most significant change for each series. [d] No absorption found around 350-450 nm.

highest T_m^{260} among the three duplexes containing azobenzenes. This result clearly indicates that **N**/**M** hetero-pair significantly stabilized the duplex more than **N**/**N** or **M**/**M** homo-pairs. Moreover, interestingly, T_m^{dye} was about 5 °C higher than T_m^{260} with T_m^{260}. Such coincidence indicates that the double-helix formation occurred **M6a**/**N6b**, whilst **N6a**/**N6b** and **M6a**/**M6b** showed a coincidence between T_m^{dye} and cooperatively. In other words, it was suggested that the dye part of **M6a**/**N6b** was so stable as to form **N**/**M** hetero pair without hybridization of native DNA part at high temperatures.

2-3-2 Sequence selectivity of donor/acceptor pairs at overhang positions

From this result, it was suggested that **N**/**M** hetero pair could be formed without any scaffolding by native DNAs. Then next, we investigated the spontaneous **N**/**M** hetero pairing using the overhang series. With the overhang series, **N** or **M** residues were

introduced at 5’ overhang positions of DNA strands and the aggregation is no longer assisted by native DNAs. Hence, the azobenzenes were allowed to form both homo- and hetero-aggregates in the overhang series. We investigated the sequence selectivity, whether the **N**/**M** hetero-aggregate is formed, through the spectroscopic measurements of overhang series.

Firstly, we investigated the **N**/**N** or **M**/**M** homo-pairing abilities within overhang series. As the temperature was lowered, hypsochromic shift of the bands, which were very similar to that of center series, were observed with both **N6Oa**/**nb** and **M6Oa**/**nb** (Fig. S2-2). When these spectra were compared to that of center series, they showed a very good coincidence, which clearly indicates that **N**/**N** or **M**/**M** homo-pairs were formed with overhang series (Fig. 2-5). CD measurements revealed that azobenzene

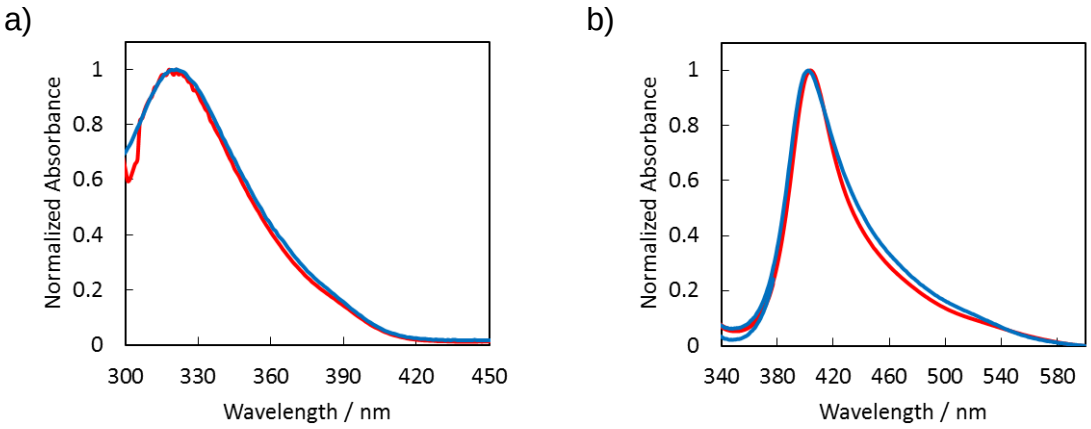

Figure 2-5. a) Comparison of UV-vis spectra of **N6Oa**/**nb** (blue line) with **N6a**/**N6b** (red line) at 0 ^{o}C. b) Comparison of UV-vis spectra of **M6Oa**/**nb** (blue line) with **M6a**/**M6b** (red line) at 0 ^{o}C; Conditions: 5.0 μM each strands. 100 mM NaCl, 10 mM phosphate buffer (pH 7.0).

residues at 5’ overhangs formed a right-handed aggregate as well as center series (Fig. S2-3). Also, single-stranded **N6Oa** and **M6Oa** were found to form **N**/**N** or **M**/**M** homo-pairs (Fig. S2-4 and Table S2-1), suggesting that the homo-azobenzene pairs are stable enough to form an aggregate without scaffolding by native DNAs.

Then, UV-vis spectra for **N**/**M** hetero-pairing were measured by mixing the same amount of **N6Oa**/**nb** and **M6Oa**/**nb** duplexes. UV-vis spectra of **N6Oa**/**nb**+**M6Oa**/**nb** showed a bathochromic shift of the band along the lowering temperature which was very similar to the spectral shift observed with center series (Fig. S2-5). Also, the spectrum of **N6Oa**/**nb**+**M6Oa**/**nb** showed a red-shifted band compared to the sum spectrum of **N6Oa**/**nb** and **M6Oa**/**nb** (Fig. 2-6a). Moreover, the spectrum of **N6Oa**/**nb**+**M6Oa**/**nb** showed a good coincidence to **M6a**/**N6b** (Fig. 2-6b). From these results, it was indicated that **N**/**M** hetero aggregate was selectively formed with overhang series. In other words, selective hetero-pairing in overhang series suggests that the thermal stability of **N**/**M** hetero-pair was far more stable compared to **N**/**N** or **M**/**M** homo pairs. Then, we measured the melting temperatures of overhang series. Table 2-2 shows the results of melting measurements. When we look at the T_m^{260}s, slight stabilization about 3-6 ^oC were observed with azobenzene containing DNAs compared to native **na**/**nb**. This stabilization seems quite natural since the azobenzene residues at

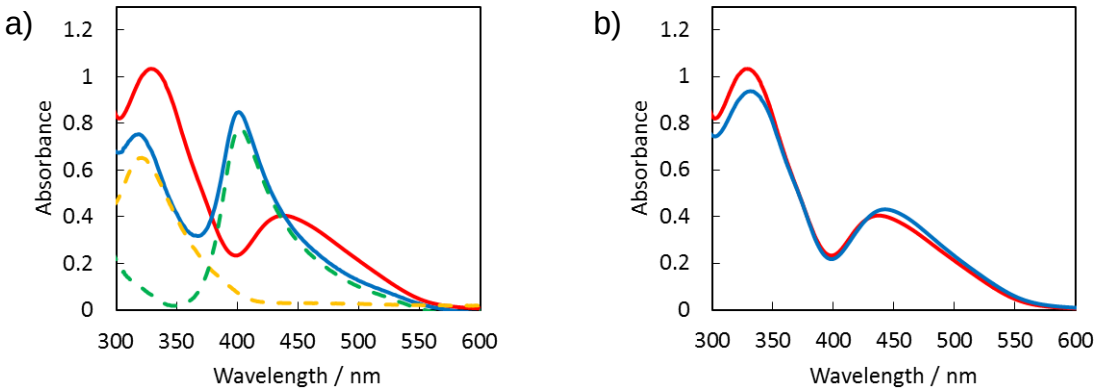

Figure 2-6. a) Comparison of UV-vis spectra of **N6Oa/nb**+**M6Oa/nb** (red line) with the mathematical sum (blue line) of single stranded **N6Oa/nb** (orange broken line) and **M6Oa/nb** (green broken line) at 0 °C; strand concentrations 5.0 μM. b) Comparison od UV-vis spectra of **N6Oa/nb**+**M6Oa/nb** (red line) with **M6a/N6b** (blue line) at 0 °C; strand concentrations 5.0 μM. Conditions: 100 mM NaCl, 10 mM phosphate buffer (pH 7.0).

Table 2-2. Melting temperatures of overhang series containing **N** or **M** residues.[a]

Sequence	T_m^{260} [°C][b]	T_m^{dye} [°C][c]
N6Oa/nb+M6Oa/nb	53.4	> 80
N6Oa/nb	50.8	30.6
M6Oa/nb	50.2	27.6
na/nb	47.7	n.d.[d]

[a] Measurement conditions: 100 mM NaCl, 10 mM phosphate buffer (pH 7.0), 5.0 μM each oligomer strand. [b] Melting temperature determined from the absorbance at 260 nm. [c] Melting temperatures determined from the absorbance due to **N**/**M**, 420 nm; **N**/**N,** 350 nm; **M**/**M,** 450 nm; these wavelengths were those of most significant change for each series. [d] No absorption found around 350-450 nm.

5' overhang position should stack with flanking native base pairs and repress the destabilization caused by the breathing of terminus base pairs.[21] On the other hand, interestingly, while the homo-pairs, **N6Oa/nb** and **M6Oa/nb**, showed T_m^{dye}s of 30.6 and 27.6 °C respectively, the T_m^{dye} of **N6Oa/nb**+**M6Oa/nb** was extremely high as more than

80 ^{o}C. Note that, no such drastic difference was observed between homo- and hetero-pairs with center series. The reason for this should be due to the cooperative effect of center series. With the homo-center series, double-helix formation of the DNA part and the dye part occurs simultaneously, and hence, the azobenzene modified strands should serve as an 18 mer long oligonucleotide sequence. This cooperative effect makes it difficult to evaluate the intrinsic stability of **N**/**N** or **M**/**M** homo-pairs which the hybridization of the DNA part and the dye part occurred simultaneously. On the other hand, with the overhang series, hybridization of the DNA part and the dye part occurs independently. Therefore, it could be considered that the intrinsic stabilities of the dye part themselves were observed with overhang sequences.[22] So, it could be concluded that the stability of **N**/**M** hetero-pair was far more stable than **N**/**N** or **M**/**M** homo-pairs. Thus, it was indicated that **N** and **M** residues form a highly stable aggregate with excellent selectivity without the scaffolding assist by native DNAs.

2-3-3 Confirmation of stabilization through electrostatic complementarity

Next, we investigated whether the extreme thermal stability of **N**/**M** pairs were due to the electrostatic complementarity of **N** and **M** residues. In order to test that, nitro group modified **M** residue, Nitro Methyl Red (**R**), was synthesized and introduced into DNA

strands (Fig. 2-7). According to DFT calculation, **R** residue showed a lowered π-electron density compared to **M** residues which induced by the electron withdrawing nitro group (Figs. S2-1b, c). Therefore, if **N**/**M** pair was stabilized by their electrostatic complementarity, the thermal stability of **N**/**R** pair should show lower thermal stability compared to **N**/**M** pair. We investigated the thermal stability of **N**/**R** pair within center or overhang series. Fig. 2-8a shows UV-vis spectrum of **R6a**/**N6b**. As the temperature was lowered, the absorption band showed a bathochromic shift, which could be assigned to **N**/**R** hetero pair formation. Also, the overhang series, **N6Oa**/**nb**+**R6Oa**/**nb**, showed red-shifted band which was not observed with **N6Oa**/**nb** or **R6Oa**/**nb** only (Figs. 2-8b, c). And the spectrum of **N6Oa**/**nb**+**R6Oa**/**nb** coincided with that of **R6a**/**N6b** which indicates that **N**/**R** hetero-aggregate was formed selectively with **N**-, **R**-overhang series (Fig.2-8d). Thus, it was confirmed that **N**/**R** hetero-aggregates were selectively formed both with the center and the overhang series.

R6a: 5'-GGTATC**RRRRRR**GCAATC-5'
R6Oa: 5'-**RRRRRR**GGTATCGCAATC-3'

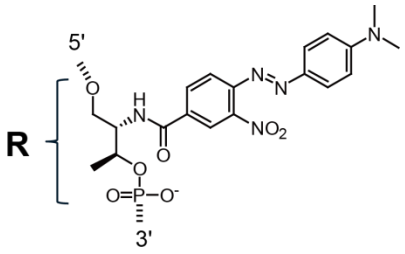

Figure 2-7. Sequences and chemical structures of oligomers containing **R** residues. A, G, C, and T represents 2'-deoxyribonucleotides.

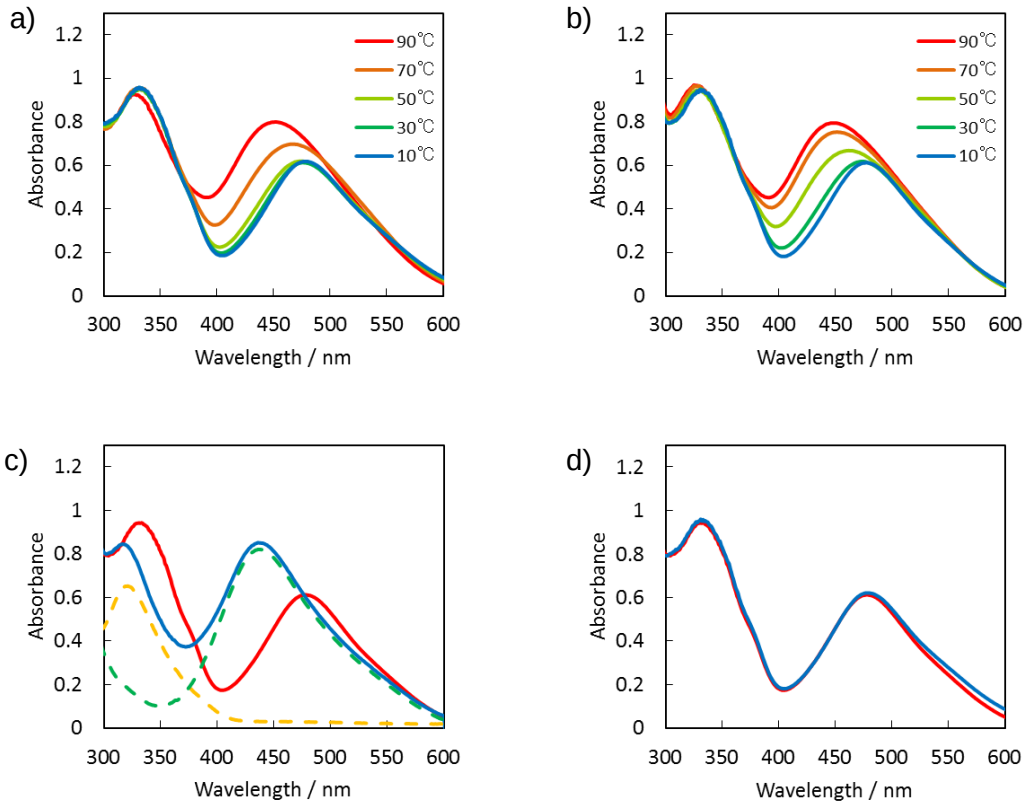

Figure 2-8. UV-vis spectra of a) **R6a**/**N6b** and b) **N6Oa**/**nb**+**R6Oa**/**nb** (5.0 μM each strand) at indicated temperatures. c) Comparison of UV-vis spectra of **R6a**/**N6b** (red line) with the mathematical sum (blue line) of single stranded **N6b** (orange broken line) and **R6a** (green broken line) at 0 ^{o}C; strand concentrations 5.0 μM. d) Comparison od UV-vis spectra of **N6Oa**/**nb**+**R6Oa**/**nb** (red line) with **R6a**/**N6b** (blue line) at 0 ^{o}C; strand concentrations 5.0 μM. Conditions: 100 mM NaCl, 10 mM phosphate buffer (pH 7.0).

Then we measured the melting temperatures of **N**/**R** hetero series to compare their thermal stability with **N**/**M** hetero series. Table 2-3 shows the results of melting measurements of **N**/**R** hetero series. The center series at first, showed the T_m^{260} of 55.5 ^{o}C which was 10.0 ^{o}C less stable compared to that of **M6a**/**N6b** of 76.7 ^{o}C. And the distinct difference between T_m^{dye} and T_m^{260}, as observed with **M6a**/**N6b**, was not

Table 2-3. Melting temperatures of **N**/**R** hetero-series.[a]

Sequence	T_m^{260} [°C][b]	T_m^{dye} [°C][c]
R6a/N6b	71.2	72.4
N6Oa/nb+R6Oa/nb	52.9	45.0

[a] Measurement conditions: 100 mM NaCl, 10 mM phosphate buffer (pH 7.0), 5.0 μM each oligomer strand. [b] Melting temperature determined from the absorbance at 260 nm. [c] Melting temperatures determined from the absorbance at 420 nm where the most significant change was observed for **N**/**R** complexation.

observed with **R6a**/**N6b**, which suggests that the stability of **/N**/**R** complex was not stable and the hybridization of DNA part and the aggregation of the azobenzenes occurred simultaneously. Also, the T_m^{dye} of **N6Oa**/**nb**+**R6Oa**/**nb** was 50.0 °C and 10 °C lower than that of **N6Oa**/**nb**+**M6Oa**/**nb** of more than 80 °C. Thus, it was identified that **N**/**R** hetero-pair is less stable compared to **N**/**M** hetero-pair both in center and overhang series. This lower stability of **N**/**R** hetero-pair is very likely due to the less electrostatic complementarity as we designed. From this result, it was suggested that electrostatic complementarity is an important factor to form a stable donor/acceptor hetero-pair, and hence, **N**/**M** hetero-pairs showed extremely high thermal stabilities.

2-3-4 Properties of L-threoninol linkers

Finally, we tried to add further recognition mechanism, which is orthogonal to donor-acceptor recognition, to the **N**/**M** hetero-pairs in order to give them more versatile

recognition. To expand the recognition mode of **N**/**M** hetero pairs, we focused on the charity of the linkers. Here, L-threoninol linker was used in addition to D-threoninol linker (Fig. 2-9). As described above, dyes tethered on D-threoninol linkers incline to form right-handed helical structures, and *vice versa*.[23,24,25] According to this disposition, we expected **N** and **M** residues to selectively recognize each other not only by electrostatic complementarity but also by the chirality of the linkers as native nucleobases with D-ribose backbones does not form a duplex with L-ribose backbones.[26,27] Sequences containing **N** or **M** residues tethered on L-threoninol ($\mathbf{N_L}$, $\mathbf{M_L}$) are shown in Fig. 2-10.

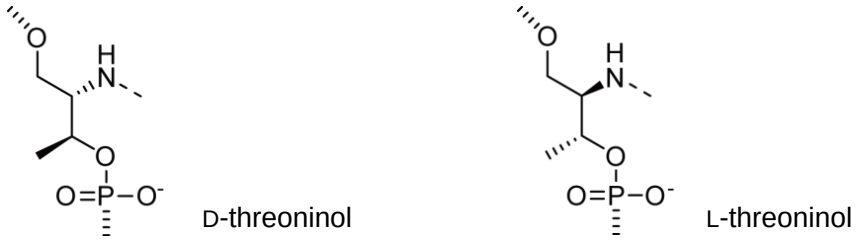

Figure 2-9. Chemical structures of D-threoninol and L-threoninol.

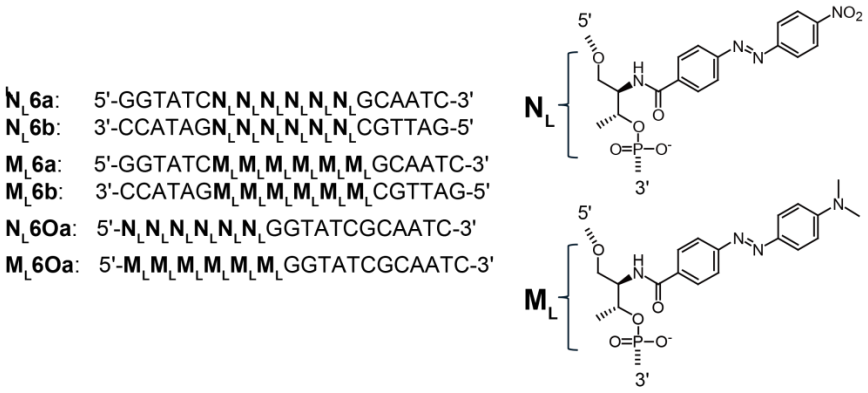

Figure 2-10. Sequences and chemical structures of oligomers containing $\mathbf{N_L}$ or $\mathbf{M_L}$ residues. A, G, C, and T represents 2'-deoxyribonucleotides.

Firstly, we investigated the spectroscopic behavior, as well as thermal stabilities, of L-threoninol series at the center position of DNA strands. Compared to D-threoninol series, all three **N_L6a**/**N_L6b**, **M_L6a**/**M_L6b** and **N_L6a**/**M_L6b** showed very similar spectral shift along the hybridization, hypsochromic- and bathochromic-shift for homo- and hetero-pairs respectively, and their spectra at duplex state showed a good coincidence with that of D-threoninol series (Figs. 2-11a, b, c). This coincidence indicates that azobenzenes tethered L-threoninol linker formed well-stacked aggregates as well as D-threoninol series. In contrast, CD spectra of L-threoninol series were totally different from D-threoninol series. As described above, azobenzenes tethered on D-threoninol

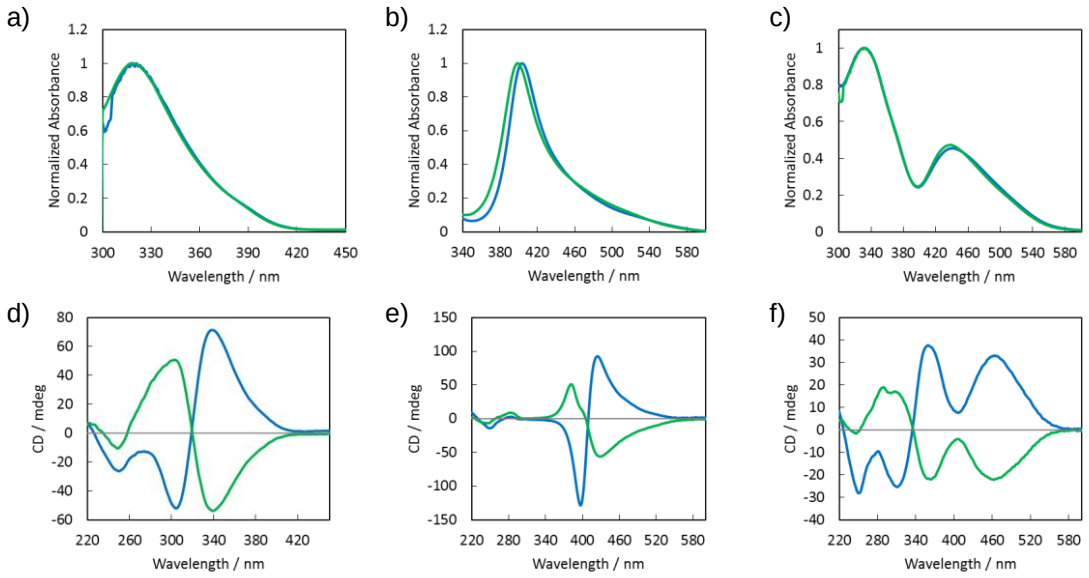

Figure 2-11. Comparison of UV-vis or CD spectra between a), c) **N6a**/**N6b** (blue line) and **N_L6a**/**N_L6b** (green line), b), e) **M6a**/**M6b** (blue line) and **M_L6a**/**M_L6b** (green line), and c), f) **M6a**/**N6b** (blue line) and **N_L6a**/**M_L6b** (green line) at 0 ^{o}C; strand concentrations 5.0 μM. Conditions: 100 mM NaCl, 10 mM phosphate buffer (pH 7.0).

Table 2-4. Melting temperatures of center series with L-threoninol linkers.[a]

Sequence	T_m^{260} [°C][b]	T_m^{dye} [°C][c]
N_L6a/M_L6b	70.9	73.5
N_L6a/N_L6b	59.5	58.9
M_L6a/M_L6b	65.0	65.8

[a] Measurement conditions: 100 mM NaCl, 10 mM phosphate buffer (pH 7.0), 5.0 μM each oligomer strand. [b] Melting temperature determined from the absorbance at 260 nm. [c] Melting temperatures determined from the absorbance due to **N**/**M**, 420 nm; **N**/**N,** 350 nm; **M**/**M,** 450 nm; these wavelengths were those of most significant change for each series.

linkers incline to form right-handed aggregate, which was identified through positive-negative cotton effect of homo-series. On the other hand, CD spectra of L-threoninol series showed absolutely inversed CD signals compared to D-threoninol series, which clearly indicate that the left-handed aggregates were formed with all three **N_L6a**/**N_L6b**, **M_L6a**/**M_L6b** and **N_L6a**/**M_L6b** (Figs. 2-11d, e, f). Then we measured the melting temperatures of L-threoninol series (Table 2-4). As a result, **N_L6a**/**M_L6b** containing **N_L**/**M_L** hetero-pair showed the highest T_m^{260} as 70.9 °C among the three duplexes, while the T_m^{260}s of **N_L6a** /**N_L6b** and **M_L6a** /**M_L6b** were 59.5 °C and 65.0 °C respectively. From this result, it was confirmed that the stabilization through theelectrostatic complementarity of the azobenzene residues was still consistent with L-threoninol linkers. On the other hand, when the melting temperatures of the L-threoninol series in Table 2-4 were compared to that of D-threoninol series in Table 2-1, it was found that the melting temperatures of D-threoninol series were higher than

L-threoninol series with all three **N**/**N**, **M**/**M** homo- and **N**/**M** hetero-pairs. This difference is very likely due to the different helicity of the dye aggregates induced by D- or L-threoinol linkers. As described above, azobenzenes tethered on D- or L-threoniol linkers tended to form right- and left-handed duplexes respectively. And of course, the native DNAs form right-handed duplexes. Therefore, it was suggested that right-handed D-threoninol linkers were more preferable for right-handed native DNAs which is unlikely to cause substantial structural disruption of the backbones and subsequent entropic loss, and *vice versa*.

Then, we investigated the spectroscopic behavior and their conformations of L-threoninol series at the 5' overhang position of DNA strands. We measured the UV-vis spectra of **N_L6Oa**/**nb**, **M_L6Oa**/**nb** and **N_L6Oa**/**nb**+**M_L6Oa**/**nb** and compared them with that of D-threoninol series. As a result, as well as center series, the UV-vis spectroscopic behavior of L-threoninol-overhang series were very similar to that of D-threoninol series, and the spectra of L-threoninol series at duplex state showed excellent coincidence with D-threoninol series (Figs. 2-12a, b, c). Thus, it was confirmed that L-threoninol-overhang series formed well-stacked aggregates as well as D-threoninol series. On the other hand the CD spectra of L-threoninol were totally different from those of D-threoninol series. As well as center series, the CD signals were definitely inversed

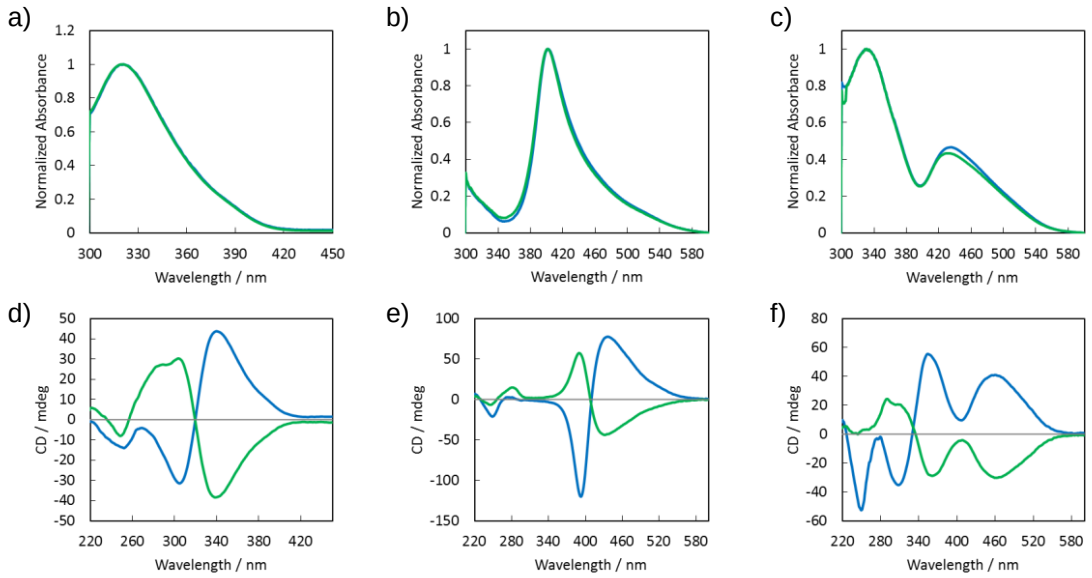

Figure 2-12. Comparison of UV-vis or CD spectra between a), c) **N6Oa/nb** (blue line) and **N_L6Oa/nb** (green line), b), e) **M6O/nb** (blue line) and **M_L6Oa/nb** (green line), and c), f) **N6Oa/nb**+**M6Oa/nb** (blue line) and **N_L6Oa/nb**+**M_L6Oa/nb** (green line) at 0 ^{o}C; strand concentrations 5.0 μM. Conditions: 100 mM NaCl, 10 mM phosphate buffer (pH 7.0).

with all three L-threoninol overhang series and was indicated that L-threoninol overhang series formed left-handed aggregates as well as L-threoninol center series described above (Figs. 2-12d, e, f). As thus, the spectroscopic behaviors of UV-vis and CDs of L-threoninol-overhang series were very similar to L-threoninol center series. Interestingly however, the results of melting measurements of L-threoninol-overhang series showed distinct difference from center series. Table 2-5 shows the melting temperatures of L-threoninol overhang series. As described above, it was found that L-threoninol series were less stable than D-threoninol series when the center series. In

Table 2-5. Melting temperatures of overhang series with L-threoninol linkers.[a]

Sequence	T_m^{260} [°C][b]	T_m^{dye} [°C][c]
N_L6Oa/nb+M_L6Oa/nb	51.0	> 80
N_L6Oa/nb	52.8	32.2
M_L6Oa/nb	49.4	27.6

[a] Measurement conditions: 100 mM NaCl, 10 mM phosphate buffer (pH 7.0), 5.0 μM each oligomer strand. [b] Melting temperature determined from the absorbance at 260 nm. [c] Melting temperatures determined from the absorbance due to **N**/**M**, 420 nm; **N**/**N,** 350 nm; **M**/**M,** 450 nm; these wavelengths were those of most significant change for each series.

contrast, the melting temperatures of the L-threoninol overhang series almost coincided with those of D-threoninol series (compare Tables 2-2 and 2-4). This result seems quite reasonable since azobenzenes are located at outside of the DNA duplexes with the overhang series and the structures at the overhang positions do not likely seem to affect the structures of native DNA parts. Thus, it was confirmed that D-threoninol linkers are preferable for center series to form stable duplexes, and both D- and L-threoninols serveas well in overhang series.

2-3-5 Recognition ability between the linkers with different chiralities

Then finally, we investigated the recognition ability through the difference of chirality between D- and L-threoninols. Here, **N** with D-threoninol and **M** with L-threoninol linkers were used. First, we confirmed **N**/$\mathbf{M_L}$ hetero aggregate formation through UV-vis measurements. Fig. 2-13a shows the result of **N6a**/$\mathbf{M_L}$**6b** duplex.

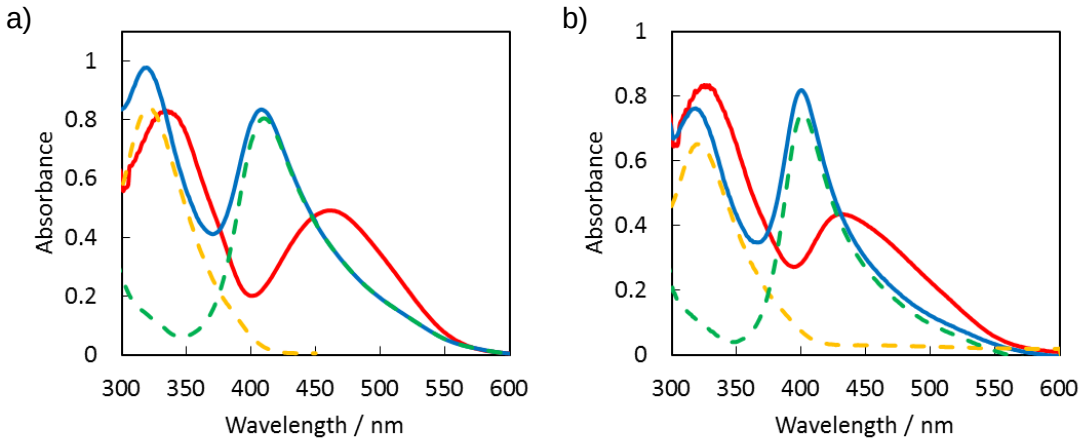

Figure 2-13. a) Comparison of UV-vis spectra of **N6a**/**M$_L$6b** (red line) with the mathematical sum (blue line) of single stranded **N6a** (orange broken line) and **M$_L$6b** (green broken line) at 0 ^{o}C; strand concentrations 5.0 μM. b) Comparison of UV-vis spectra of **N6Oa**/**nb**+**M$_L$6Oa**/**nb** (red line) with the mathematical sum (blue line) of **N6Oa**/**nb** (orange broken line) and **M$_L$6Oa**/**nb** (green broken line) at 0 ^{o}C; strand concentrations 5.0 μM. Conditions: 100 mM NaCl, 10 mM phosphate buffer (pH 7.0).

Similar to the above described **N**/**M** or **N$_L$**/**M$_L$** hetero-pairs, red-shifted was observed compared to the sum spectrum of each single strands. Such red-shift was also observed with **N6Oa**/**nb**+**M$_L$6Oa**/**nb**. Thus, it was indicated that **N**/**M$_L$** hetero aggregate were formed, even though their chirality of the linkers were different. Then we investigated the thermal stability of **N**/**M$_L$** hetero-pairs. Table 2-6 shows the result of melting measurements. As a result, the melting temperature of **N6a**/**M$_L$6b** was 74.2 ^{o}C which was in between of **M6a**/**N6b** (T_m =76.7 ^{o}C) and **N$_L$6a**/**M$_L$6b** (T_m =70.9 ^{o}C). Thus, it was indicated that the duplex was most stabilized with D-/D-threoniol pair and least with L-/L-threoninol pair. This result suggests that right handed D-/D-threoniol pair was

Table 2-6. Melting temperatures of **N**/**M** hetero-series with L-threoninol linkers.[a]

Sequence	T_m^{260} [°C][b]	T_m^{dye} [°C][c]
N6a/M$_L$6b	74.2	77.7
N6Oa/nb+M$_L$6Oa/nb	49.7	66.5

[a] Measurement conditions: 100 mM NaCl, 10 mM phosphate buffer (pH 7.0), 5.0 μM each oligomer strand. [b] Melting temperature determined from the absorbance at 260 nm. [c] Melting temperatures determined from the absorbance at 420 nm where the most significant change was observed for **N**/**M** complexation.

most preferable for right handed DNA duplex as described above. And the higher thermal stability of **N6a**/**M$_L$6b** than **N$_L$6a**/**M$_L$6b** might be due to the less entropic loss compared to left-handed **N$_L$**/**M$_L$** pair. Hence, the recognition ability through the chiralities of the linkers was yet unclear through the measurements of center series. In contrast, the melting temperature of **N**/**M$_L$** pairs at overhang position (T_m =66.5 °C) was far more lower than **N**/**M** or **N$_L$**/**M$_L$** pairs (T_m >80 °C). As described above, pseudo base pairs introduced at overhang positions were not affected by the right-handed helicity of native DNA parts. Therefore, the difference of melting temperature between **N**/**M**, **N$_L$**/**M$_L$**, **N**/**M$_L$** pairs at overhang positions should represent the effect of recognition ability through the chiralities of the linkers. Hence, it was indicated that N and M residues recognizes each other not only by electrostatic complementarity but also by chiralities of the linkers and D- or L-donors formed more stable pair with D- or L-acceptors respectively.

2-4 Conclusions

In summary, we successfully demonstrated hetero-selective pseudo base pair formation using *p*-nitroazobenzene and Methyl Red. UV-vis measurements indicated predicted homo- or hetero-aggregates were formed at the center positon of DNA duplex and the duplex was significantly stabilized with hetero-pairs compared to homo-pairs. Also, *p*-nitroazobenzene/Methyl Red pairs showed excellent sequence selectivity and high thermal stability when they were introduced at 5' overhang positions. Nitro group modification to the donor residues indicated that the high thermal stability of the hetero-pairs were due to the electrostatic complementarity of the azobenzene residues.

Moreover, *p*-nitroazobenzene/Methyl Red pairs showed the sequence selectivity through the chirality of the linkers. *p*-Nitroazobenzene tethered on right-handed D-threoninol linkers formed a more stable duplex with Methyl Red tethered on D-threoninol linkers, and also L- with L-. The donor/acceptor azobenzene pseudo base pairs showed high thermal stability and excellent sequence selectivity, and also its recognition through electrostatic complementarity or chirality of the linker are orthogonal to the hydrogen bonding recognition of native nucleobases. Therefore, this hetero-selective azobenzene pseudo base pair is a promising candidate which allows us to construct more stable and complicated nano-architectures.

2-5 Experimental section

Materials

All conventional phosphoramidite monomers, CPG columns, and reagents for DNA synthesis were purchased from Glen Research. Other reagents for the syntheses of phosphoramidite monomers were purchased from Tokyo Chemical Industry, Wako, and Aldrich. Unmodified oligonucleotides were purchased from Integrated DNA Technologies.

Synthesis of ODNs

All the modified ODNs were synthesized on an automated DNA synthesizer (H-8-SE, Gene World) by using phosphoramidite monomers bearing **N**, **M**, **R,** $\mathbf{N_L}$, or $\mathbf{M_L}$. Syntheses of phosphoramidite monomers **M** and **Z** were reported previously. **N** was synthesized as described in the Appendix Information. After workup, ODNs were purified by reversed phase HPLC and characterized using a matrix-assisted laser desorption ionization time-of-flight mass spectrometer (MALDI-TOF; Autoflex II, Bruker Daltonics).

Spectroscopic Measurements

UV-vis spectra were measured on a Shimadzu UV-1800 equipped with programmed temperature-controllers using 10-mm quartz cells. CD spectra were measured on a JASCO model J-820 equipped with programmed temperature-controllers using 10-mm quartz cells.

Melting Temperature Measurements

The melting curves were obtained with a Shimadzu UV-1800 by measuring the change in absorbance at 260, 350, 400, 420, or 450 nm versus temperature. Both the heating and the cooling curves were measured, and the melting temperatures (T_m) were determined from the maximum in the first derivative of the melting curves. The shown T_ms were obtained from the average between the heating and the cooling, and only the heating curves are shown. The temperature ramp was 0.2 °C min^{-1}.

2-6 References

(1) Varghese, R.; Wagenknecht, H.-A. *Chem. Commun.* **2009**, 2615.

(2) Malinovskii, V. L.; Wenger, D.; Haner, R. *Chem. Soc. Rev.* **2010**, *39*, 410.

(3) Asanuma, H.; Fujii, T.; Kato, T.; Kashida, H. *J. Photochem. Photobiol., C* **2012**, *13*, 124.

(4) Kelley, S. O.; Barton, J. K. *Science* **1999**, *283*, 375.

(5) Murphy, C. J.; Arkin, M. R.; Jenkins, Y.; Ghatlia, N. D.; Bossmann, S. H.; Turro, N. J.; Barton, J. K. *Science* **1993**, *262*, 1025.

(6) Thazhathveetil, A. K.; Vura-Weis, J.; Trifonov, A.; Wasielewski, M. R.; Lewis, F. D. *J. Am. Chem. Soc.* **2012**, *134*, 16434.

(7) Börjesson, K.; Preus, S.; El-Sagheer, A. H.; Brown, T.; Albinsson, B.; Wilhelmsson, L. M. *J. Am. Chem. Soc.* **2009**, *131*, 4288.

(8) Kato, T.; Kashida, H.; Kishida, H.; Yada, H.; Okamoto, H.; Asanuma, H. *J. Am. Chem. Soc.* **2013**, *135*, 741.

(9) Iqbal, A.; Arslan, S.; Okumus, B.; Wilson, T. J.; Giraud, G.; Norman, D. G.; Ha, T.; Lilley, D. M. J. *Proc. Natl. Acad. Sci. U.S.A.* **2008**, *105*, 11176.

(10) Fujii, T.; Kashida, H.; Asanuma, H. *Chem. Eur. J.* **2009**, *15*, 10092.

(11) Brotschi, C.; Leumann, C. J. *Angew. Chem. Int. Ed.* **2003**, *42*, 1655.

(12) Zahn, A.; Leumann, C. J. *Chem. Eur. J.* **2008**, *14*, 1087.

(13) Grigorenko, N. A.; Leumann, C. J. *Chem. Eur. J.* **2009**, *15*, 639.

(14) Kashida, H.; Fujii, T.; Asanuma, H. *Org. Biomol. Chem.* **2008**, *6*, 2892.

(15) Kashida, H.; Doi, T.; Sakakibara, T.; Hayashi, T.; Asanuma, H. *J. Am. Chem. Soc.* **2013**, *135*, 7960.

(16) Kashida, H.; Ito, H.; Fujii, T.; Hayashi, T.; Asanuma, H. *J. Am. Chem. Soc.* **2009**, *131*, 9928.

(17) Kashida, H.; Hayashi, T.; Fujii, T.; Asanuma, H. *Chem. Eur. J.* **2011**, *17*, 2614.

(18) Scott Lokey, R.; Iverson, B. L. *Nature* **1995**, *375*, 303.

(19) Gabriel, G. J.; Sorey, S.; Iverson, B. L. *J. Am. Chem. Soc.* **2005**, *127*, 2637.

(20) Das, A.; Molla, M. R.; Maity, B.; Koley, D.; Ghosh, S. *Chem. Eur. J.* **2012**, *18*, 9849.

(21) About 3 ^{o}C stabilization observed in **N6Oa**/**nb**+**M6Oa**/**nb** compared to homo-pairs might be due to the high stability of **N**/**M** hetero-aggregate. With **N6Oa**/**nb**+**M6Oa**/**nb**, the aggregation of azobenzenes should occur before than the hybridization of native DNA part, which contributes to stabilize the base pairing of flanking bases due to their relatively fixed structures.

(22) Though, the stabilization by stacking of the flanking nucleobases still remains.

(23) Kashida, H. *Doctoral Dissertation of the University of Tokyo*, 2006.

(24) This preference is true only when the dye molecules were directly tethered on threoninol linkers. The helicities are likely to inverse when native nucleobases are tethered on threoninol linkers via methylene group. See the reference below.

(25) Murayama, K.; Kashida, H.; Asanuma, H. *Chem. Commun.* **2015**, *51*, 6500.

(26) Urata, H.; Shinohara, K.; Ogura, E.; Ueda, Y.; Akagi, M. *J. Am. Chem. Soc.* **1991**, *113*, 8174.

(27) Garbesi, A.; Capobianco, M. L.; Colonna, F. P.; Tondelli, L.; Arcamone, F.; Manzini, G.; Hilbers, C. W.; Aelen, J. M.; Blommers, M. J. *Nucleic Acids Res.* **1993**, *21*, 4159.

2-7 Appendixes

Synthesis of *p*-nitroazobenzene phosphoramidite monomer

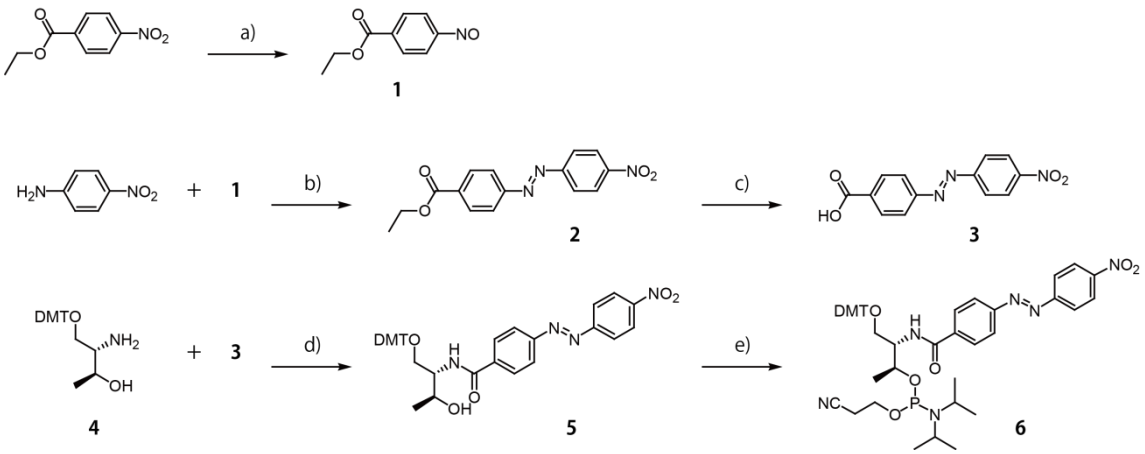

Scheme S2-1. Synthesis of phosphoramidite monomers tethering *p*-nitroazobenzene. Reagents and conditions: a) NH_4Cl, Zn, 2-methoxyethanol, $FeCl_3$, methanol, r.t., 30 min, yield: 87.0%. b) Acetic acid, r.t., few days, yield: 49.0%. c) NaOHaq, ethanol, chloroform, r.t., overnight, yield: quant. d) DCC, HOBt, NEt_3, DMF, r.t., overnight, yield: 51.0%. e) $(iPr)_2NP(Cl)(OCH_2CH_2CN)$, NEt_3, THF, 0 ^oC, 20 min, yield: quant.

Compound **4** was synthesized according to the previous report.[1] The phosphoramidite monomer tethering *p*-nitroazobenzene was synthesized as follows:

Synthesis of Compound 1: To a stirred solution of ethyl-4-nitrobenzoate (20.0 mmol, 3.90 g) in 2-methoxyethanol (45 mL), NH_4Cl (30.0 mmol, 1.60 g) in water (12 mL) was added. To the stirring mixture on water bath, Zn powder (52.0 mmol, 3.40 g) was gradually added. After 30 min stirring, Zn powder was removed by filtration and the solution was substituted with nitrogen gas. To the stirred solution, solution of $FeCl_3$ (50.0 mmol, 8.11 g) in water (90 mL) and ethanol (25 mL) was added dropwise at –5 ^oC under nitrogen atmosphere. After 40 min stirring, water (200 mL) was added and the precipitated solid was collected by filtration. The obtained solid was used for next reaction without further purification. Yield: 87.0%

Synthesis of Compound 2: Compound 1 (17.4 mmol, 3.12 g) and 4-nitroaniline (28.0 mmol, 3.86g) were dissolved in glacial acetic acid (100 mL) and stirred for few days under light shielding condition. After few days, ethyl acetate was added to the mixture and the organic layer was washed with water, saturated solution of $NaHCO_3$ (twice), and brine. After drying over $MgSO_4$, the solvent was removed by evaporation. The obtained residue was suspended in hexane (50 mL) and refluxed. To the suspension, ethyl acetate was gradually added until the all solid dissolved. The solution was keeped at 4 ^oC for overnight, and precipitate was collected by filtration. The obtained residue was purified by silica gel column chromatography using toluene as eluent. Yield: 49.0%. ^1H NMR [DMSO-d_6, 500 MHz] δ=8.44 ppm (d, 2H, *J*= 9.0 Hz, aromatic protons), δ=8.18 ppm (d, 2H, *J*= 8.5 Hz, aromatic protons), δ=8.12 ppm (d, 2H, *J*= 7.0 Hz, aromatic protons), δ=8.05 ppm (d, 2H, *J*= 8.0 Hz , aromatic protons), δ=4.43 ppm (q, 2H, *J*=7.5 Hz, CH_3-CH_2-O-CO-R), δ=1.34 ppm (t, 3H, *J*=7.5 Hz, CH_3-CH_2-O-CO-R).

Synthesis of Compound 3: To a stirred suspension of Compound 2 in ethanol (360 mL), aqueous NaOH (2 mmol/L, 120 mL) was added, then chloroform was added until the all solid dissolved. The solution was stirred for overnight under light shielding condition. After overnight stirring, the solution was acidified with aqueous HCl to pH 5, and then solvent was removed by evaporation. The obtained residue was suspended in water and filtered. On filter, the residue was washed with water and dried *in vacuo*. Yield: quant. ^1H NMR [DMSO-d_6, 500 MHz] δ=13.4 ppm (s, 1H, R-CO-O*H*), δ=8.50 ppm (m, 2H, aromatic protons), δ=8.22 ppm (m, 2H, aromatic protons), δ=8.18 ppm (m, 2H, aromatic protons), δ=8.08 ppm (m, 2H, aromatic protons).

Synthesis of Compound 5: To a stirred suspension of HOBt (2.24 mmol, 0.34 g), DCC (2.58 mmol, 0.53 g) and Compound 3 (2.06 mmol, 0.56 g) in DMF, Compound 4 (1.72 mmol, 0.70 g) in DMF was added dropwise, and then stirred for overnight. To the mixture, ethyl acetate was added and the organic layer was washed with saturated aqueous solution of $NaHCO_3$ and NaCl. After drying over $MgSO_4$, the solvent was removed by evaporation, followed by silica gel column chromatography using hexane and ethyl acetate as eluent (3% triethylamine was added). Yield: 51.0%. ^1H NMR

[DMSO-d_6, 500MHz] δ=8.50 ppm (d, 2H, *J*=8.5 Hz, aromatic protons), δ=8.34 ppm (d, 1H, *J*=9.0 Hz, -N*H*-CO-), δ=8.18 ppm (m, 4H, aromatic protons), δ=8.11 ppm (d, 2H, *J*=8.5Hz, aromatic protons), δ=7.44 ppm (d, 2H, *J*=7.0 Hz, aromatic protons), δ=7.30 ppm (m, 6H, aromatic protons), δ=7.24 ppm (m, 1H, *J*=8.0 Hz, aromatic protons), δ=6.88 ppm (m, 4H, aromatic protons), δ=4.67 ppm (d, 1H, *J*=6.0 Hz, -O*H*), δ=4.17 ppm (m, 1H, HO-CH_2-CH(NHR)-), δ=4.17 ppm (m, 1H, -C*H*(NHR)-), δ=4.07 ppm (m, 1H, HO-CH_2-CH(NHR)-), δ=4.07 ppm (m, 1H, -C*H*(CH_3)OH), δ=3.76 ppm (s, 6H, -O-CH_3), δ=1.07 ppm (d, 3H, *J*=6.0 Hz, -CH(CH_3)OH).

Synthesis of Compound 6: To a solution of Compound 5 (0.80 mmol, 0.53g) in dry THF, triethylamine (4.0 mmol, 0.55 mL) was added and the solution was cooled to 0 ^{o}C. To the solution, 2-cyanoethyl *N*,*N*-diisopropylchlorophosphoramidite (1.6 mmol, 0.36 mL) was added dropwise at 0 ^{o}C. After 20 min of vigorous stirring on ice, ethyl acetate was added and the organic layer was washed with saturated aqueous solution of $NaHCO_3$ and with NaCl. After drying over $MgSO_4$, the solvent was removed by evaporation, followed by silica gel column chromatography using hexane and ethyl acetate as eluent (3% triethylamine was added). Yield: quant.

Reference

1. Hara, Y.; Fujii, T.; Kashida, H.; Sekiguchi, K.; Liang, X.G.; Yoshida, Y.; Asanuma, H. *Angew. Chem. Int. Ed.* **2010**, *49*, 5502 –5506.

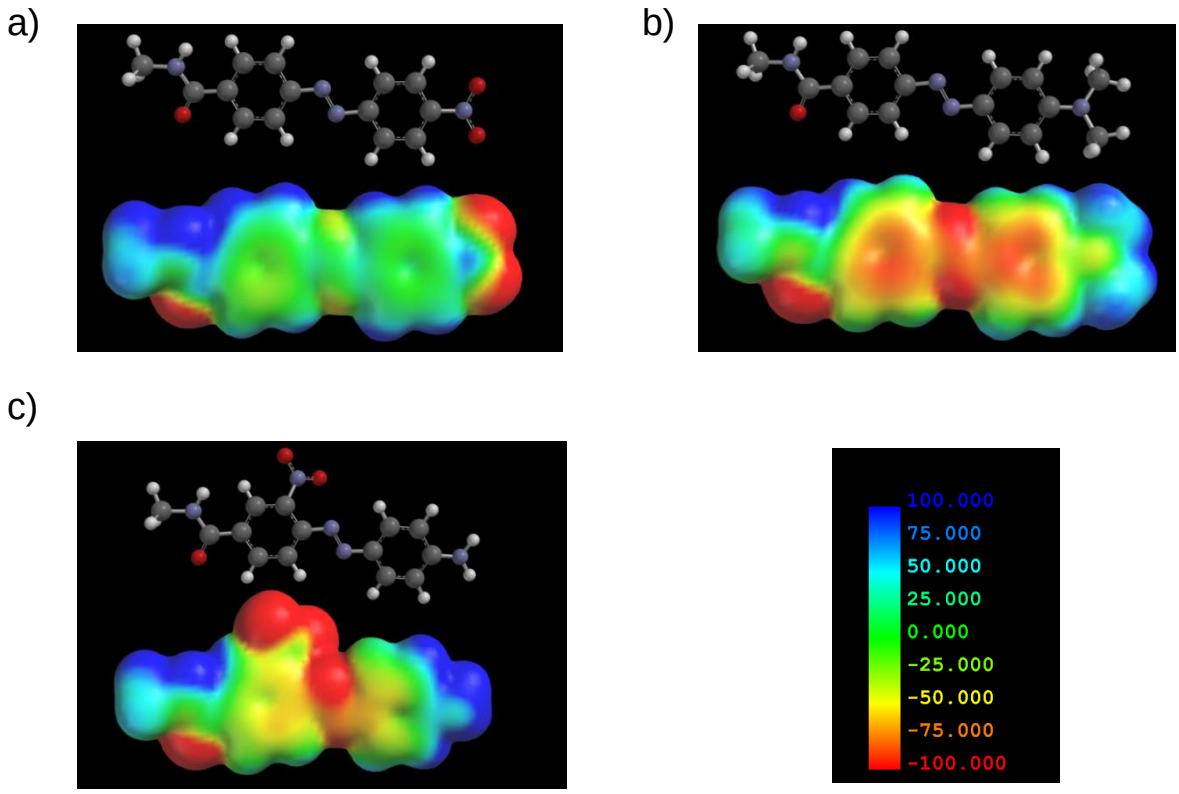

Fig. S2-1. Electrostatic potential surfaces of a) *p*-nitroazobenzene, b) Methyl Red, and c) Nitro Methyl Red. DFT calculation: B3LYP/6-31G(d), solvent: water.

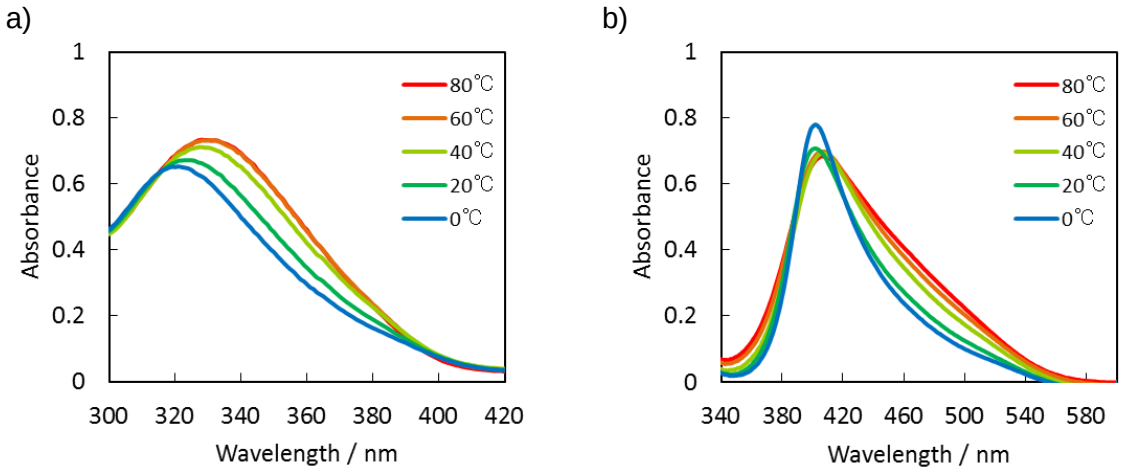

Figure S2-2. UV-vis spectra of a) **N6Oa**/**nb**, and b) **M6Oa**/**nb** (5.0 μM each strand) at indicated temperatures. Conditions: 100 mM NaCl, 10 mM phosphate buffer (pH 7.0).

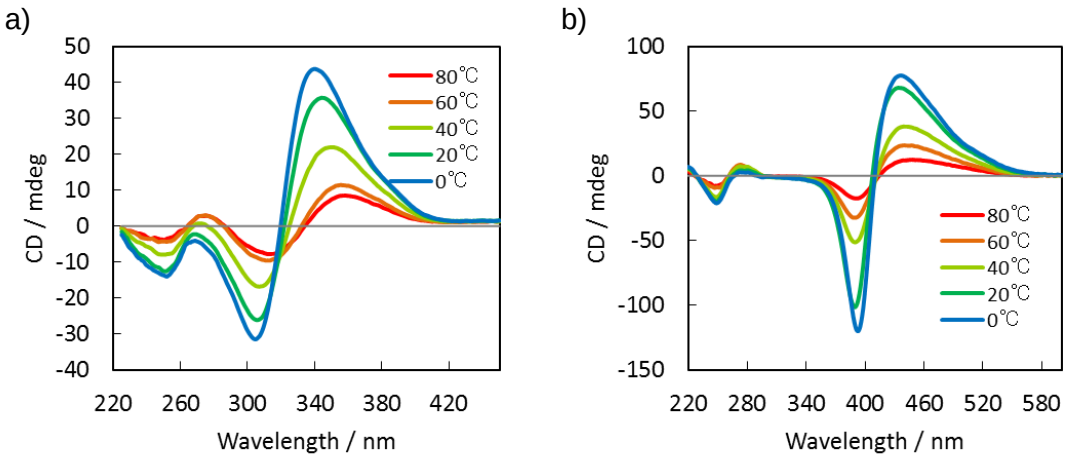

Figure S2-3. CD spectra of a) **N6Oa**/**nb** and b) **M6Oa**/**nb** (5.0 μM each duplex) at indicated temperatures. Conditions: 100 mM NaCl, 10 mM phosphate buffer (pH 7.0).

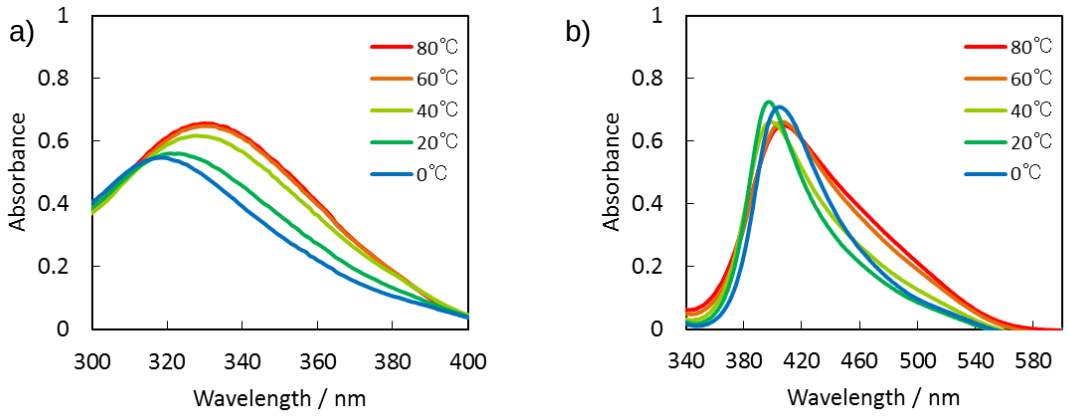

Figure S2-4. UV-vis spectra of a) **N6Oa**, and b) **M6Oa** (5.0 μM each strand) at indicated temperatures. Conditions: 100 mM NaCl, 10 mM phosphate buffer (pH 7.0).

Table S2-1. Melting temperatures of single-stranded overhang sequences.[a]

Sequence	T_m^{260} [°C][b]	T_m^{dye} [°C][c]
N6Oa+M6Oa	n.d.[d]	> 80
N6Oa	n.d.[d]	25.4
M6Oa	n.d.[d]	43.7

[a] Measurement conditions: 100 mM NaCl, 10 mM phosphate buffer (pH 7.0), 5.0 μM each oligomer strand. [b] Melting temperature determined from the absorbance at 260 nm. [c] Melting temperatures determined from the absorbance due to **N**/**M**, 420 nm; **N**/**N,** 350 nm; **M**/**M,** 450 nm; these wavelengths were those of most significant change for each series. [d] No significant melting temperature observed.

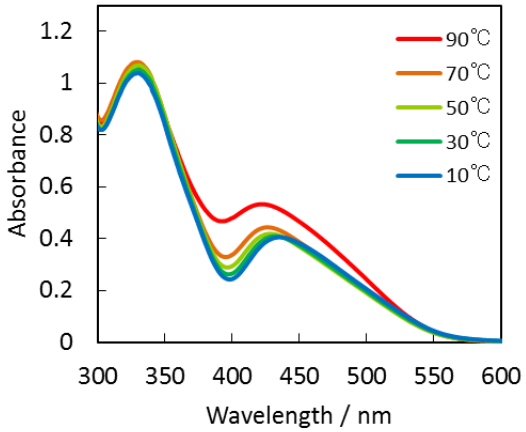

Figure S2-5. UV-vis spectra of **N6Oa**/**nb**+**M6Oa**/**nb** (5.0 μM each duplex) at indicated temperatures. Conditions: 100 mM NaCl, 10 mM phosphate buffer (pH 7.0).

Table S2-2. Melting temperatures of **N**/**N** homo-series.[a]

Sequence	T_m^{260} / °C [b]	T_m^{dye} / °C [c]
N1a/N1b	58.2	58.3
N2a/N2b	60.1	60.3
N3a/N3b	61.6	61.7
N6a/N6b	65.9	67.5
N_L1a/N_L1b	50.2	50.1
N_L2a/N_L2b	51.4	51.7
N_L3a/N_L3b	54.6	54.8
N_L6a/N_L6b	59.5	58.9
N_L1a/N1b	54.1	54.1
N_L2a/N2b	54.3	54.3
N_L3a/N3b	57.6	57.6
N_L6a/N6b	59.5	58.9
N6Oa/nb	50.8	30.6
N6Oa	n.d	25.4
N_L6Oa/nb	52.8	32.2
N_L6Oa	n.d	31.6

[a] Sequences: **N*n*a**: 5'-GGTATC(**N**)$_n$GCAATC-3' (*n*=1-3, 6); **N*n*b**: 5'-GATTGC(**N**)$_n$GCAATC-3' (*n*=1-3, 6); **N_L*n*a**: 5'-GGTATC(**N_L**)$_n$GCAATC-3' (*n*=1-3, 6); **N_L*n*b**: 5'-GATTGC(**N**)$_n$GCAATC-3' (*n*=1-3, 6); **N*6*Oa**: 5'-(**N**)$_6$GGTATCGCAATC-3'; **N_L*6*Oa**: 5'-(**N_L**)$_6$GGTATCGCAATC-3'; **nb**: 5'-GATTGCGATACC-3'; Measurement conditions: 100 mM NaCl, 10 mM phosphate buffer (pH 7.0), 5.0 μM each oligomer. [b] Melting temperature determined from the absorbance at 260 nm. [c] Melting temperature determined from the absorbance at 350 nm.

Table S2-3. Melting temperatures of **M**/**M** homo-series.[a]

Sequence	T_m^{260} / °C [b]	T_m^{dye} / °C [c]
M1a/M1b	50.5	n.d.[d]
M2a/M2b	51.2	n.d.[d]
M3a/M3b	58.0	n.d.[d]
M6a/M6b	65.9	67.5
M_L1a/M_L1b	41.8	43.1
M_L2a/M_L2b	44.9	45.5
M_L3a/M_L3b	51.4	51.2
M_L6a/M_L6b	65.0	65.8
M1a/M_L1b	46.4	n.d.[e]
M2a/M_L2b	49.2	51.3
M3a/M_L3b	56.4	56.4
M6a/M_L6b	70.4	74.9
M6Oa/nb	50.2	27.6
M6Oa	n.d	43.7
M_L6Oa/nb	49.4	27.6
M_L6Oa	n.d	41.9

[a] Sequences: **M*n*a**: 5'-GGTATC(**M**)$_n$GCAATC-3' (*n*=1-3, 6); **M*n*b**: 5'-GATTGC(**M**)$_n$GCAATC-3' (*n*=1-3, 6); **M_L*n*a**: 5'-GGTATC(**M_L**)$_n$GCAATC-3' (*n*=1-3, 6); **M_L*n*b**: 5'-GATTGC(**M**)$_n$GCAATC-3' (*n*=1-3, 6); **M*6*Oa**: 5'-(**M**)$_6$GGTATCGCAATC-3'; **M_L*6*Oa**: 5'-(**M_L**)$_6$GGTATCGCAATC-3'; **nb**: 5'-GATTGCGATACC-3'; Measurement conditions: 100 mM NaCl, 10 mM phosphate buffer (pH 7.0), 5.0 μM each oligomer. [b] Melting temperature determined from the absorbance at 260 nm. [c] Melting temperature determined from the absorbance at 450 nm. [d] Not measured. It should coincide with T_m^{260} since such results were observed with all other center series. [e] Hyperchromicity was too slight to calculate the melting temperature.

Table S2-4. Melting temperatures of **N**/**M** hetero-series.[a]

Sequence	T_m^{260} / °C [b]	T_m^{dye} / °C [c]
N1a/N1b	55.5	56.1
N2a/N2b	60.5	60.9
N3a/N3b	64.9	65.3
M6a/N6b	76.7	81.3
N_L1a/N_L1b	46.3	46.5
N_L2a/N_L2b	51.4	51.5
N_L3a/N_L3b	57.6	57.8
N_L6a/M_L6b	70.9	73.5
N_L1a/N_L1b	50.9	50.5
N_L2a/N_L2b	55.1	55.6
N_L3a/N_L3b	61.8	61.9
N6a/M_L6b	74.2	77.7
N6Oa/nb + **M6Oa/nb**	53.4	> 80
N6Oa + **M6Oa**	n.d.	> 80
N_L6Oa/nb + **M_L6Oa/nb**	51.0	> 80
N_L6Oa + **M_L6Oa**	n.d.	> 80
N6Oa/nb + **M_L6Oa/nb**	49.7	66.5
N_L6Oa + **M_L6Oa**	n.d.	59.3

[a] Sequences: Refer Tables S2-3 and S2-4. Measurement conditions: 100 mM NaCl, 10 mM phosphate buffer (pH 7.0), 5.0 μM each oligomer. [b] Melting temperature determined from the absorbance at 260 nm. [c] Melting temperature determined from the absorbance at 400 nm.

Chapter 3. Formation of a hetero-selective artificial duplex stabilized by donor-acceptor interaction

3-1 Abstract

Here we report characterization of a novel hetero-selective DNA-like duplex of pyrene and anthraquinone pseudo base pairs. The pyrene/anthraquinone pairs showed excellent selectivity in hetero-recognition and even trimers were found to form a hetero-duplex. Pyrene and anthraquinone moieties were tethered on acyclic D-threoninol linkers and linked to adjacent residues using standard phosphoramidite chemistry. When pyrene and anthraquinone were incorporated at pairing positions in complementary strands of natural DNA oligonucleotides, the duplex was significantly stabilized. Moreover, a pyrene hexamer and an anthraquinone hexamer formed a stable artificial hetero-duplex without the assistance of natural base pairs. The pyrene/anthraquinone pair was so stable that even trimers formed a hetero-duplex under conditions in which natural DNA strands of three residues do not.

3-2 Introduction

Each of the four nucleobases of natural DNA has a complementary base that enables formation of a canonical B-type duplex. Over the past several decades, chemists have attempted to prepare artificial duplexes that mimicking natural nucleic acids. A number of *de novo* designed double helices have been reported by chemists in the field of supramolecular and polymer chemistry.[1-4] Nucleic acid chemists have also prepared hetero-selective artificial base pairs by modifying natural nucleic acids. These base pairs have expanded the genetic alphabet and have utility in DNA-based nanotechnology. For example, artificial base pairs with unique hydrogen bonding patterns selectively form hetero-pairs,[5-10] and hetero-selective artificial base pairs with shape complementarity have also been reported[11-13] Artificial base pairs stabilized by hydrophobic interactions,[14,15] π-stacking interactions,[16-21] and *via* metal binding have also been described;[22-24] however, these non-natural bases pair homo-selectively.

We previously reported that azobenzene derivatives recognize each other through π-stacking interactions in the context of a natural DNA duplex, and azobenzene derivatives also show excellent orthogonality with native nucleobases.[25] We also reported that pairs of a cationic stilbazole derivative strongly stabilize an otherwise DNA duplex through π-stacking and electrostatic interactions.[26] However,

hetero-selective recognition was not achieved with these designs. Recently, Leumann *et al.*,[27] Iverson *et al.*,[28] and Häner *et al.*[29,30] have reported π-stacked hetero-selective pseudo base pairs using designs based on electrostatic complementarity. These hetero-pairs introduced into the middle or at the termini of DNA duplexes were found to stabilize the duplex than the homo-pairs. However, hetero-duplex formation of these hetero-pairs in the absence of flanking DNA pairs has not been investigated.

Herein, we report a totally artificial duplex of *de novo* designed nucleotides. The structure is completely different from that of natural nucleic acid duplexes, i.e., no hydrogen bondings, no (deoxy) ribose. The hetero-selective pairings were stabilized by donor-acceptor interactions between pyrene (**P**) and anthraquinone (**Q**). Since **P** and **Q** residues function as electron donors and acceptors, respectively, **P**/**Q** hetero-pairs in the context of a DNA duplex were more stable than homo pairs. Furthermore, these **P** and **Q** residues were stable enough to form a completely artificial hetero-duplex. To the best of our knowledge, this is the first report of a hetero-duplex stabilized by electrostatic complementarity between pseudo base pairs.

3-3 Results and discussions

3-3-1 Spectroscopic behaviors along the pyrene/anthraquinone hetero-pair formation

Pyrene and anthraquinone were tethered on D-threoninol, and the oligomers were synthesized using standard solid-phase DNA synthesis protocols (Fig. 3-1). Three types of duplexes were investigated. Firstly, we incorporated **P**/**Q** pairs into the center of DNA duplex (Scheme 3-1a). With this design, the **P** and **Q** residues form hetero-pairs oriented by flanking natural base pairs; this type of duplex allows investigation of spectroscopic behavior as previously described.[31] Oligomers were also synthesized to allow evaluation of **P**/**P** and **Q**/**Q** homo-pairs. Second, **P** or **Q** residues were introduced at the 5' end of the duplex (Scheme 3-1b). In this context, formation of the native duplex

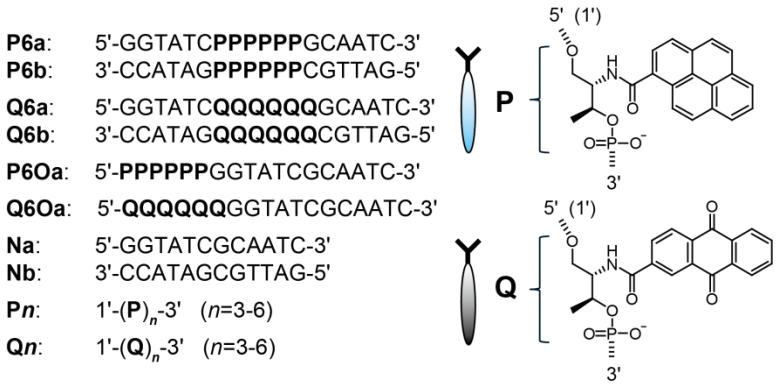

Figure 3-1. Sequences and chemical structures of oligomers synthesized in this study. formed by **P** and **Q** oligomers only were studied (Scheme 3-1c). Hetero-duplex A, G, C, and T represents 2'-deoxyribonucleotides.

Scheme 3-1. Schematic illustration of **P**/**Q** hetero-pair formation in oligomers a) **P6a**/**Q6b** b) **P6Oa**/**Nb**+**Q6Oa**/**Nb**, and c) **P6**/**Q6**.

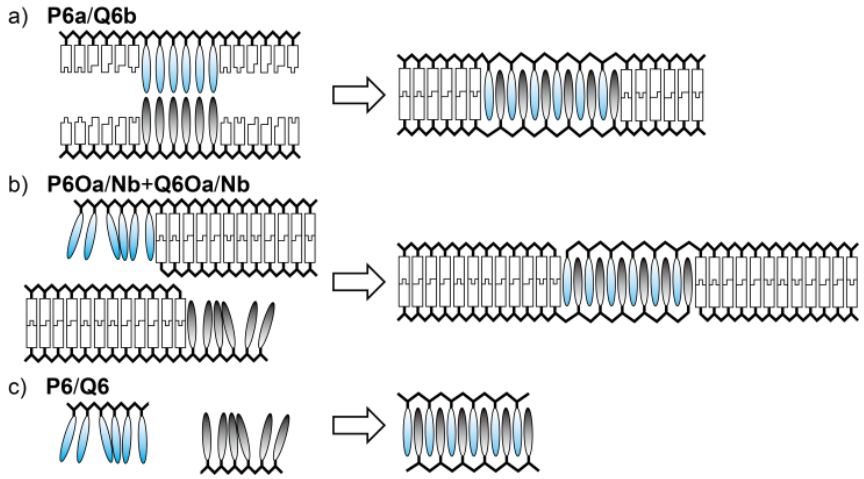

and aggregation of the dye occur independently.[32] Study of these oligomers allowed us to evaluate the selectivity of hetero-pairing over homo-pairing. Finally, duplexes formation was evaluated by comparing their spectroscopic behaviors with those of designs in Scheme 3-1a and 3-1b.

First, we investigated the spectroscopic behaviors and the thermal stabilities of **P**/**Q** pairs by analysis of the duplex formed by **P6a** and **Q6b**. The UV-vis spectra of **P6a**/**Q6b** were characterized by distinct broadening of a band at around 340 nm as temperature decreased from 90 ^{o}C to 0 ^{o}C (Fig. 3-2a). This band was not present in a simple sum of the spectra of single- stranded **P6a** and **Q6b** at 0 ^{o}C (Fig. 3-2b). These observations were characteristic to hetero-aggregate formation and it was indicated that **P** and **Q** residues formed a hetero-aggregate within the duplex scaffold.[31] An absorption

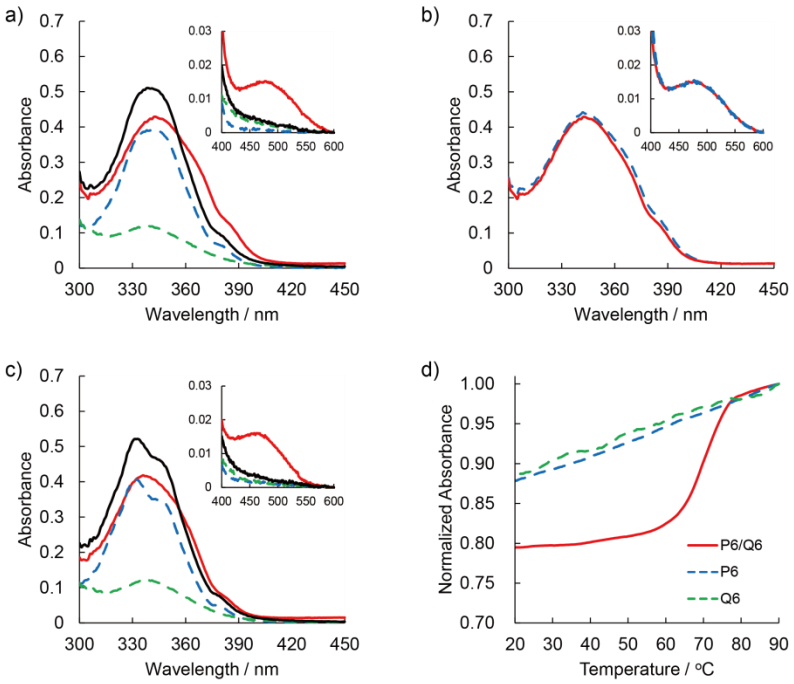

Figure 3-2. a) UV-vis spectra of **P6a**/**Q6b** (5.0 μM each strand) at indicated temperatures. b) Comparison of UV-vis spectra of **P6a**/**Q6b** (red line) with the mathematical sum (gray line) of single stranded **P6a** (blue broken line) and **Q6b** (green dotted line) at 0 ^{o}C; strand concentrations 5.0 μM. c) Fluorescence emission spectra of **P6a**/**Q6b** (green line) and **P6a** (blue broken line) at 0 ^{o}C; strand concentrations 1.0 μM each. d) Melting profiles of **P6a**/**Q6b** monitored at 260 nm (black line) and 342 nm (red broken line); strand concentrations 5.0 μM each. Conditions: 100 mM NaCl, 10 mM phosphate buffer (pH 7.0).

band at 480 nm also appeared when **P6a** and **Q6b** were hybridized (Fig. 3-2b, inset). This new band is characteristic of a charge-transfer complex, confirming that **P** and **Q** residues interact in **P6a**/**Q6b**. In the fluorescence emission spectra, strong emission around 500 nm corresponding to excimer emission of pyrene was observed with single stranded **P6a**. This emission was effectively quenched upon addition of **Q6b** (Fig. 3-2c). We hypothesize that this significant quenching is due to the physical inhibition of

pyrene excimer formation by anthraquinone residues[33], followed by electron transfer from excited pyrene to ground stated anthraquinone. The slight emission around 500 nm in **P6a**/**Q6b** was probably due to pyrene-anthraquinone exciplex formation (*vide infra*). We concluded from these results that **P**/**Q** hetero-pairing can be monitored both from appearance of a charge-transfer band in UV-vis spectrum and quenching of excimer emission in emission spectrum.[34-36]

3-3-2 Thermal stability of pyrene/anthraquinone pairs at the center position of DNA duplexes

We further investigated the recognition ability of **P** and **Q** in a DNA duplex by measuring the thermal stability of the **P6a**/**Q6b** duplex (Table 3-1). The melting temperature was determined by monitoring the absorbance at 260 nm (T_m^{260}). **P6a**/**Q6b** was significantly more stable than **Na**/**Nb**, the native duplex without **P** and **Q** residues. The T_m^{260} of **P6a**/**Q6b** was 77.1 ^oC, about 30 ^oC higher than that of **Na**/**Nb** (47.7 ^oC). The duplexes designed to contain **P**/**P** or **Q**/**Q** pairs were also more stable than the native duplex due to the π-stacking interactions (54.6 ^oC for **P6a**/**P6b** and 71.9 ^oC for **Q6a**/**Q6b**). As **P6a**/**Q6b** was more stable than either **P6a**/**P6b** or **Q6a**/**Q6b**, the **P**/**Q** hetero-pair was more stable than the homo-pairs in the context of a DNA duplex. The

Table 3-1. Melting temperatures of duplexes.[a]

Sequence	T_m^{260} [°C][b]	T_m^{dye} [°C][c]
P6a/Q6b	77.1	78.2
P6a/P6b	54.6	54.2
Q6a/Q6b	71.9	71.8
Na/Nb	47.7	n.d.[d]
P6Oa/Nb+Q6Oa/Nb	56.1	55.3
P6Oa/Nb	50.1	n.d.[e]
Q6Oa/Nb	54.7	n.d.[e]

[a] Measurement conditions: 100 mM NaCl, 10 mM phosphate buffer (pH 7.0), 5 μM each oligomer strand. [b] Melting temperature determined from the absorbance at 260 nm. [c] Melting temperatures determined from the absorbance due to **P**/**P**, 345 nm; **Q**/**Q,** 334 nm; **P**/**Q,** 342 nm; these wavelengths were those of most significant change for each series. [d] No absorption found around 340 nm. [e] No significant melting temperature observed.

melting profile of **P6a**/**Q6b** monitored at 342 nm was sigmoidal (Fig. 3-2d), and T_m^{dye}, the melting temperature obtained from analysis of this curve was almost the same as T_m^{260}. This indicates that the dye pairing and natural base pairings occurred simultaneously.

We also investigated thermal stabilities of duplexes with one to five hetero-pairs (Table S3-1-S3-3). When the number of dye pair was less than three, **P*n*a**/**Q*n*b** (n = 1, 2), the T_m was similar to that of **Q*n*a**/**Q*n*b**. We have reported that electron deficient molecules stabilize a duplex when they are intercalated.[37] Accordingly, **Q**/**Q** pairs strongly stabilized the duplex through π-stacking interactions between **Q** residues and the native nucleobases. As the numbers of **P**/**Q** pairs was increased, donor-acceptor

interactions between **P** and **Q** dominated the duplex stability, and for **P*n*a**/**Q*n*b** (*n* = 3-6) the T_m was higher than that of **Q*n*a**/**Q*n*b**.

3-3-3 Thermal stability and sequence selectivity of pyrene/anthraquinone pairs at overhang positions of DNA duplexes

Next, we investigated the hetero-recognition selectivity of **P**/**Q** pair using **P6Oa**/**Nb** and **Q6Oa**/**Nb** in which the **P** and **Q** residues are located at the 5' ends of the oligomers (Scheme 3-1b). If **P**/**Q** hetero-pairs are formed, the spectroscopic behavior of **P6Oa**/**Nb**+**Q6Oa**/**Nb** should be similar to that of **P6a**/**Q6b**. UV-vis spectrum of **P6Oa**/**Nb**+**Q6Oa**/**Nb** showed a charge-transfer band at 480 nm (Fig. S3-2a), indicating charge-transfer complexation between **P** and **Q** residues. The spectrum of **P6Oa**/**Nb**+**Q6Oa**/**Nb** was much different from summed spectra of **P6Oa**/**Nb** and **Q6Oa**/**Nb** (compare black and gray lines in Fig. 3-3a) and very similar to that of **P6a**/**Q6b** (Fig. 3-3b). In addition, efficient quenching of pyrene excimer emission was observed in fluorescence spectra of **P6Oa**/**Nb**+**Q6Oa**/**Nb** (Fig. S3-2b). From these results, we concluded that **P** and **Q** residues selectively formed **P**/**Q** hetero-pairs but not homo-pairs. Thus, **P** and **Q** residues selectively paired without the assistance of a DNA scaffold. Even three **P**/**Q** pairs were sufficient to form this type of duplex (Table S3-4).

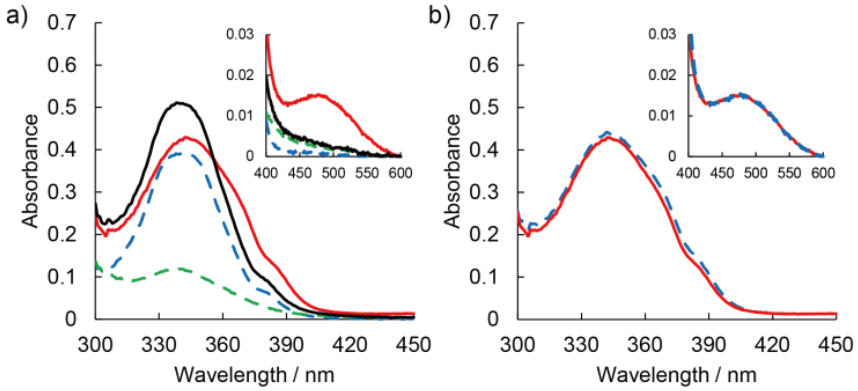

Figure 3-3. a) Comparison of UV-vis spectra of **P6Oa**/**Nb**+**Q6Oa**/**Nb** (red line) with the mathematical sum (black line) of **P6Oa**/**Nb** (blue broken line) and **Q6Oa**/**Nb** (green broken line) at 0 ^{o}C. b) Comparison of UV-vis spectra of **P6Oa**/**Nb**+**Q6Oa**/**Nb** (red line) with the spectrum of **P6a**/**Q6b** (blue broken line) at 0 ^{o}C. Conditions: 100 mM NaCl, 10 mM phosphate buffer (pH 7.0), 5.0 μM each strand.

Interestingly, T_m^{dye} of **P6Oa**/**Nb**+**Q6Oa**/**Nb** coincided with T_m^{260}, indicating that duplex formation and **P**/**Q** hetero-pair formation were synchronized. Therefore, hetero-pair formation was likely facilitated by DNA duplex formation probably due to π-stacking interactions.[32] Single-stranded **P6Oa** and **Q6Oa** also formed a duplex (Fig. S3-3 and Table S3-5), suggesting that the **P**/**Q** pair is stable enough to form a cluster without the assistance of natural base pairs.

3-3-4 Totally artificial duplex formation composed of pseudo base pairs

We then investigated artificial duplex formation by **P** and **Q** oligomers (Scheme 3-1c). The UV-vis spectrum of **P6**/**Q6** differed from the summed spectra of single-stranded **P6**

and **Q6** (Figs. 3-4a, S3-4). A charge-transfer absorption band at 460 nm was observed for **P6**/**Q6**. The slight hypsochromic shift compared with **P6a**/**Q6b** is probably due to the absence of excitonic interactions with nucleobases (Fig. S3-5), which may also cause hypsochromic shift in the fluorescence emission (Figs. 3-2c, 3-5a).[38, 39] These results clearly indicate formation of hetero-pairs between **P** and **Q** residues. Furthermore, **P6**/**Q6** showed a sigmoidal melting profile and had a high melting temperature (T_m^{dye}: 69.7 °C); **P6** or **Q6** alone did not have sigmoidal melting curves (Fig. 3-4b). From these results, we concluded that **P6** and **Q6** formed a complex stabilized by hetero-pairing of **P** and **Q**.

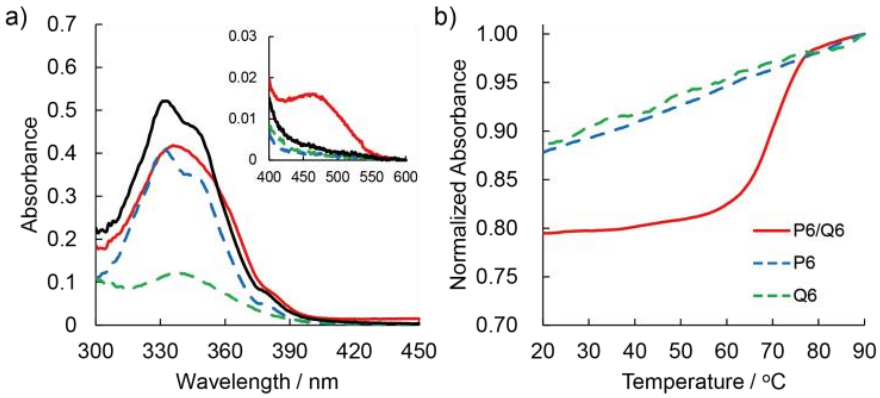

Figure 3-4. a) Comparison of UV-vis spectrum of **P6**/**Q6** (red line) with the mathematical sum (black line) of spectra of the single-stranded **P6** (blue broken line) and **Q6** (green broken line) at 0 °C. b) Melting profiles of **P6**/**Q6** (red line), **P6** (blue broken line), and **Q6** (green broken line) monitored at 342, 345, and 334 nm respectively. Conditions: 100 mM NaCl, 10 mM phosphate buffer (pH 7.0), 5.0 μM each strand.

Next, we performed titration experiment to determine the stoichiometry of **P6**:**Q6** binding; this analysis was based on the quenching of **P6** excimer emission by **Q6** (Fig. 3-5a).[40] As the concentration of **Q6** was increased, fluorescence intensity decreased, reaching a plateau after the ratio of equivalents of **Q6** to **P6** exceeded 1 (Fig. 3-5b).[41] This result suggests that **P6** and **Q6** formed a 1:1 complex, that is, a duplex.[42] Hence, a hetero-duplex containing no natural base pairs and no ribose scaffold was successfully prepared; this duplex is stabilized by electrostatic complementarity between pyrene and anthraquinone.

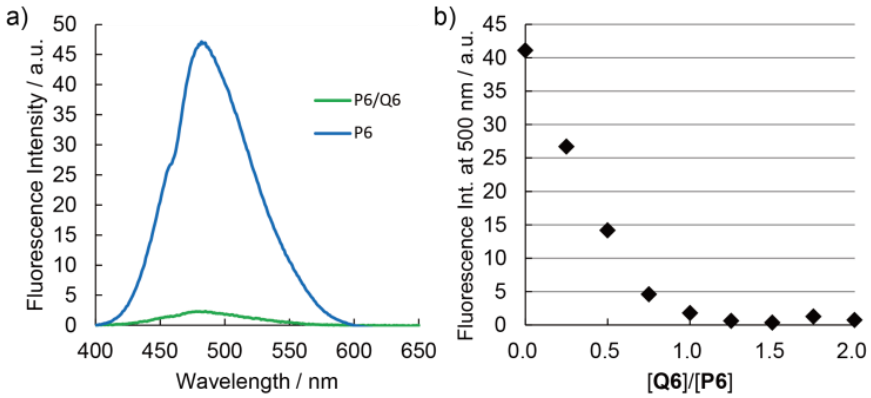

Figure 3-5. a) Fluorescence emission spectra of **P6**/**Q6** (green line) and **P6** (blue line) at 0 ^{o}C. Conditions: 100 mM NaCl, 10 mM phosphate buffer (pH 7.0), 1.0 μM each strand. b) Titration of 1.0 μM **P6** with **Q6** over the range from 0 to 2.0 μM, excited at 350 nm in 100 mM NaCl, 10 mM phosphate buffer (pH 7.0).

3-3-5 Lifetime measurements of pyrene, anthraquinone pseudo bases

Curiously, the excimer emission of **P6** was not completely quenched in the presence of one equivalent of **Q6** (Fig. 3-5a), and this slight emission was also observed in **P6a**/**Q6b** and **P6Oa**/**Nb**+**Q6Oa**/**Nb** (Figs. 3-2c and S3-2b). We measured the fluorescent lifetimes of these samples in order to investigate whether this emission wascaused by single-stranded **P6** (resulting from incomplete duplex formation) or from the **P**/**Q** complex. Table 3-2 shows the results of lifetime measurements obtained using a streak camera. In the three samples lacking anthraquinones, **P6a**, **P6Oa**/**Nb**, and **P6**, two lifetime components of about 15 ns and 35 ns were observed. On the basis of previous reports, these two lifetime components were assigned to partially stacked

Table 3-2. Lifetimes of fluorescent species.[a]

Sequence	τ_1 [ns]	τ_2 [ns]	α_1	α_2	χ^2
P6a	15	35	0.37	0.63	1.1
P6a/Q6b	0.76	4.4	0.46	0.54	1.2
P6Oa/Nb	13	33	0.36	0.64	1.1
P6Oa/Nb+Q6Oa/Nb	0.47	5.1	0.39	0.61	1.3
P6	16	38	0.44	0.56	1.2
P6/Q6	0.47	3.8	0.38	0.62	1.1

[a] Measurement conditions: 100 mM NaCl, 10 mM phosphate buffer (pH 7.0); **P6a**: 100 μM **P6a**; **P6a**/**Q6b**: 132.5 μM **P6a**, 267.5 μM **Q6b**; **P6Oa**/**Nb**: 100 μM **P6Oa**/**Nb**; **P6Oa**/**Nb**+**Q6Oa**/**Nb**: 132.5 μM **P6Oa**/**Nb**, 267.5 μM **Q6Oa**/**Nb**; **P6**: 50 μM **P6**; **P6**/**Q6**: 132.5 μM **P6**, 267.5 μM **Q6**, excited at 390 nm. Decay curves obtained from the integration of the region from 475 to 525 nm of streak images were fit to a bi-exponential curve of $\alpha_1\exp(-t/\tau_1)+\alpha_2\exp(-t/\tau_2)$, where τ is lifetime and α is pre-exponential factor of lifetime component.

excimer (15 ns) and fully stacked excimer (35 ns).[43,44] The samples containing anthraquinones showed completely different profiles. In all three samples involving anthraquinones, **P6a**/**Q6b**, **P6Oa**/**Nb**+**Q6Oa**/**Nb**, **P6**/**Q6**, sub-nanosecond- to nanosecond-order two-lifetime components (0.5-0.8 ns and 3-5 ns) were observed. The absence of long lifetime components (15 and 35 ns) clearly demonstrated that the pyrene excimer was not present in the **P**/**Q** hetero series duplexes. Furthermore, steady-state fluorescence measurements revealed that the emission wavelength of the **P**/**Q** hetero-complex slightly differed from those of the pyrene excimer series (Fig. S3-6). Thus, the weak emission observed in **P**/**Q** hetero series samples was likely due to exciplex-like emission from the pyrene-anthraquinone hetero-pairs, since no fluorescence was observed by excitating at CT absorption which indicates that the excited CT state is non-fluorescent.[45]

3-3-6 Thermal stability of totally artificial duplexes along the length of the sequences

Finally, we investigated the effects of oligomer length on the stability of the **P**/**Q** artificial duplex. Fig. 3-6 shows the melting curves and T_ms of **P*n***/**Q*n*** (*n*=3-6) determined from the change of absorbance at 342 nm. **P6**/**Q6** had the highest melting

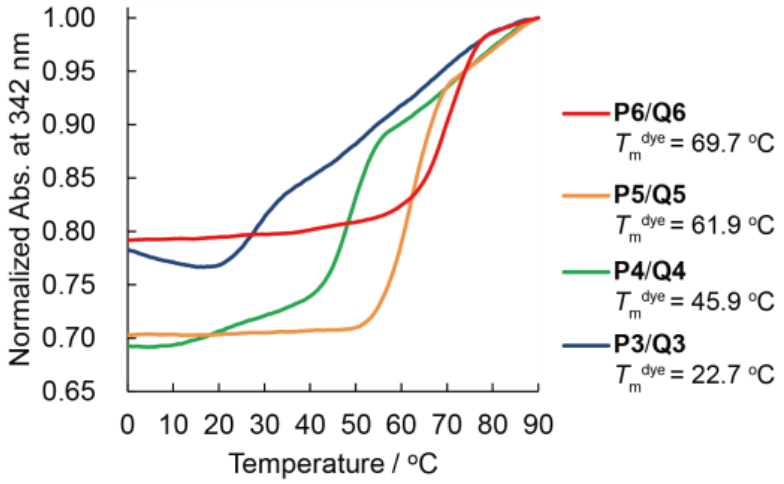

Figure 3-6. Melting profiles of **P6**/**Q6**, **P5**/**Q5**, **P4**/**Q4**, and **P3**/**Q3** monitored at 342 nm. Conditions: 100 mM NaCl, 10 mM phosphate buffer (pH 7.0), 5.0 μM each strand.

temperature (T_m^{dye} 69.7 °C). This melting temperature was considerably higher than that of the native DNA duplex with six G/C pairs (T_m^{260} 39 °C)[46] and only 10 °C lower than that of **P6a**/**Q6b** containing the hetero-pairs and 12 natural base pairs. T_m^{dye}s were61.9 °C and 45.9 °C for **P5**/**Q5** and **P4**/**Q4**, respectively. To our surprise, the **P3**/**Q3** duplex had a T_m^{dye} of 22.7 °C. Spectral shift and appearance of CT band in UV-vis spectra also indicated a hetero-complexation unambiguously (Fig.S3-7). Native DNAs do not form duplexes with fewer than 4 base pairs under the conditions employed in this study. No duplex formation was observed with **P*n*** or **Q*n*** (*n*=3-6) alone. Additionally, the T_m^{dye} of **P3**/**Q3** was strongly dependent on concentration (Fig. S3-8), indicative of inter-molecular complexation between **P3** and **Q3**. **P6**/**Q6** showed much different CD signals from **P6a**/**Q6b** (Fig. S3-9), indicating that the stacked structure of **P**/**Q** pairs in

P6/**Q6** differs from that in **P6a**/**Q6b**. These results suggest that the conformation of the **P** and **Q** residues in **P6**/**Q6** optimized donor-acceptor interactions, whereas the conformation of the hetero-pairs in **P6a**/**Q6b** differs from this optimum due to the surrounding natural nucleobases.

3-4 Conclusions

In conclusion, we successfully designed and prepared novel artificial hetero-duplexes using pyrene/anthraquinone pseudo base pairs. Pyrene/anthraquinone pairs significantly stabilized the native DNA duplex, and the appearance of an absorption band at 480 nm upon duplex formation clearly indicated that pyrene and anthraquinone formed a charge-transfer complex. The pyrene/anthraquinone pairs showed excellent selectivity in hetero-recognition when linked to the 5' ends of natural DNA. Furthermore, even trimers of pyrene and anthraquinone formed a stable hetero-duplex. Exceptionally-stable pseudo base-pair allowed a new hetero-duplex formation in aqueous conditions; pyrene/anthraquinone pair includes no ribose scaffold, no hydrogen bondings based on natural base-pairs, but stably forms duplex. The pyrene/anthraquinone hetero-pairs will be useful in the field of supramolecular chemistry and in nano-architectures and fluorescent probes.

3-5 Experimental section

Materials

All conventional phosphoramidite monomers, CPG columns, and reagents for DNA synthesis were purchased from Glen Research. Other reagents for the syntheses of phosphoramidite monomers were purchased from Tokyo Chemical Industry, Wako, and Aldrich. Unmodified oligonucleotides were purchased from Integrated DNA Technologies.

Synthesis of oligomers

All the modified oligomers were synthesized on an automated DNA synthesizer (H-8-SE, Gene World) using phosphoramidite monomers bearing **P** or **Q**. The oligomers **P*n*** and **Q*n*** (*n*=3-6) were synthesized using **P**- or **Q**-modified CPGs. **P**- or **Q**-modified CPGs were synthesized as described previously.[32] Phosphoramidite monomer bearing **P** or **Q** were synthesized as described in the Appendix Information. After workup, oligomers were purified by reversed-phase HPLC. The purification was confirmed by HPLC and matrix-assisted laser desorption ionization time-of-flight mass spectrometer (MALDI-TOF; Autoflex II, Bruker Daltonics). MALDI-TOF MS data for the synthesized oligomers: **P6a**, obsd 6017 (calcd for [**P6a** + H^+], 6015); **P6b**, obsd 6017 (calcd for [**P6b** + H^+], 6015); **Q6a**, obsd 6057 (calcd for [**Q6a** + H^+], 6051); **Q6b**, obsd 6057 (calcd for [**Q6b** + H^+], 6051); **P6Oa**, obsd 6016 (calcd for [**P6Oa** + H^+], 6015); **Q6Oa**, obsd 6054 (calcd for [**Q6Oa** + H^+], 6051); **P3**, obsd 1124 (calcd for [**P3** + H^+], 1124); **P4**, obsd 1519 (calcd for [**P4** + H^+], 1519);**P5**, obsd 1915 (calcd for [**P5** + H^+], 1915); **P6**, obsd 2310 (calcd for [**P6** + H^+], 2310); **Q3**, obsd 1144 (calcd for [**Q3** + H^+], 1142); **Q4**, obsd 1546 (calcd for [**Q4** + H^+], 1543); **Q5**, obsd 1948 (calcd for [**Q5** + H^+], 1944); **Q6**, obsd 2350 (calcd for [**Q6** + H^+], 2345); **P1a**, obsd 4041 (calcd for [**P1a** + H^+], 4040); **P1b**, obsd 4041 (calcd for [**P1b** + H^+], 4040); **P2a**, obsd 4437 (calcd for [**P2a** + H^+], 4435); **P2b**, obsd 4437 (calcd for [**P2b** + H^+], 4435); **P3a**, obsd 4830 (calcd for [**P3a** + H^+], 4830); **P3b**, obsd 4829 (calcd for [**P3b** + H^+], 4830); **P4a**,

obsd 5225 (calcd for [**P4a** + H^+], 5225); **P4b**, obsd 5224 (calcd for [**P4b** + H^+], 5225); **P5a**, obsd 5621 (calcd for [**P5a** + H^+], 5620); **P5b**, obsd 5622 (calcd for [**P5b** + H^+], 5620); **Q1a**, obsd 4046 (calcd for [**Q1a** + H^+], 4046); **Q1b**, obsd 4047 (calcd for [**Q1b** + H^+], 4046); **Q2a**, obsd 4450 (calcd for [**Q2a** + H^+], 4447); **Q2b**, obsd 4448 (calcd for [**Q2b** + H^+], 4447); **Q3a**, obsd 4850 (calcd for [**Q3a** + H^+], 4848); **Q3b**, obsd 4848 (calcd for [**Q3b** + H^+], 4848); **Q4a**, obsd 5252(calcd for [**Q4a** + H^+], 5249); **Q4b**, obsd 5252 (calcd for [**Q4b** + H^+], 5249); **Q5a**, obsd 5655 (calcd for [**Q5a** + H^+], 5650); **Q5b**, obsd 5655 (calcd for [**Q5b** + H^+], 5650); **P3Oa**, obsd 4833 (calcd for [**P3Oa** + H^+], 4830); **P4Oa**, obsd 5225 (calcd for [**P4Oa** + H^+], 5225); **P5Oa**, obsd 5621(calcd for [**P5Oa** + H^+], 5620); **Q3Oa**, obsd 4850 (calcd for [**Q3Oa** + H^+], 4848); **Q4Oa**, obsd 5252 (calcd for [**Q4Oa** + H^+], 5249); **Q5Oa**, obsd 5654 (calcd for [**Q5Oa** + H^+], 5650). The extinction coefficients for **P** and **Q** residues: **P**; $\varepsilon_{260}=7.9\times10^2$ m^2/mol, $\varepsilon_{342}=1.6\times10^3$ m^2/mol, **Q**; $\varepsilon_{260}=2.3\times10^3$ m^2/mol, $\varepsilon_{340}=4.4\times10^2$ m^2/mol. On the determination of concentrations, absorbance at 260 nm was used for **P**- or **Q**- DNA conjugates, and absorbance at 342 nm or 340 nm were used for **P*n*** and **Q*n*** (*n*=3-6) respectively.

Spectroscopic Measurements

UV-vis spectra were measured on a Shimadzu UV-1800 equipped with programmed temperature-controllers using 10-mm quartz cells. CD spectra were measured on a JASCO model J-820 equipped with programmed temperature-controllers using 10-mm quartz cells. Fluorescence spectra were measured on a JASCO model FP-6500 equipped with a microcell holder.

Melting Temperature Measurements

The melting curves were obtained with a Shimadzu UV-1800 by measuring the change in absorbance at 260, 334, 342, or 345 nm versus temperature. Both the heating and the cooling curves were measured, and the melting temperatures (T_m) were determined from the maximum in the first derivative of the melting curves. The shown T_ms were obtained

from the average between the heating and the cooling, and only the heating curves are shown. The temperature ramp was 0.2 °C min^{-1}.

Time-Resolved Fluorescence Measurements

A pulse at 780 nm was generated by a Ti:sapphire laser system (Spectra-Physics, Tsunami 3950-L2S, fwhm 150 fs, 82 MHz). The repetition rate was reduced to 4 MHz by a pulse selector (Spectra-Physics Model 3980). The exciting source was a laser with wavelength converted to 390 nm by passage through SHG crystals. Fluorescence emission was captured by a streak camera (Hamamatsu C4334) operating in photon counting mode. Measurements were performed at room temperature.

Curve Fitting

Decay curves were obtained from the integration of the photon counts in the spectral region from 375 to 425 nm in the streak image. The fluorescence decay curve was analyzed by using the U8167-01 program (Hamamatsu). The decay curves were fitted with the bi-exponential function $\alpha_1 \exp(-t/\tau_1) + \alpha_2 \exp(-t/\tau_2)$.

3-6 References

(1) Yashima, E.; Maeda, K.; Iida, H.; Furusho, Y.; Nagai, K. *Chem. Rev.* **2009**, *109*, 6102.

(2) Piguet, C.; Bernardinelli, G.; Hopfgartner, G. *Chem. Rev.* **1997**, *97*, 2005.

(3) Haldar, D.; Schmuck, C. *Chem. Soc. Rev.* **2009**, *38*, 363.

(4) Gabriel, G. J.; Iverson, B. L. *J. Am. Chem. Soc.* **2002**, *124*, 15174.

(5) Kool, E. T.; Morales, J. C.; Guckian, K. M. *Angew. Chem. Int. Ed.* **2000**, *39*, 990.

(6) Switzer, C.; Moroney, S. E.; Benner, S. A. *J. Am. Chem. Soc.* **1989**, *111*, 8322.

(7) Piccirilli, J. A.; Benner, S. A.; Krauch, T.; Moroney, S. E. *Nature* **1990**, *343*, 33.

(8) Minakawa, N.; Kojima, N.; Hikishima, S.; Sasaki, T.; Kiyosue, A.; Atsumi, N.; Ueno, Y.; Matsuda, A. *J. Am. Chem. Soc.* **2003**, *125*, 9970.

(9) Liu, H.; Gao, J.; Lynch, S. R.; Saito, Y. D.; Maynard, L.; Kool, E. T. *Science* **2003**, *302*, 868.

(10) Gao, J.; Liu, H.; Kool, E. T. *Angew. Chem. Int. Ed.* **2005**, *44*, 3118.

(11) Schweitzer, B. A.; Kool, E. T. *J. Am. Chem. Soc.* **1995**, *117*, 1863.

(12) Kimoto, M.; Kawai, R.; Mitsui, T.; Yokoyama, S.; Hirao, I. *Nucleic Acids Res.* **2009**, *37*, e14.

(13) Malyshev, D. A.; Seo, Y. J.; Ordoukhanian, P.; Romesberg, F. E. *J. Am. Chem. Soc.* **2009**, *131*, 14620.

(14) Kaufmann, M.; Gisler, M.; Leumann, C. J. *Angew. Chem. Int. Ed.* **2009**, *48*, 3810.

(15) Kashida, H.; Sekiguchi, K.; Higashiyama, N.; Kato, T.; Asanuma, H. *Org. Biomol. Chem.* **2011**, *9*, 8313.

(16) Schmucker, W.; Wagenknecht, H.-A. *Synlett* **2012**, *23*, 2435.

(17) Varghese, R.; Wagenknecht, H.-A. *Chem. Commun.* **2009**, 2615.

(18) Hainke, S.; Seitz, O. *Angew. Chem. Int. Ed.* **2009**, *48*, 8250.

(19) Brotschi, C.; Leumann, C. J. *Angew. Chem. Int. Ed.* **2003**, *42*, 1655.

(20) Guckian, K. M.; Schweitzer, B. A.; Ren, R. X. F.; Sheils, C. J.; Tahmassebi, D. C.; Kool, E. T. *J. Am. Chem. Soc.* **2000**, *122*, 2213.

(21) Häner, R.; Garo, F.; Wenger, D.; Malinovskii, V. L. *J. Am. Chem. Soc.* **2010**, *132*, 7466.

(22) Tanaka, K.; Tengeiji, A.; Kato, T.; Toyama, N.; Shiro, M.; Shionoya, M. *J. Am. Chem. Soc.* **2002**, *124*, 12494.

(23) Tanaka, K.; Tengeiji, A.; Kato, T.; Toyama, N.; Shionoya, M. *Science* **2003**, *299*, 1212.

(24) Clever, G. H.; Kaul, C.; Carell, T. *Angew. Chem. Int. Ed.* **2007**, *46*, 6226.

(25) Kashida, H.; Fujii, T.; Asanuma, H. *Org. Biomol. Chem.* **2008**, *6*, 2892.

(26) Kashida, H.; Ito, H.; Fujii, T.; Hayashi, T.; Asanuma, H. *J. Am. Chem. Soc.* **2009**, *131*, 9928.

(27) Grigorenko, N. A.; Leumann, C. J. *Chem. Eur. J.* **2009**, *15*, 639.

(28) Ikkanda, B. A.; Samuel, S. A.; Iverson, B. L. *J. Org. Chem.* **2014**, *79*, 2029.

(29) Häner, R.; Biner, S. M.; Langenegger, S. M.; Meng, T.; Malinovskii, V. L. *Angew. Chem. Int. Ed.* **2010**, *49*, 1227.

(30) Winiger, C. B.; Langenegger, S. M.; Khorev, O.; Häner, R. *Beilstein J. Org. Chem.* **2014**, *10*, 1589.

(31) Fujii, T.; Kashida, H.; Asanuma, H. *Chem. Eur. J.* **2009**, *15*, 10092.

(32) Kashida, H.; Hayashi, T.; Fujii, T.; Asanuma, H. *Chem. Eur. J.* **2011**, *17*, 2614.

(33) Weak monomer like emission was observed with **P6a**/**Q6b** (Fig. S3-1). This monomeric emission may have resulted from physical inhibition by anthraquinone residues to form a pyrene excimer, which is anticipated with fully alternative sequence.

(34) Fischbach, M.; Resch-Genger, U.; Seitz, O. *Angew. Chem. Int. Ed.* **2014**, *53*, 11955.

(35) Bouquin, N.; Malinovskii, V. L.; Häner, R. *Eur. J. Org. Chem.* **2008**, *2008*, 2213.

(36) May, J. P.; Brown, L. J.; Rudloff, I.; Brown, T. *Chem. Commun.* **2003**, 970.

(37) Doi, T.; Kashida, H.; Asanuma, H. *Org. Biomol. Chem.* **2015**, *13*, 4430.

(38) Bathochromic shift is often observed when the dyes are introduced at neighboring position to nucleobases.

(39) Asanuma, H.; Fujii, T.; Kato, T.; Kashida, H. *J. Photochem. Photobiol., C* **2012**, *13*, 124.

(40) Photobleaching was observed with single-stranded **P*n*** (*n*=3-6) upon repetitive photoexcitation by fluorophotometer. We used freshly prepared sample for each measurement. No difference was observed between the first and the second time measurement, but only the first value is reported. Note that, no significant photobleaching was observed with **P6a**, **P6Oa**/**Nb**, or **P6Oa**.

(41) Slight discrepancy was observed from perfect 1:1 complexation. However, other possible stoichiometry (such as 0.82:1) than 1:1 seems rather unlikely. We think that the slight discrepancy might be due to an experimental error of the molar coefficients of **P6** and **Q6**. Especially for the coefficient of **Q6**, it might include error due to so small absorbance at the maximum (340 nm) compared with that of **P6**.

(42) Though several structures are possible for **P6**/**Q6** complexation, 1:1 duplex with alternatively stacked **P** and **Q** residues are most likely to be formed. Because the duplex is entropically most favorable than other high ordered 1:1 complexes, and the fully alternative structure has the most number of interactions between the donor and the acceptor residues.

(43) Lewis, F. D.; Zhang, Y.; Letsinger, R. L. *J. Am. Chem. Soc.* **1997**, *119*, 5451.

(44) Nakamura, M.; Fukuda, M.; Takada, T.; Yamana, K. *Org. Biomol. Chem.* **2012**, *10*, 9620.

(45) We assign the longer component as exciplex emission of pyrene and anthraquinone and the shorter lifetime as exciplex emission quenched by electron transfer to/from the exciplex. However, structural distribution may have also caused several lifetime components.

(46) The T_m value of 6-mer DNA duplex (5'-GCGGCG-3'/3'-CGCCGC-5') was calculated using OligoAnalyzer 3.1 from Integrated DNA Technologies, Inc.

3-7 Appendixes

Synthesis of pyrene phosphoramidite monomer

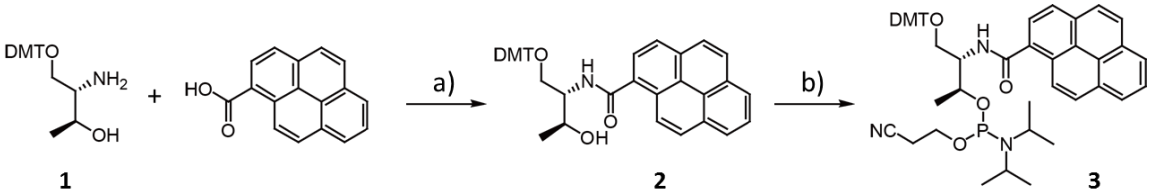

Scheme S3-1. Synthesis of phosphoramidite monomer tethering pyrene. Reagents and conditions: a) EDC, HOBt, NEt_3, DMF, r.t., overnight, 78.5 %; b) $(i\text{Pr})_2\text{NP(Cl)(OCH}_2\text{CH}_2\text{CN})$, NEt_3, THF, 0 ^{o}C, 20 min, 58.6 %.

Compound **1** was synthesized according to the previous report.[1] The phosphoramidite monomer tethering pyrene was synthesized as follows:

Synthesis of Compound 2: To a stirred solution of **1** (4.83 mmol, 1.97 g), triethylamine (16.9 mmol, 2.36 mL), 1-hydroxybenzotriazole (8.56 mmol, 1.31 g), and 1-pyrenecarboxylic acid (4.83 mmol, 1.19 g) in DMF was added 1-ethyl-3-(3-dimethylaminopropyl)carbodiimide hydrochloride (9.66 mmol, 1.85 g) and the mixture was stirred overnight. The solvent was removed *in vacuo*. Then $CHCl_3$ was added, and the organic layer was washed with saturated aqueous solution of $NaHCO_3$ and NaCl. After drying over $MgSO_4$, the solvent was removed by evaporation, followed by silica gel column chromatography using hexane and chloroform as eluent (3% triethylamine was added). Yield: 78.5%.

^{1}H-NMR [DMSO-d_6, 500 MHz] δ = 8.61 (d, J = 9.0 Hz, 1H), 8.50 (d, J = 9.0 Hz, 1H), 8.40 (m, 4H), 8.29 (m, 2H), 8.22 (m, 2H), 8.16 (t, J = 9.0 Hz, 1H), 7.53 (d, J = 8.5 Hz, 2H), 7.37 (m, 6H), 7.26 (m, 1H), 6.91 (m, 4H), 4.67 (d, J = 6.0 Hz, 1H), 4.41 (m, 1H), 4.05 (m, 1H), 3.76 (s, 6H), 3.51 (m, 1H), 3.15 (m, 1H), 1.16 (d, J = 8.0 Hz, 3H), ^{13}C-NMR [DMSO-d_6, 125 MHz] δ = 130.2, 128.7, 128.4, 128.3, 127.7, 127.1, 127.0, 126.2, 125.8, 125.4, 124.9, 113.6, 113.6, 79.7, 66.2, 63.8, 55.8, 55.5, 20.8.

Synthesis of Compound 3: *N*,*N*-diisopropylethylamine (5.0 mmol, 0.85 mL) and 2-cyanoethyl *N*,*N*-diisopropylchlorophosphoramidite (2.0 mmol, 0.46 mL) were added to a solution of compound **2** (1.0 mmol, 0.635g) in dry CH_2Cl_2 at 0 ^oC. After 20 min of vigorous stirring on ice, an excess of ethyl acetate was added to the reaction mixture, and the mixture was washed with saturated aqueous solution of $NaHCO_3$ and with NaCl. After drying over $MgSO_4$, the solvent was removed by evaporation, followed by silica gel column chromatography using hexane and ethyl acetate as eluent (3% triethylamine was added). Yield: 58.6%.^{31}P-NMR [DMSO-d_6, 121 MHz] δ =147.7, 147.6.

Synthesis of anthraquinone phosphoramidite monomer

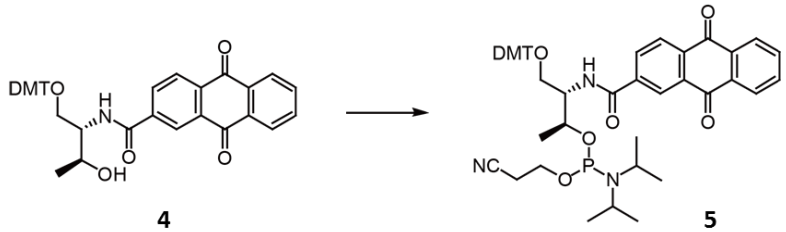

Scheme S3-2. Synthesis of phosphoramidite monomer tethering anthraquinone. Reagents and conditions: (iPr)$_2$NP(Cl)(OCH$_2$CH$_2$CN), NEt$_3$, CH_2Cl_2, 0 ^oC, 20 min, 69.5 %.

Compound **4** was synthesized according to the previous report.[2] The phosphoramidite monomer tethering anthraquinone was synthesized as follows:

Synthesis of Compound 5: *N*,*N*-diisopropylethylamine (7.5 mmol, 1.2 mL) and 2-cyanoethyl *N*,*N*-diisopropylchlorophosphoramidite (3.0 mmol, 0.67 mL) were added to a solution of compound **4** (1.5 mmol, 0.963g) in dry CH_2Cl_2 at 0 ^oC. After 20 min of vigorous stirring on ice, an excess of ethyl acetate was added to the reaction mixture, and the mixture was washed with saturated aqueous solution of $NaHCO_3$ and with NaCl. After drying over $MgSO_4$, the solvent was removed by evaporation, followed by silica gel column chromatography using hexane and ethyl acetate as eluent (3% triethylamine was added). Yield: 69.5%.^{31}P-NMR [DMSO-d_6, 121 MHz] δ =148.0, 147.9.

References

1. Y. Hara *et al. Angew. Chem. Int. Ed.* **2010**, *49*, 5502.

2. H. Asanuma *et al. Chem. Commun.* **2006**, 5062-5064.

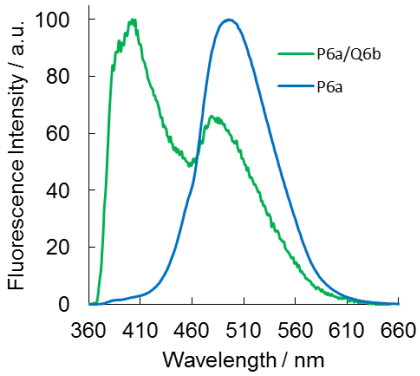

Fig. S3-1. Normalized fluorescence emission spectra of **P6a**/**Q6b** (green line) and **P6a** (blue line) for 360-660 nm region. Emission in **P6a**/**Q6b** around 400 nm and 470 nm could be assigned to the emission from monomeric pyrene and pyrene/anthraquinone exciplex respectively. Conditions: 100 mM NaCl, 10 mM phosphate buffer (pH 7.0), 1.0 μM oligomer at 0 °C.

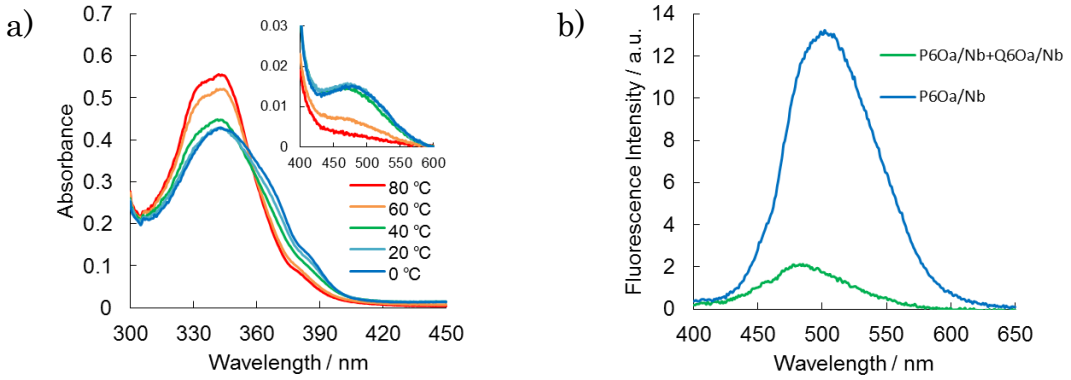

Fig. S3-2. a) UV-vis spectra of **P6Oa**/**Nb**+**Q6Oa**/**Nb** at indicated temperatures in 100 mM NaCl, 10 mM phosphate buffer (pH 7.0), 5.0 μM oligomer. b) Fluorescence emission spectra of **P6Oa**/**Nb**+**Q6Oa**/**Nb** (green line) and **P6Oa**/**Nb** (blue line) in 100 mM NaCl, 10 mM phosphate buffer (pH 7.0), 1.0 μM oligomer at 0 °C.

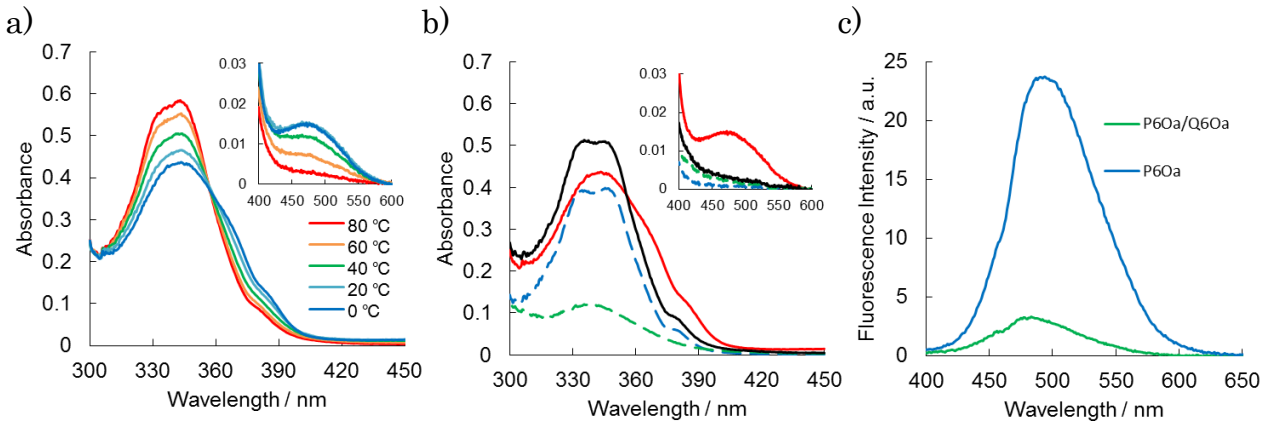

Fig. S3-3. a) UV-vis spectra of **P6Oa**/**Q6Oa** at indicated temperatures. b) Comparison of UV-vis spectrum of **P6Oa**/**Q6Oa** (red line) with the mathematical sum (black line) of the spectra of **P6Oa** (blue broken line) and **Q6Oa** (green broken line) in 100 mM NaCl, 10 mM phosphate buffer (pH 7.0), 5.0 μM oligomer at 0 ^{o}C. c) Fluorescence emission spectra of **P6Oa**/**Q6Oa** (green line) and **P6Oa** (blue line) in 100 mM NaCl, 10 mM phosphate buffer (pH 7.0), 5.0 μM oligomer at 0 ^{o}C. Conditions: 100 mM NaCl, 10 mM phosphate buffer (pH 7.0), 1.0 μM oligomer.

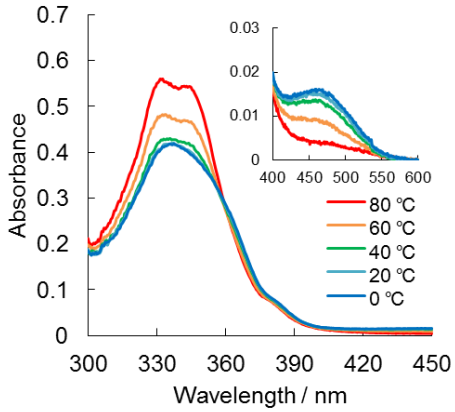

Fig. S3-4. UV-vis spectra of **P6**/**Q6** at indicated temperatures. Conditions: 100 mM NaCl, 10 mM phosphate buffer (pH 7.0), 5.0 μM oligomer.

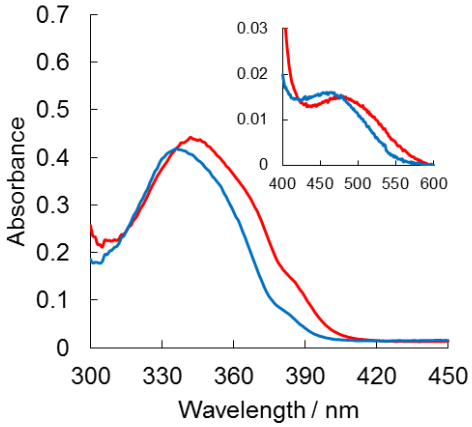

Fig. S3-5. UV-vis spectra of **P6a**/**Q6b** (red line) and **P6**+**Q6** (blue line) at 0 ^{o}C. Conditions: 100 mM NaCl, 10 mM phosphate buffer (pH 7.0), 5.0 μM oligomer.

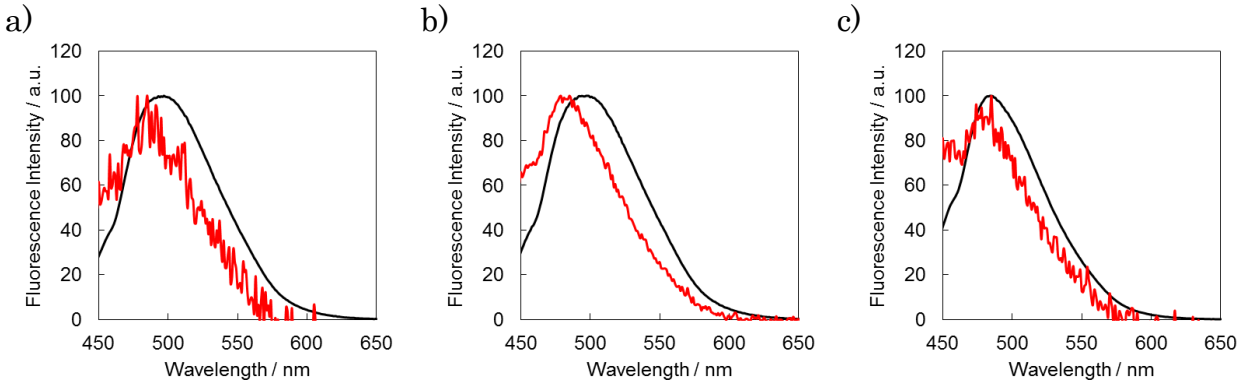

Fig. S3-6. Normalized fluorescence emission spectra of a) **P6a**/**Q6b** (red line) and **P6a** (black line), b) **P6Oa**/**Nb**+**Q6Oa**/**Nb** (red line) and **P6Oa**/**Nb** (black line), c) **P6**+**Q6** (red line) and **P6** (black line). Conditions: 100 mM NaCl, 10 mM phosphate buffer (pH 7.0) at 0 ^{o}C. Oligomer concentrations were **P6a**, **P6Oa**/**Nb**, and **P6** 1.0 μM and **Q6b**, **Q6Oa**/**Nb**, and **Q6** 2.0 μM.

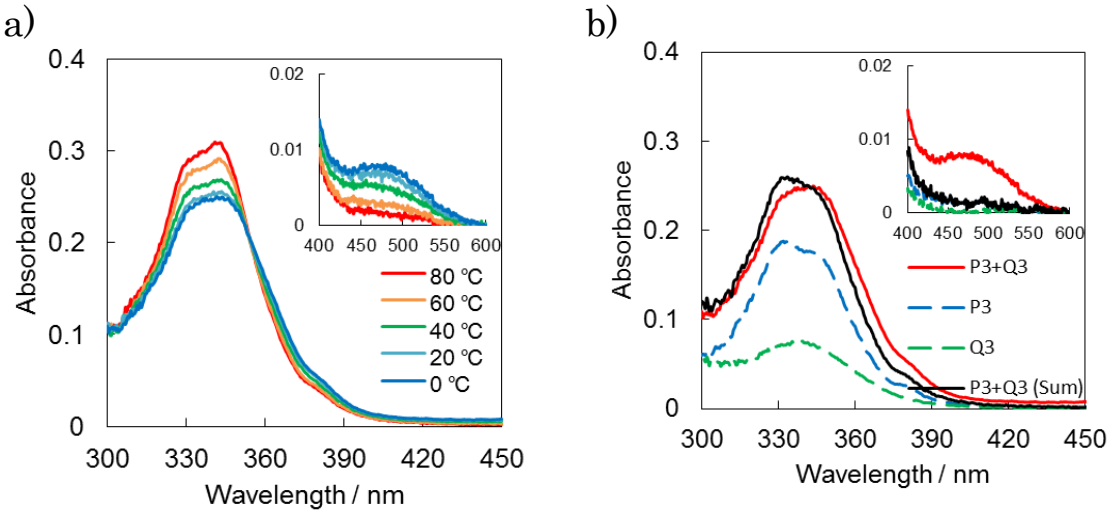

Fig. S3-7. a) UV-vis spectra of **P3**/**Q3** (5.0 μM each strand) at indicated temperatures. b) Comparison of UV-vis spectra of **P3**/**Q3** (red line) with the mathematical sum (black line) of single stranded **P3** (blue broken line) and **Q3** (green broken line) at 0 °C; strand concentrations 5.0 μM. Conditions: 100 mM NaCl, 10 mM phosphate buffer (pH 7.0).

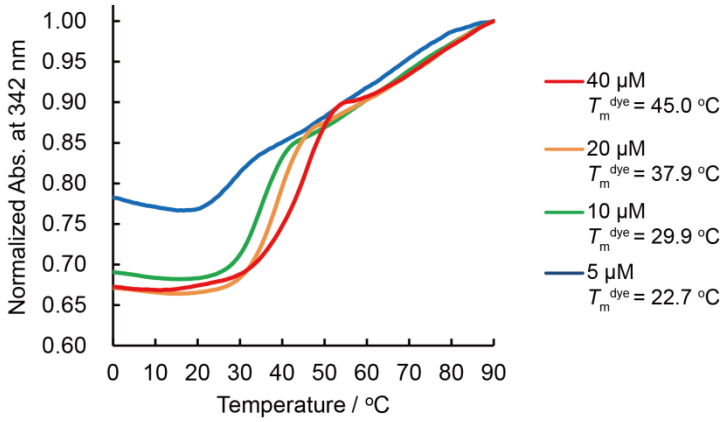

Fig. S3-8. Melting profiles of **P3**/**Q3** at indicated concentrations. Conditions: 100 mM NaCl, 10 mM phosphate buffer (pH 7.0). Absorbance at 342 nm was monitored.

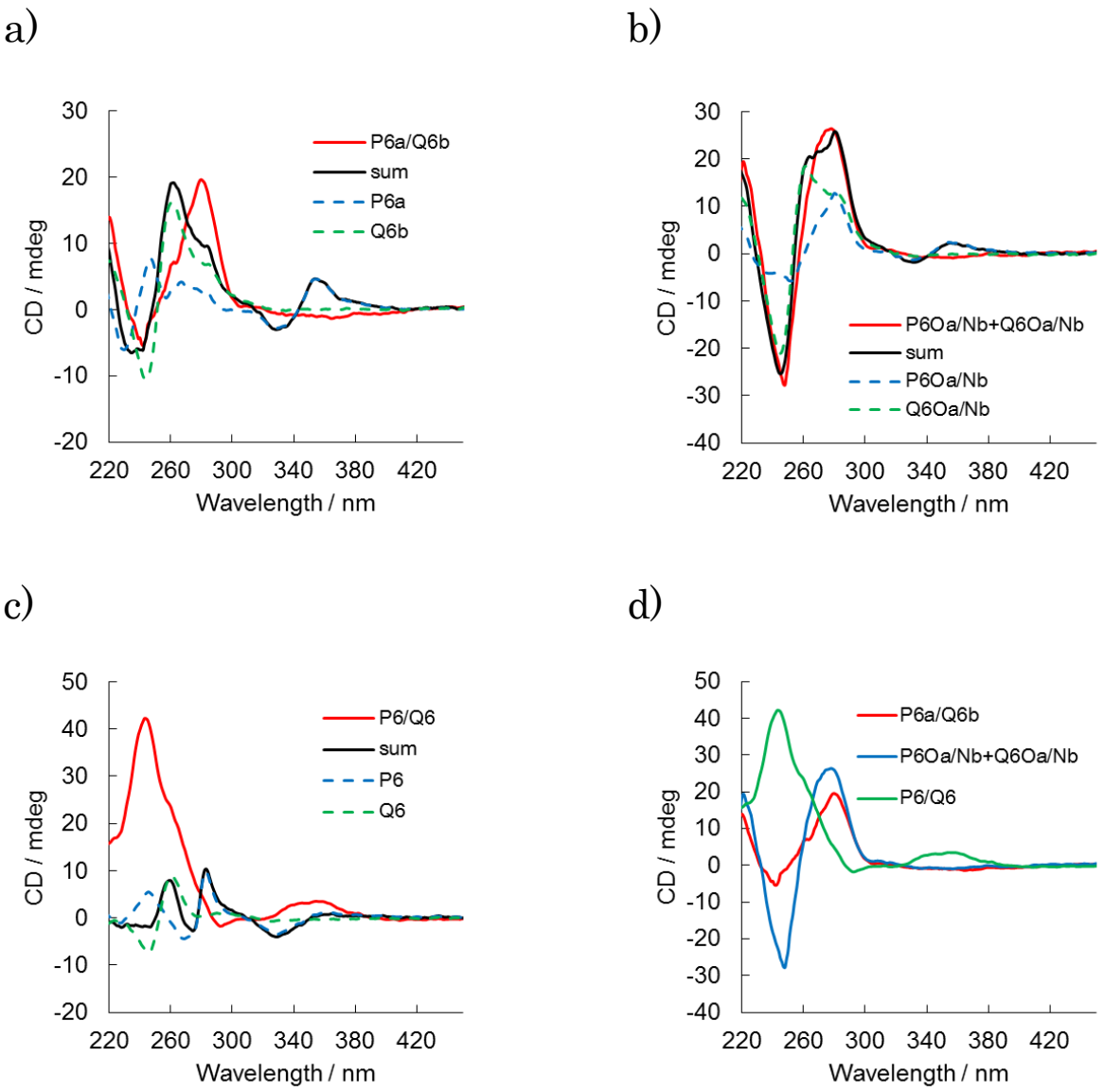

Fig. S3-9. CD spectra of a) **P6a**/**Q6b**, b) **P6Oa**/**Nb**+**Q6Oa**/**Nb**, and c) **P6**+**Q6**, (red lines in each graph) compared with the mathematically summed spectra of each component strand (black lines in each graph). d) Comparison of CD spectra of **P6a**/**Q6b**, **P6Oa**/**Nb**+**Q6Oa**/**Nb**, and **P6**+**Q6**. Conditions: 100 mM NaCl, 10 mM phosphate buffer (pH 7.0), 5.0 μM oligomer at 0 ^{o}C.

Table S3-1. Melting temperatures of center series oligomers with **P**/**Q** pairs.[a]

Sequence	T_m^{260} / °C [b]	T_m^{dye} / °C [c]
P1a/Q1b	59.2	58.5
P2a/Q2b	64.1	63.3
P3a/Q3b	69.7	69.5
P4a/Q4b	72.6	72.4
P5a/Q5b	75.6	75.3
P6a/Q6b	77.1	78.2

[a] Sequences: **P*n*a**: 5'- GGTATC (**P**)$_n$ GCAATC -3' (n=1-6) and **Q*n*b**: 3'- CCATAG (**Q**)$_n$ CGTTAG -5' (n=1-6). Measurement conditions: 100 mM NaCl, 10 mM phosphate buffer (pH 7.0), 5.0 μM oligomer. [b] Melting temperature determined from the absorbance at 260 nm. [c] Melting temperature determined from the absorbance at 342 nm.

Table S3-2. Melting temperatures of center series with **P**/**P** pairs.[a]

Sequence	T_m^{260} / °C [b]	T_m^{dye} / °C [c]
P1a/P1b	51.1	51.4
P2a/P2b	48.5	47.9
P3a/P3b	49.7	49.4
P4a/P4b	53.7	56.4
P5a/P5b	55.2	54.3
P6a/P6b	54.6	54.2

[a] Sequences: **P*n*a**: 5'- GGTATC (**P**)$_n$ GCAATC -3' (n=1-6) and **P*n*b**: 3'- CCATAG (**P**)$_n$ CGTTAG -5' (n=1-6). Measurement conditions: 100 mM NaCl, 10 mM phosphate buffer (pH 7.0), 5.0 μM oligomer. [b] Melting temperature determined from the absorbance at 260 nm. [c] Melting temperature determined from the absorbance at 345 nm.

Table S3-3. Melting temperatures of center series oligomers with **Q**/**Q** pairs.[a]

Sequence	T_m^{260} / °C [b]	T_m^{dye} / °C [c]
Q1a/Q1b	60.3	59.9
Q2a/Q2b	64.4	63.9
Q3a/Q3b	67.5	67.5
Q4a/Q4b	69.5	69.2
Q5a/Q5b	71.2	70.8
Q6a/Q6b	71.9	71.8

[a] Sequences: **Q*n*a**: 5'- GGTATC (**Q**)$_n$ GCAATC -3' (*n*=1-6) and **Q*n*b**: 3'- CCATAG (**Q**)$_n$ CGTTAG -5' (*n*=1-6). Measurement conditions: 100 mM NaCl, 10 mM phosphate buffer (pH 7.0), 5.0 μM oligomer. [b] Melting temperature determined from the absorbance at 260 nm. [c] Melting temperature determined from the absorbance at 334 nm.

Table S3-4. Melting temperatures of overhang series.[a]

Sequence	T_m^{260} / °C [b]	T_m^{dye} / °C [c]
P3Oa/Nb+Q3Oa/Nb	54.8	31.0
P4Oa/Nb+Q4Oa/Nb	54.4	50.2
P5Oa/Nb+Q5Oa/Nb	55.3	53.2
P6Oa/Nb+Q6Oa/Nb	56.1	55.3
P3Oa/Nb	51.3	n.d.
P4Oa/Nb	51.8	n.d.
P5Oa/Nb	50.6	n.d.
P6Oa/Nb	50.1	n.d.
Q3Oa/Nb	55.4	n.d.
Q4Oa/Nb	54.9	n.d.
Q5Oa/Nb	55.0	n.d.
Q6Oa/Nb	54.7	n.d.

[a] Sequences: **P*n*Oa**: 5'- (**P**)$_n$ GGTATCGCAATC -3' (*n*=3-6); **Nb**: 5'- GATTGCGATACC-3'; **Q*n*Oa**: 5'- (**Q**)$_n$ GGTATCGCAATC -3' (*n*=3-6). Measurement conditions: 100 mM NaCl, 10 mM phosphate buffer (pH 7.0), 5.0 μM each oligomer. [b] Melting temperature determined from the absorbance at 260 nm. [c] Melting temperature determined from the absorbance at 345 nm for **P** series, 334 nm for the **Q** series, and 342 nm for the **P**/**Q** series.

Table S3-5. Melting temperatures of single-stranded overhang sequences.[a]

Sequence	T_m^{260} / °C [b]	T_m^{dye} / °C [c]
P3Oa+Q3Oa	n.d.	n.d.
P4Oa+Q4Oa	n.d.	n.d.
P5Oa+Q5Oa	n.d.	34.1
P6Oa+Q6Oa	n.d.	45.6
P3Oa	n.d.	n.d.
P4Oa	n.d.	n.d.
P5Oa	n.d.	n.d.
P6Oa	n.d.	n.d.
Q3Oa	n.d.	n.d.
Q4Oa	n.d.	n.d.
Q5Oa	n.d.	n.d.
Q6Oa	n.d.	n.d.

[a] Sequences: **P*n*Oa**: 5'- $(\mathbf{P})_n$ GGTATCGCAATC -3' (*n*=3-6) and **Q*n*Oa**: 5'- $(\mathbf{Q})_n$ GGTATCGCAATC -3' (*n*=3-6). Measurement conditions: 100 mM NaCl, 10 mM phosphate buffer (pH 7.0), 5.0 μM oligomer. [b] Melting temperature determined from the absorbance at 260 nm. [c] Melting temperature determined from the absorbance at 345 nm for **P** series, 334 nm for **Q** series, and 342 nm for **P**/**Q** series.

Chapter 4. Cross-linking of DNA duplex using [2+2] photodimerization reaction of stilbazole derivatives

4-1 Abstract

In this study, we report a photo-cross-linking reaction between *p*-stilbazole moieties. *p*-Stilbazoles were introduced into base-paring positions of complementary DNA strands. The [2 + 2] photocycloaddition reaction occurred rapidly upon light irradiation at 340 nm. Consequently, duplex was cross-linked and highly stabilized after 3 min irradiation. The CD spectrum of the cross-linked duplex indicated that the B-form double-helical structure was not severely distorted. NMR analysis revealed only one conformation of the duplex prior to UV irradiation, whereas two diastereomers were detected after the photo-cross-linking reaction. Before UV irradiation, *p*-stilbazole can adopt two different stacking modes because of rotation around the single bond between the phenyl and vinyl groups; these conformations cannot be discriminated on the NMR time scale due to rapid interconversion. However, photo-cross-linking fixed the conformation and enabled discrimination both by NMR and HPLC. The artificial base pair of *p*-methylstilbazolium showed almost the same reactivity as *p*-stilbazole, indicating that positive charge does not affect the reactivity. When a natural nucleobase

was present in the complementary strand opposite *p*-stilbazole, the duplex was significantly destabilized relative to the duplex with paired *p*-stilbazole moieties and no photoreaction occurred between *p*-stilbazole and the nucleobase. The *p*-stilbazole pair has potential as a "third base pair" for nanomaterials due to its high stability and superb orthogonality.

4-2 Introduction

Watson–Crick base pairs stabilize DNA duplexes through hydrogen-bonding and stacking interactions. Extremely high orthogonality of base pairing is realized by strict control of these two interactions. It has become possible to synthesize oligodeoxyribonucleotides of essentially any sequence in an automated fashion. This has made DNA an ideal material to construct nanostructures and nanodevices.[1,2] DNA duplexes dissociate into single strands at high temperature. Although the reversibility is essential for biological processes, such as replication and transcription, the heat lability of DNA duplex in some cases restricts applications of DNA-based nanomaterials. To make DNA nanomaterials more heat tolerant, it is necessary to increase the thermal stability of DNA structures.[3]

Photo-cross-linking or photoligation has been widely studied not only for its

biological relevance but also for nucleic detection and duplex stabilization.[4-7] For example, Lewis et al. reported photo-cross-linking system by introducing stilbene units into main chain of a DNA duplex.[8] Fujimoto et al. reported several vinyldeoxyuridine and vinylcarbazole derivatives that form adducts with natural nucleo-bases.[9] Cross-linking has been used in SNP detection, DNA computing, and nano-structure stabilization.[10-14] Furthermore, photoligation via [4 + 4] cycloaddition reaction between anthracene moieties has been reported by Ihara et al. and other groups.[15-18]

Herein, we propose a photo-cross-linking system using *p*-stilbazoles as an artificial base pair. We have previously reported that planar molecules incorporated via D-threoninol linkers serve as "artificial base pairs" to stabilize a DNA duplex.[19] For example, when azobenzene derivatives were introduced into the base-pairing positions of both strands, the duplex was highly stabilized relative to the unmodified DNA due to intermolecular stacking interactions.[20,21] Interestingly, this "base pair" showed high orthogonality with natural base pairs. We have also reported that base pairs of *p*-methylstilbazolium, which has a positive charge, stabilize duplexes even more strongly than natural base pairs due to electrostatic interactions between the positive charge on*p*-methylstilbazolium and the phosphate anion.[22,23] In this paper, we used the photocycloaddition reaction between stilbazole derivatives to further improve the heat

tolerance of a DNA duplex.

p-Stilbazole derivatives are known to form dimers upon UV irradiation via a [2 + 2] photocycloaddition reaction.[24-26] Therefore, if a duplex containing an artificial base pair of *p*-stilbazole moieties is irradiated with UV light, the *p*-stilbazoles should react with each other and the duplex should be cross-linked (Scheme 4-1). If the *p*-stilbazole base pair shows high orthogonality, *p*-stilbazoles could serve as a "third base pair" for preparation of complex nanomaterials. Here, we introduced *p*-stilbazole moieties (**B** in Figure 4-1) into DNA and investigated their photoreactivity and effect on duplex stability. *p*-Methylstilbazolium (**Z** in Figure 4-1), which has a similar structure but a positive charge, was also incorporated into DNA to investigate the effects of positive charge on photoreactivity. Orthogonality of stilbazole moieties with natural base pairs was also evaluated.

Scheme 4-1. Schematic Illustration of Photo-Cross-Linking via [2 + 2] Photocyclo-addition Between *p*-Stilbazole Moieties

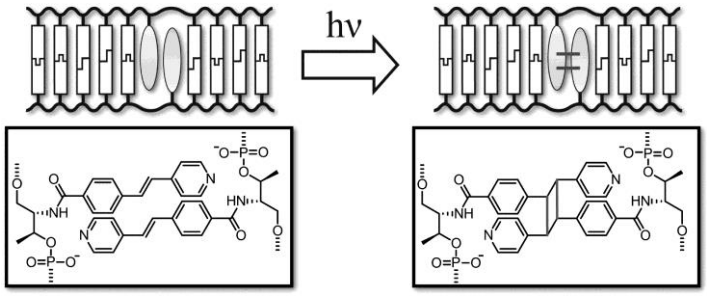

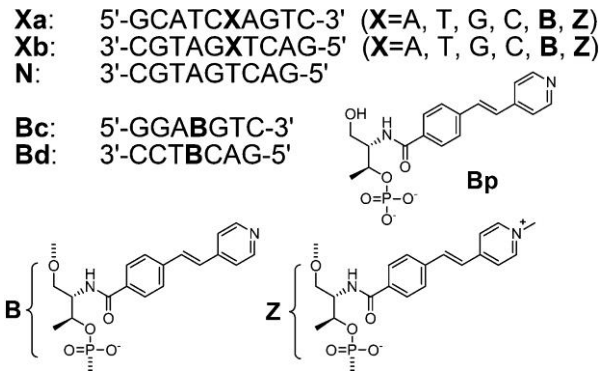

Figure 4-1. Sequences of ODNs synthesized in this study. Chemical structure of *p*-stilbazole monophosphate is also shown.

4-3 Results and discussions

4-3-1 Photochemical Properties of *p*-Stilbazole Monophosphate and *p*-Stilbazole-Modified DNA

We first investigated the photochemical properties of *p*-stilbazole monophosphate (**Bp** in Figure 4-1) before evaluating photochemical properties in DNA. Figure 4-2a shows the UV–vis spectra of **Bp** before and after photoirradiation. Before photoirradiation, **Bp** showed peaks at 303 and 312 nm arising from the π-π* transition of *trans p*-stilbazole (black line). When the sample was irradiated with 340 nm UV light for 1 min, these peaks immediately disappeared, and a new broad peak appeared at 297 nm due to photoisomerization to the *cis* form (purple line).[27] Thus, the photoisomerization rate of free *p*-stilbazole is intrinsically very rapid. Further

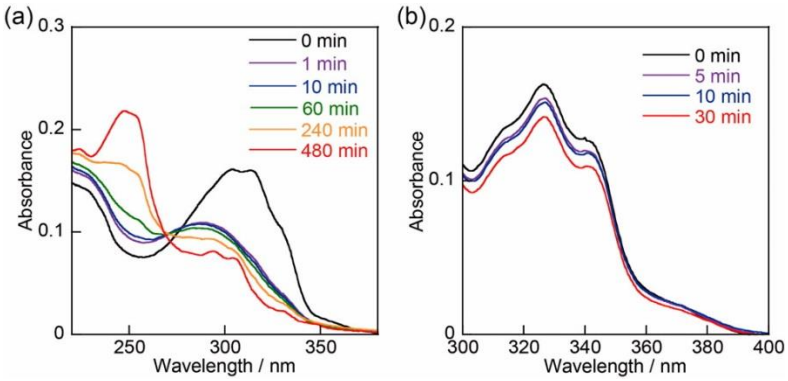

Figure 4-2. UV–vis spectra of (a) stilbazole monophosphate **Bp** and (b) **Ba**/**N**before and after UV irradiation (340 nm). T_m of **Ba**/**N** was 43.2 °C. Solution conditions were 5.0 μM **Bp**, 5.0 μM DNA, 100 mM NaCl, 10 mM phosphate buffer (pH 7.0), 0 °C.

photoirradiation at 340 nm for 480 min resulted in a decrease in absorbance at around 300 nm and appearance of a peak at 247 nm (red line). These spectral shifts are due to cyclization and subsequent oxidation to a benzoquinoline derivative as shown in Scheme 4-2a.[28] The cyclized product was detected by ESI-MS (see appendix). The peak at around 300 nm did not disappear even after 480 min irradiation, indicating that the [2 + 2] photocycloaddition reaction did not occur under these conditions. These results show that photoirradiation of *p*-stilbazole potentially causes several side reactions but not the desired [2 + 2] photocycloaddition (Scheme 4-2a).

In striking contrast, incorporation of *p*-stilbazole into DNA drastically suppressed these side reactions. The **Ba**/**N** duplex with a stilbazole moiety in one strand of the DNA duplex showed absorption maximum (λ_{max}) at 327 nm (black line in Figure 4-2b). The

Scheme 4-2. Photochemical Reaction Observed with (a) *p*-Stilbazole Monophosphate and (b) *p*-Stilbazole Moiety in DNA Duplex

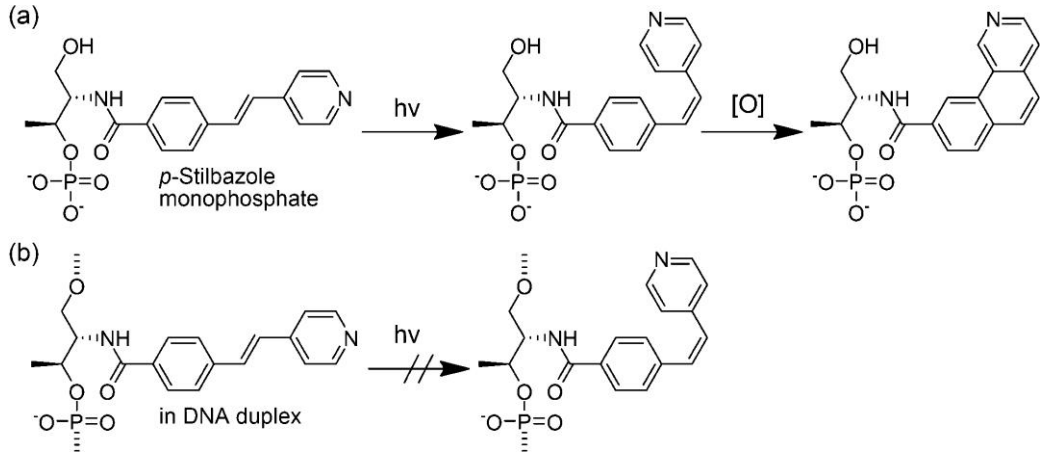

peak did not change after irradiation at 340 nm for 5 min. Although the peak slightly decreased after 30 min irradiation, these results clearly demonstrated that introduction of *p*-stilbazole moiety into DNA strongly suppressed photoisomerization to *cis* form (Scheme 4-2b). This is in sharp contrast to azobenzene, which can isomerize even within DNA duplex.[29] This difference in isomerization is attributable to differences in the isomerization mechanisms: Isomerization of the stilbene derivative proceeds exclusively through rotation, whereas that of azobenzene occurs via both rotation and inversion.[30] Consistently, photoisomerization of stilbene derivatives is suppressed in viscous solution, whereas isomerization of azobenzene is not affected significantly by viscosity.[31] Within a DNA duplex, isomerization of *p*-stilbazole is presumably suppressed by stacking interactions with natural base pairs.

4-3-2 Photo-Cross-Linking of *p*-Stilbazole in DNA Duplex

The photochemical properties of the duplex **Ba**/**Bb**, which has **B** residues in complementary positions on the two strands, were investigated in order to evaluate the photo-cross-linking of *p*-stilbazole within a duplex.[32] Before photoirradiation, the UV–vis spectrum of the **Ba**/**Bb** duplex had a peak at 323 nm (Figure 4-3). A slight hypsochromic shift compared with the single-stranded **Ba** (λ_{max} 325 nm) indicated that **B** residues formed an H dimer (Figure S4-1).[33] Upon irradiation at 340 nm for 3 min, the peak at 323 nm had completely disappeared. This disappearance of the π–π* absorption band assigned to the *p*-stilbazole moieties strongly suggested that a [2 + 2] photocycloaddition reaction between two *p*-stilbazole moieties had occurred. The λ_{max} of **Ba**/**Bb** did not shift upon photoirradiation, indicating that trans-to-cis

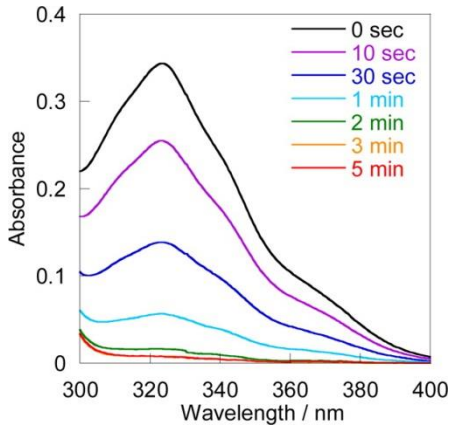

Figure 4-3. UV–vis spectra of **Ba**/**Bb** before and after photoirradiation. Solution conditions were 5.0 μM DNA, 100 mM NaCl, 10 mM phosphate buffer (pH 7.0), 0 °C.

isomerization did not occur and that neither *p*-stilbazoles were in the *cis* form. Instead, the *trans* forms reacted. Note that isomerization to the *cis* form causes a blue-shift in the absorption spectrum as shown in Figure 4-2a.

The photo-cross-linked product of **Ba**/**Bb** was further analyzed by reversed-phase HPLC (Figure 4-4). Before photoirradiation, two peaks corresponding to the single-stranded forms of **Ba** and **Bb** were observed. After 3 min photoirradiation, however, the two peaks disappeared and a new peak appeared at a shorter retention time. MALDI-TOF MS analysis of this new peak proved it to be a photo-cross-linked duplex (Figure S4-2). From these results, we conclude that a [2 + 2] photocycloaddition reaction occurred between *p*-stilbazole moieties in the DNA duplex upon UV irradiation at 340 nm.

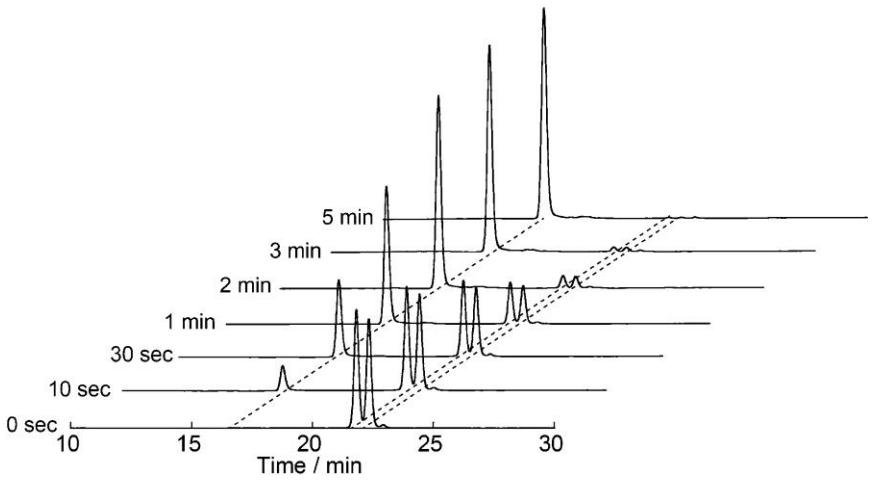

Figure 4-4. HPLC chromatograms of **Ba**/**Bb** before and after indicated times of photoirradiation.

4-3-3 Structure of Photodimer of *p*-stilbazole

Photocycloaddition of stilbene derivatives usually produces several isomers.[24] When the stilbene derivatives are within a DNA scaffold, the orientations of *p*-stilbazoles should be restricted, and thus the stereochemistry of photodimerized product should be controlled. In order to investigate the structure of photo-cross-linked product, the **Bc**/**Bd** duplex was analyzed by NMR. The imino region of the 1D spectrum of **Bc**/**Bd** had six peaks corresponding to imino protons from the six natural base pairs (Figure 4-5a). These sharp peaks indicated that hydrogen bonding of natural base pairs was not disturbed by the presence of the *p*-stilbazole moieties. After irradiation at 340 nm, these peaks disappeared, and eight new peaks appeared. Although several peaks overlap, the appearance of more than six peaks indicates that there are at least two species in the photo-cross-linked product.

The aromatic regions of the 1D NMR spectra in D_2O of **Bc**/**Bd** before and after irradiation are shown in Figure 4-5b. In the nonirradiated sample, 11 peaks corresponded to 4 vinyl and 8 phenyl protons of 2 *p*-stilbazole moieties.[34] In the spectrum of the irradiated sample, 4 peaks assigned to vinyl protons disappeared as expected, and 12 new, partially overlapping peaks appeared. If the photo-cross-linked product were a single species, only eight peaks should be observed. Hence, the

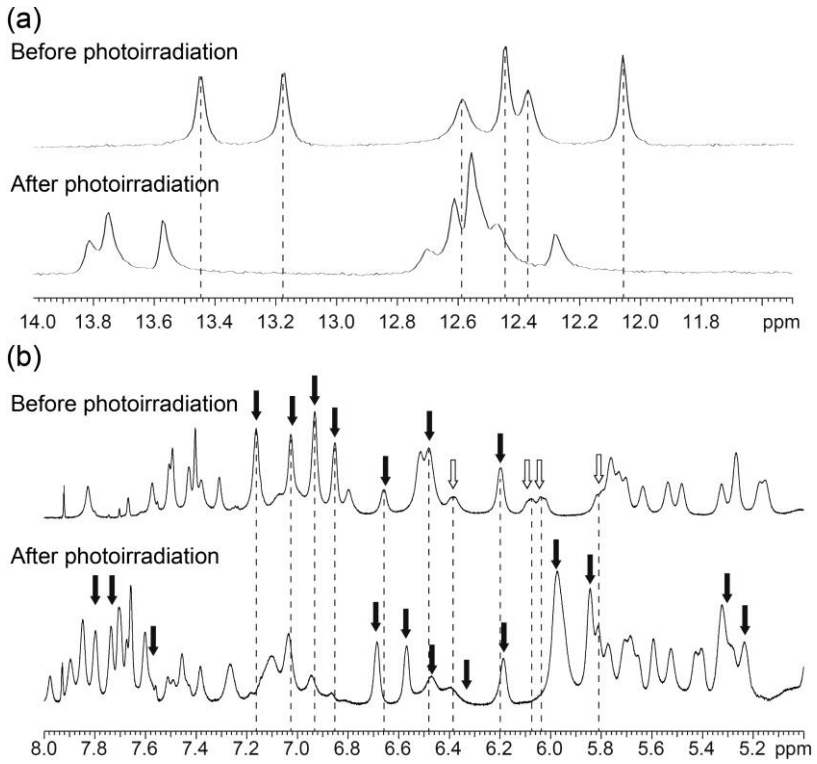

Figure 4-5. 1H NMR spectra of **Bc**/**Bd** in (a) imino regions measured in H_2O/D_2O and (b) aromatic regions in D_2O. White and black arrows in (b) indicate vinyl and phenyl protons of the *p*-stilbazole moiety, respectively.

appearance of 12 peaks clearly shows that more than one species was produced upon photoirradiation. Furthermore, TOCSY in D_2O gave eight cross-peaks in the aromatic region after photoirradiation, whereas four cross-peaks were observed before photoirradiation (Figure S4-3). These results undoubtedly show that there are two diastereomers of the photo-cross-linked product. The existence of two diastereomers was further supported by the appearance of two peaks in the HPLC chromatogram of **Bc**/**Bd** after irradiation (Figure S4-4).[35]

Previously, we prepared DNA duplexes containing heterodimers of azo compounds. NMR structural analyses revealed that the dyes were stacked in an antiparallel manner and located at 3′ side of the complementary strand.[21] Thus, *p*-stilbazole moieties in this study are expected to adopt similar stacking structures. A *trans*-to-*cis* isomerization within the duplex could be ruled out based on the fact that the λ_{max} of **Ba**/**Bb** did not shift during photoirradiation (Figure 4-3). Furthermore, NMR and HPLC analyses revealed that equal amounts of diastereomers were produced. Thus, we concluded that the two observed products are diastereomers (Figure 4-6, right panel). The very fast rotation around the single bond between phenyl and vinyl groups of *p*-stilbazole results in the production of the two diastereomers upon irradiation. Before photo-irradiation, *p*-stilbazole can adopt either of two stable stacking modes (Figure 4-6, left

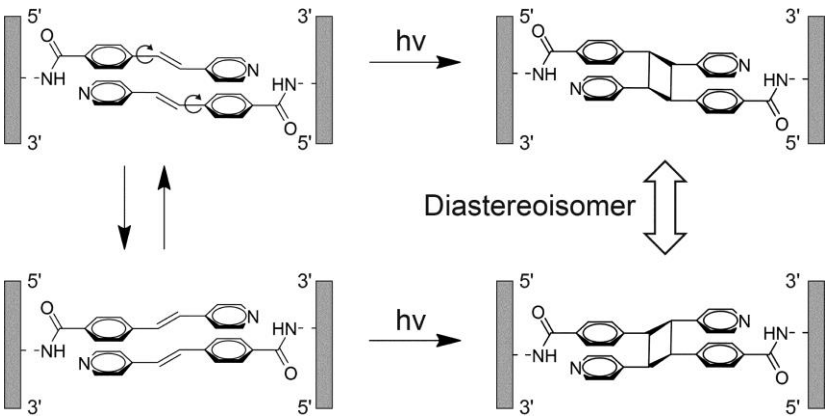

Figure 4-6. Presumed structures of diastereoisomers produced upon photocycloaddition.

panel). Since interconversion between the two conformers is rapid, NMR does not distinguish these two conformers. Photo-cross-linking prevents interconversion and fixes the conformation. As a result, duplexes containing each of these two "fixed" conformers are observed both by NMR and HPLC. We have also conducted molecular dynamics simulations of **Ba**/**Bb** (Figure S4-5). These simulations indicate that the *p*-stilbazoles in **Ba**/**Bb** may adopt either of the possible conformations without disturbing the overall B-form structure.

4-3-4 Thermal Stability of Photo-Cross-Linked Duplex

We next evaluated thermal stability of the cross-linked duplex. Melting curves of **Ba**/**Bb** before and after photoirradiation are shown in Figure 4-7a. Before photoirradiation, the T_m of **Ba**/**Bb** was 46.4 °C (Figure 4-7a and Table 4-1), which was 8.2 °C higher than that of a native duplex without **B**residues (38.2 °C). The T_m increased to more than 80 °C after photoirradiation. Thus, thermal stability of duplex was dramatically improved through photodimerization of the *p*-stilbazole moieties. The overall structure of photo-cross-linked duplex was analyzed by CD spectroscopy (Figure 4-7b). Before photoirradiation, positive exciton couplet was observed at around 260 nm, showing that natural nucleobases adopted B-form duplex. An induced CD was ob served at 320 nm, indicating that the *p*-stilbazoles are located in the chiral

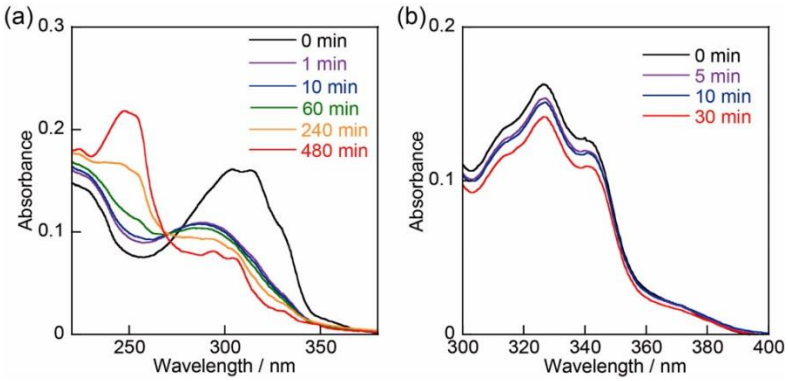

Figure 4-7. UV–vis spectra of (a) stilbazole monophosphate **Bp** and (b) **Ba**/**N**before and after UV irradiation (340 nm). T_m of **Ba**/**N** was 43.2 °C. Solution conditions were 5.0 μM **Bp**, 5.0 μM DNA, 100 mM NaCl, 10 mM phosphate buffer (pH 7.0), 0 °C.

Table 4-1. Comparison of Thermal Stabilities and Photoreactivities of Duplexes Containing *p*-Stilbazole and *p*-Methylstilbazolium

	T_m/°C[a]		
sequence	before UV irradiation	after UV irradiation[b]	k_{obs}/min^{-1}[c]
Ba/**Bb**	46.4	>80	1.1
Za/**Zb**	51.5	>80	1.5
Ba/**Zb**	49.7	>80	0.9

[a]Conditions: 5.0 μM DNA, 100 mM NaCl, 10 mM phosphate buffer (pH 7.0), 20 °C. [b]UV light at 340 nm was irradiated for 30 (**Ba**/**Zb**), 60 (**Ba**/**Bb**) or 120 min (**Za**/**Zb**). T_m of native duplex without stilbazole was 38.2 °C. [c]Observed rate constant determined from initial slope of Figure 4-9.

environment of DNA duplex. This induced CD band disappeared upon light irradiation because π–π* absorption of *p*-stilbazole at 325 nm disappears upon photocycloaddition. In the cross-linked species, the CD couplet at 260 nm remained almost unchanged to that prior to irradiation. These results indicated that overall B-form double-helical

structure remained intact in spite of nonplanar structure of photo-dimerized *p*-stilbazoles.[24]

4-3-5 Effect of Positive Charge on Photo-Cross-Linking Properties

We then investigated photo-cross-linking of *p*-methylstilbazolium, a stilbazole derivative containing a positive charge (**Z** in Scheme 4-1). The UV–vis spectra of a duplex tethering these moieties, **Za**/**Zb**, are shown in Figure 4-8. Before photoirradiation, an absorption maximum was observed at 340 nm. This peak completely disappeared after photoirradiation for 3 min, unambiguously demonstrating that the photocycloaddition reaction between **Z** moieties occurred. The photo-cross-linking between **Z** moieties was further confirmed by HPLC and

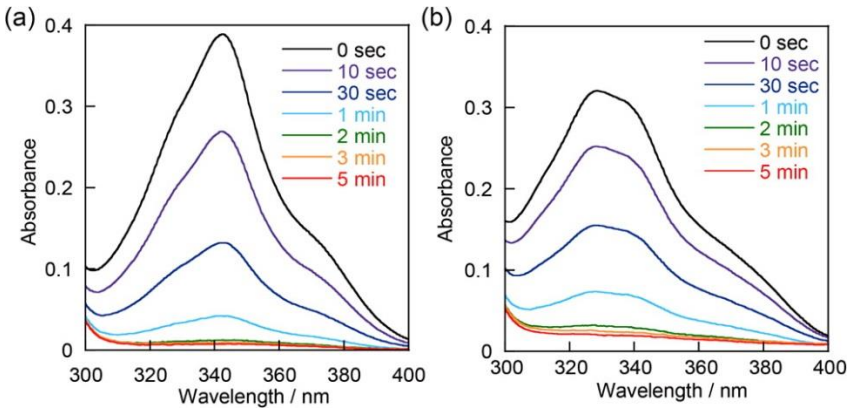

Figure 4-8. UV–vis spectra of (a) **Za**/**Zb** and (b) **Ba**/**Zb** before and after photoirradiation. Solution conditions were 5.0 μM DNA, 100 mM NaCl, 10 mM phosphate buffer (pH 7.0), 0 °C.

MALDI-TOF MS analyses (Figure S4-6). The T_m of **Za**/**Zb** before photoirradiation was 51.5 °C (Table 4-1 and Figure S4-7), about 5.1 °C higher than that of **Ba**/**Bb** (46.4 °C). The high stability of the **Z**-**Z** pair is due to electrostatic interactions between phosphate anions and cations of **Z** residues as we reported previously.[22] In addition, cation−π interaction should also contribute to the high stability. The T_m of the **Za**/**Zb** increased to over 80 °C after photoirradiation at 340 nm, demonstrating significant stabilization upon photo-cross-linking of the **Z**-**Z** pair. We also investigated photocycloaddition of the hetero combination between **B** and **Z** residues (Figure 4-8b). Absorption maxima of **B** and **Z** residues at about 320 and 350 nm, respectively, simultaneously decreased upon irradiation. Thus, the **B**–**Z** pair can be photo-cross-linked in the context of DNA duplexes.

The observed rate constant of the reaction between *p*-methylstilbazolium residues was also determined from UV–vis spectra (Table 4-1 and Figure 4-9). The observed rate constants measured under the conditions of the same absorbance and light intensity are a measure of the relative quantum yields of reaction.[36] The observed rate constant of **Za**/**Zb** was 1.5 min^{-1}, which was almost the same order as that of the *p*-stilbazole duplex (1.1 min^{-1}).[37] The observed rate constant of hetero **B**-**Z** pair was also similar (0.9

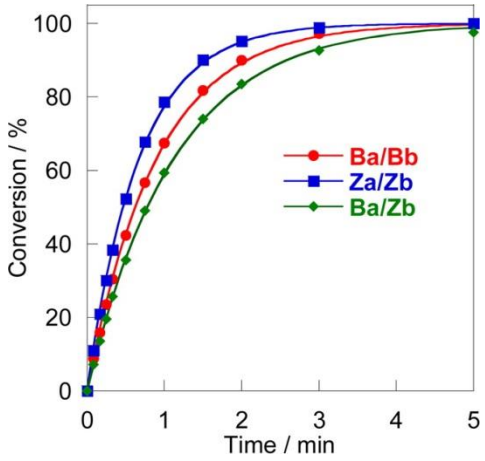

Figure 4-9. Reaction kinetics of **Ba**/**Bb** (red line), **Za**/**Zb** (blue line), and **Ba**/**Zb** (green line) determined from UV–vis spectra. Absorbances of all duplexes were adjusted to be almost the same (**Ba**/**Bb**: 0.186, **Ba**/**Zb**: 0.196, **Za**/**Zb**: 0.187).

min^{-1}). Thus, the cationic charge on the **Z** moiety did not significantly affect photoreactivity. In photodimerization reactions of *p*-stilbazole and *p*-methylstilbazolium not conjugated with DNA, the positive charge played important roles in both yield and stereoselectivity.[24,38] Although the positive charge does affect the association process of stilbazoles, the "intrinsic" reactivity should be almost the same between *p*-stilbazole and *p*-methylstilbazolium. In other words, intrinsic photoreactivity of molecules can be evaluated by using DNA as a scaffold. Use of a DNA scaffold also allows reactivity of hetero combinations to be investigated while excluding the corresponding homo combinations.

4-3-6 Orthogonality with Natural Nucleobases

In order to serve as artificial base pairs, orthogonality is one of the most important prerequisites. Thus, we investigated orthogonality of **B**-**B** or **Z**-**Z** pairs with natural base pairs. Melting temperatures of **Xa**/**Xb** duplexes (where **X** was A, T, G, C, **B**, or **Z**) before photoirradiation are shown in Table 4-2. The **B** residue more strongly hybridizes when the complementary residue is **B** than when it is a natural nucleobase. For example, **Ba**/**Bb** had a T_m of 46.4 °C, whereas duplexes of **Ba** with **Ab**, **Tb**, **Gb**, and **Cb** had much lower T_ms (31.6, 34.0, 33.9, and 35.1 °C, respectively). These T_ms were also significantly lower than those of duplexes with natural A-T or G-C pairs: The T_m of **Aa**/**Tb** (42.8 °C) was much higher than that of **Ab**/**Bb** (33.7 °C). The same tendency was observed with **Z**-**Z** pairs (Table 4-2). These results clearly demonstrated that **B**-**B** and **Z**-**Z** pairs show excellent orthogonality with natural nucleobases. In other words, the **B**-**B** or **Z**-**Z** pair could be used as "third base pair" for construction of DNA-based nanomaterials. The instability of a natural base paired with either **B** or **Z** is attributable to the sizes of the **B** and **Z** moieties; these stilbazoles are much larger than nucleobases, and intercalation of these moieties should cause steric hindrance with D-ribose. In contrast, when **B** and **Z** moieties are paired, steric hindrance is likely lessened by flexible D-threoninol linkers. In addition, strong intermolecular stacking

Table 4-2. Orthogonality of **B** or **Z** Moiety with Natural Nucleobases before Photoirradiation

	T_m/°C[a]					
	Aa	**Ta**	**Ga**	**Ca**	**Ba**	**Za**
Ab	25.7	40.3	30.6	24.4	31.6	30.4
Tb	42.8	28.7	33.6	26.4	34.0	31.8
Gb	30.7	31.9	29.8	45.9	33.9	32.4
Cb	27.3	26.8	48.8	23.8	35.1	32.2
Bb	33.7	37.4	36.3	36.0	46.4	50.9
Zb	32.5	34.4	35.1	34.7	49.7	51.5

[a]Conditions: 5.0 μM DNA, 100 mM NaCl, 10 mM phosphate buffer (pH 7.0), 20 °C.

interactions between **B** and **Z** moieties should contribute to high stabilities of the duplexes containing two of these residues.

Next, orthogonality in the photo-cross-linking reaction was evaluated. When a **B** or **Z** moiety was located counter to A, T, G, or C, the UV–vis spectra did not change even after photoirradiation for 30 min (Figure S4-9).[39] Spectra of **Ba**/**N** (Figure 4-2b) and **Za**/**N** (Figure S4-10) did not change upon photoirradiation of the sample. This indicates that neither **B** nor **Z** react with natural nucleobases, whereas fast reactions occurred between **B**-**B**, **Z**-**Z**, and **B**-**Z** pairs. It has been reported that natural nucleobases, especially pyrimidine bases, may cause [2 + 2] photocycloaddition reactions. For example, a thymine dimer is formed upon UV irradiation that may induce

point mutations.[40] Photo-cross-linking agents, such as psoralen, form interstrand cross-link with thymine via photocycloaddition reactions.[41,42] In our design, the vinyl group of *p*-stilbazole was located near the center of the natural base pair (Figure S4-11), but the reaction sites of nucleobases (e.g., C5 and C6 of pyrimidine bases) are toward the outside of the DNA duplex. Separation of vinyl group from pyrimidine inhibited cycloaddition reaction between *p*-stilbazole and natural nucleobases.

4-4 Conclusions

In conclusion, we have successfully developed artificial base pairs that can be photo-cross-linked in the context of a DNA duplex. When a duplex with a pair of *p*-stilbazoles located on opposite strands was irradiated with UV light, a [2 + 2] photocycloaddition reaction occurred significantly stabilizing the duplex. Both UV–vis spectra and HPLC analyses revealed that photo-cross-linking reaction was complete within 3 min. NMR analyses indicated that two diastereomers are produced on photo-cross-linking due to rotation of vinyl group. We have also demonstrated that *p*-stilbazole and *p*-methylstilbazolium showed high orthogonality with natural nucleobases in terms of both stability and photo-cross-linking reaction.

DNA has recently been used for construction of nanomaterials, such as nanoarchitecture and devices. However, the two natural base pairs, A-T and G-C, are not necessarily optimal in these materials. Furthermore, it is not necessary to mimic natural nucleobases when DNA is chemically synthesized and used as materials. The high stability and superb orthogonality of artificial base pairs of stilbazoles make them candidates for use in DNA nanomaterials. The photo-cross-linking reaction contributes remarkable stability to the DNA duplex. We believe that these pairs should be added to the “genetic alphabet” of DNA-based nanomaterials.

4-5 Experimental section

Materials

All the conventional phosphoramidite monomers, CPG columns, and reagents for DNA synthesis were purchased from Glen Research. Other reagents for the synthesis of phosphoramidite monomers were purchased from Tokyo Chemical Industry, Wako, and Aldrich. Unmodified oligodeoxyribonucleotides (ODNs) were purchased from Integrated DNA Technologies.

Synthesis of ODNs

All modified ODNs were synthesized on an automated DNA synthesizer (H-8-SE, Gene World) by using phosphoramidite monomers bearing **B** or **Z**. Syntheses of phosphoramidite monomers **B** and **Z** were reported previously.[22] *p*-Stilbazole monophosphate was synthesized as described in the appendix information. Sample handling was conducted under dark conditions. After the workup, ODNs were purified by reversed phase HPLC and characterized using a MALDI-TOF MS (Autoflex II, Bruker Daltonics). Matrix-assisted laser desorption ionization time-of-flight mass spectrometry (MALDI-TOF MS) data for the synthesized ODNs: **Ba**: obsd 3072 (calcd for [**Ba** + H^+]: 3073). **Bb**: obsd 3112 (calcd for [**Bb** + H^+]: 3113). **Bc**: obsd 2206 (calcd for [**Bc** + H^+]: 2206).**Bd**: obsd 2126 (calcd for [**Bd** + H^+]: 2126). **Za**: obsd 3088 (calcd for [**Za** + H^+]: 3088). **Zb**: obsd 3128 (calcd for [**Zb** + H^+]: 3128).

NMR Measurements

NMR samples were prepared by dissolving lyophilized DNA in an H_2O/D_2O 9:1 solution containing 10 mM sodium phosphate (pH 7.0) to give a duplex concentration of 1.0 mM. NaCl was added to give a final sodium concentration of 200 mM. NMR spectra were measured with a Varian INOVA spectrometer (700 MHz) equipped for triple resonance at a probe temperature of 275 K. Resonances were assigned by standard methods using a combination of 1D, totally correlated spectroscopy (TOCSY) (60 ms of mixing time), and nuclear Overhauser effect spectroscopy (NOESY) (150 ms of mixing time) experiments. All spectra in the H_2O/D_2O 9:1 solution were recorded using the 3–9–19 WATERGATE pulse sequence for water suppression.[43]

Spectroscopic Measurements

UV spectra were measured on a JASCO model J-560 equipped with a programmed temperature controller; 10 mm quartz cells were used. CD spectra were measured on a JASCO model J-820 equipped with programmed temperature-controllers using 10 mm quartz cells.

Measurement of the Melting Temperature

The melting curves were obtained with a JASCO model J-560 by measuring the change in absorbance at 260 nm versus temperature. The melting temperature (T_m) was determined from the maximum in the first derivative of the melting curve. Both the heating and the cooling curves were measured, and the calculated T_ms agreed to within 2.0 °C. The temperature ramp was 1.0 °C min^{-1}.

UV Irradiation

A xenon light source (MAX-301, Asahi Spectra) equipped with interference filters centered at 341.5 nm (half bandwidth 9 nm, power density 0.15 mW/cm^2) was used for photo-cross-linking. The sample solution was added to a cuvette, and the temperature of light irradiation was controlled using a programmable temperature controller. Photoirradiation was conducted at 0 °C.

HPLC Analyses

A Merck LiChrospher 100 RP-18(e) column heated at 50 °C was used for HPLC analyses. The flow rate was 0.5 mL/min. A solution of 50 mM ammonium formate (solution A) and a mixture of 50 mM ammonium formate and acetonitrile (50/50, v/v) (solution B) were used as mobile phases. A linear gradient of 5–35% solution B over 30 min was employed. HPLC chromatograms were monitored at 260 nm absorption.

Molecular Dynamic Simulation

The Insight II/Discover 98.0 program package was used for conformational energy minimization. The duplex tethering *p*-stilbazole was built from canonical B-form DNA by a graphical program. The AMBER95 force field was used for the calculation. All the structures were energy minimized to an RMS derivative of <0.001 kcal $Å^{-1}$. Computations were carried out on a Silicon Graphics O2+ workstation with the IRIX64 OS release 6.5.

4-6 References

(1) Krishnan, Y.; Simmel, F. C. *Angew. Chem., Int. Ed.* **2011**, *50*, 3124.

(2) Seeman, N. C. *Annu. Rev. Biochem.* **2010**, *79*, 65.

(3) Rajendran, A.; Endo, M.; Katsuda, Y.; Hidaka, K.; Sugiyama, H. *J. Am. Chem. Soc.* **2011**, *133*, 14488.

(4) Meisenheimer, K. M.; Koch, T. H. *Crit. Rev. Biochem. Mol. Biol.* **1997**, *32*, 101.

(5) Noll, D. M.; Mason, T. M.; Miller, P. S. *Chem. Rev.* **2005**, *106*, 277.

(6) Cai, J.; Li, X.; Taylor, J. S. *Org. Lett.* **2005**, *7*, 751.

(7) Lewis, R. J.; Hanawalt, P. C. *Nature* **1982**, *298*, 393.

(8) Lewis, F. D.; Wu, T.; Burch, E. L.; Bassani, D. M.; Yang, J. S.; Schneider, S.; Jaeger, W.; Letsinger, R. L. *J. Am. Chem. Soc.* **1995**, *117*, 8785.

(9) Fujimoto, K.; Matsuda, S.; Takahashi, N.; Saito, I. *J. Am. Chem. Soc.* **2000**, *122*, 5646.

(10) Ogino, M.; Fujimoto, K. *Angew. Chem., Int. Ed.* **2006**, *45*, 7223.

(11) Ogasawara, S.; Fujimoto, K. *Angew. Chem., Int. Ed.* **2006**, *45*, 4512.

(12) Ogasawara, S.; Ami, T.; Fujimoto, K. *J. Am. Chem. Soc*. **2008**, *130*, 10050.

(13) Fujimoto, K.; Konishi-Hiratsuka, K.; Sakamoto, T.; Yoshimura, Y. *ChemBioChem* **2010**, *11*, 1661.

(14) Tagawa, M.; Shohda, K.; Fujimoto, K.; Sugawara, T.; Suyama, A. *Nucleic Acids Res.* **2007**, *35*, e140.

(15) Pasternak, K.; Pasternak, A.; Gupta, P.; Veedu, R. N.; Wengel, J. *Bioorg. Med. Chem.* **2011**, *19*, 7407.

(16) Manchester, J.; Bassani, D. M.; Duprey, J. L. H. A.; Giordano, L.; Vyle, J. S.; Zhao, Z. y.; Tucker, J. H. R. *J. Am. Chem. Soc.* **2012**, *134*, 10791.

(17) Ihara, T.; Fujii, T.; Mukae, M.; Kitamura, Y.; Jyo, A. *J. Am. Chem. Soc.* **2004**, *126*, 8880.

(18) Mukae, M.; Ihara, T.; Tabara, M.; Jyo, A. *Org. Biomol. Chem.* **2009**, *7*, 1349.

(19) Artificial base pairs, which can be synthesized enzymatically, have been reported by several groups. (a) Malyshev, D. A.; Dhami, K.; Quach, H. T.; Lavergne, T.; Ordoukhanian, P.; Torkamani, A.; Romesberg, F. E. Proc. Natl. Acad. Sci. U.S.A. 2012, 109, 12005. (b) Yang, Z.; Chen, F.; Alvarado, J. B.; Benner, S. A. J. Am. Chem. Soc. 2011, 133, 15105. (c) Kimoto, M.; Kawai, R.; Mitsui, T.; Yokoyama, S.; Hirao, I. Nucleic Acids Res. 2009, 37, e14. (d) Kaul, C.; Müller, M.; Wagner, M.; Schneider, S.; Carell, T. Nat. Chem. 2011, 3, 794.

(20) Kashida, H.; Fujii, T.; Asanuma, H. *Org. Biomol. Chem.* **2008**, *6*, 2892.

(21) Fujii, T.; Kashida, H.; Asanuma, H. *Chem.—Eur. J.* **2009**, *15*, 10092.

(22) Kashida, H.; Ito, H.; Fujii, T.; Hayashi, T.; Asanuma, H. *J. Am. Chem. Soc.* **2009**, *131*, 9928.

(23) Kashida, H.; Hayashi, T.; Fujii, T.; Asanuma, H. *Chem.—Eur. J.* **2011**, *17*, 2614.

(24) Yamada, S.; Nojiri, Y.; Sugawara, M. *Tetrahedron Lett.* **2010**, *51*, 2533.

(25) Quina, F. H.; Whitten, D. G. *J. Am. Chem. Soc.* **1977**, *99*, 877.

(26) Yamada, S.; Uematsu, N.; Yamashita, K. *J. Am. Chem. Soc.* **2007**, *129*, 12100.

(27) Daku, L. M. L.; Linares, J.; Boillot, M. L. *Phys. Chem. Chem. Phys.* **2010**, *12*, 6107.

(28) Turanova, O. A.; Gafiyatullin, L. G.; Gnezdilov, O. I.; Turanov, A. N. *Russ. J. Gen. Chem.* **2011**, *81*, 937.

(29) Liang, X. G.; Asanuma, H.; Kashida, H.; Takasu, A.; Sakamoto, T.; Kawai, G.; Komiyama, M. *J. Am. Chem. Soc.* **2003**, *125*, 16408.

(30) Bandara, H. M. D.; Burdette, S. C. *Chem. Soc. Rev.* **2012**, *41*, 1809.

(31) Gegiou, D.; Muszkat, K. A.; Fischer, E. *J. Am. Chem. Soc.* **1968**, *90*, 12.

(32) Here, we did not introduce spacers at the counter positions of *p*-stilbazole because incorporation of spacers rather destabilize duplex. See ref 20.

(33) **B** residues should be stacked in antiparallel manner in DNA. See also ref 21.

(34) Because peaks of *p*-stilbazole in *cis* form were not observed, all the *p*-stilbazole took trans form in DNA.

(35) On the other hand, only single peak was observed with **Ba**/**Bb** after photoirradiation as shown in Figure 4-4. Longer DNA portion of **Ba**/**Bb** would lessen the effect of structural difference of diastereomers compared with **Bc**/**Bd**.

(36) It is known that rate constant of photoreaction is affected by light intensity, absorbance, and quantum yield. Here, absorbances of **Ba**/**Bb**, **Ba**/**Zb**, and **Za**/**Zb** were adjusted to about 0.19. In addition, reaction kinetics of all duplexes was measured within several hours to avoid change of light intensity during the experiments. As a result, initial slope of Figure 4-9 (observed rate constant in Table 4-1) should be proportional to quantum yields.

(37) We also investigated effects of flanking sequence and mismatch on reaction rate constant of **B**-**B** combination. As a result, flanking AT pairs strongly facilitated photocrosslinking of *p*-stilbazole. Incorporation of mismatches decreased the rate constant. See Figure S4-8 for

actual data.

(38) Takagi, K.; Suddaby, B. R.; Vadas, S. L.; Backer, C. A.; Whitten, D. G. *J. Am. Chem. Soc.* **1986**, *108*, 7865.

(39) Although absorbance of *p*-stilbazole (**B** residue) slightly decreased probably due to photodegradation, the reaction was much slower than photocrosslinking reaction.

(40) Lukin, M.; de los Santos, C. *Chem. Rev.* **2006**, *106*, 607.

(41) Hearst, J. E. *Annu. Rev. Biophys. Bioeng.* **1981**, *10*, 69.

(42) Lee, B. L.; Murakami, A.; Blake, K. R.; Lin, S. B.; Miller, P. S. *Biochemistry* **1988**, *27*, 3197.

(43) Liu, M.; Mao, X. a.; Ye, C.; Huang, H.; Nicholson, J. K.; Lindon, J. C. *J. Magn. Reson.* **1998**, *132*, 125.

4-7 Appendixes

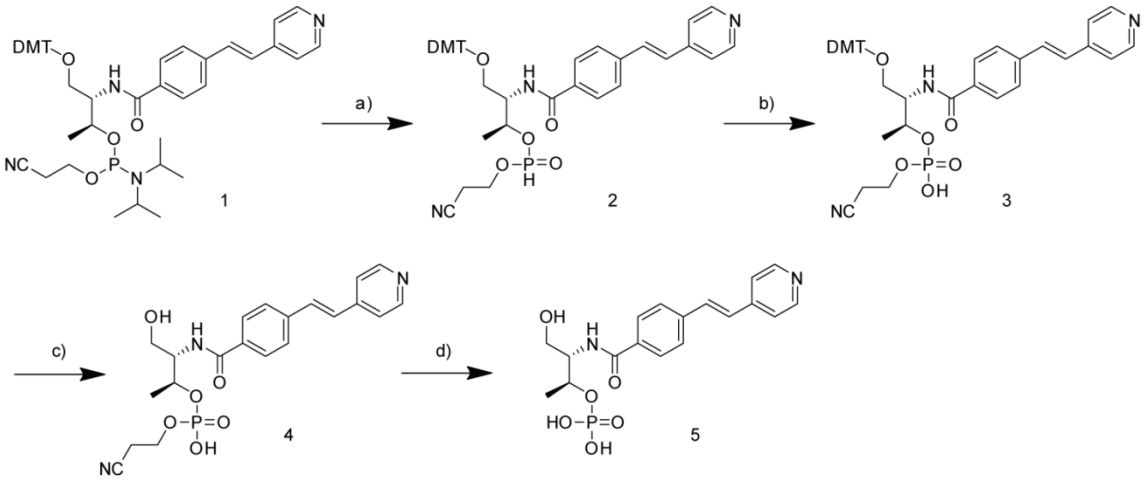

Scheme S4-1. Synthesis of *p*-stilbazole monophosphate. Reagents and conditions: a) 1*H*-tetrazole, CH_3CN, H_2O, rt, overnight.; b) I_2, THF, pyridine, H_2O, rt, 4 days.; c) TFA, rt, 5 minutes.; d) NH_3aq, rt, overnight.

The *p*-stilbazole monophosphate was synthesized as follows:

Compound **1** was synthesized according to the previous report.[1]

Compound **1** (61.1 mg, 0.075 mmol) was dissolved in CH_3CN and 1*H*-tetrazole (0.051 g, 0.728 mmol) in 2ml of CH_3CN was added. Then 8 ml of H_2O was added. After stirring for overnight, 18.5 ml of Oxidizing Solution (0.02 M iodine in THF/pyridine/H_2O, Glen Research) and ammonium hydroxide was added. After 3 days, iodine (0.282g, 1.11 mmol) in THF was added. After stirring for overnight, excessive amount of ammonium hydroxide was added and stirred for 3 hours, followed by partial purification and detritylation conducted on Poly Pak Ⅱ (Glen Research). Ammonium

hydroxide was added to the eluate and laid for overnight. Then the solvent was removed by evaporation, and purified by HPLC. ^{1}H-NMR [D_2O, 500 MHz] δ = 7.82 (d, J = 8.5 Hz, 2H, aromatic protons), 7.71 (d, J = 8 Hz, 2H, aromatic protons), 7.67 (d, J = 8 Hz, 2H, aromatic protons), 7.61 (d, J = 6 Hz, 2H, aromatic protons), 7.52 (d, J = 16.5 Hz, 1H, -C*H*=C*H*- of *trans* isomer), 7.32 (d, 8 Hz, 2H, aromatic protons), 7.28 (d, 16.5 Hz, 1H, -C*H*=C*H*- of *trans* isomer), 7.25 (d, 6 Hz, 2H, aromatic protons), 6.94 (d, 12 Hz, 1H, -C*H*=C*H*- of *cis* isomer), 6.71 (d, 12.5 Hz, 1H, -C*H*=C*H*- of *cis* isomer), 4.46 (m, 2H, -C*H*(CH_3)-OH of *cis*/*trans* isomers), 4.07 (m, 2H, -CH_2C*H*(NH-)- of *cis*/*trans* isomers), 3.77, 3.66 (each m, 2H, -CH_2-OH of *cis*/*trans* isomers), 1.25, 1.23 (each d, 6.5 Hz, 3H, CH_3-CH- of *cis*/*trans* isomers). MS (ESI) Calcd for $C_{18}H_{20}N_2O_6P$ ($M\text{-}H^+$) 391.1059. Found 391.1073.

[1]Kashida, H.; Ito, H.; Fujii, T.; Hayashi, T.; Asanuma, H. *J. Am. Chem. Soc.* **2009**, *131*, 9928.

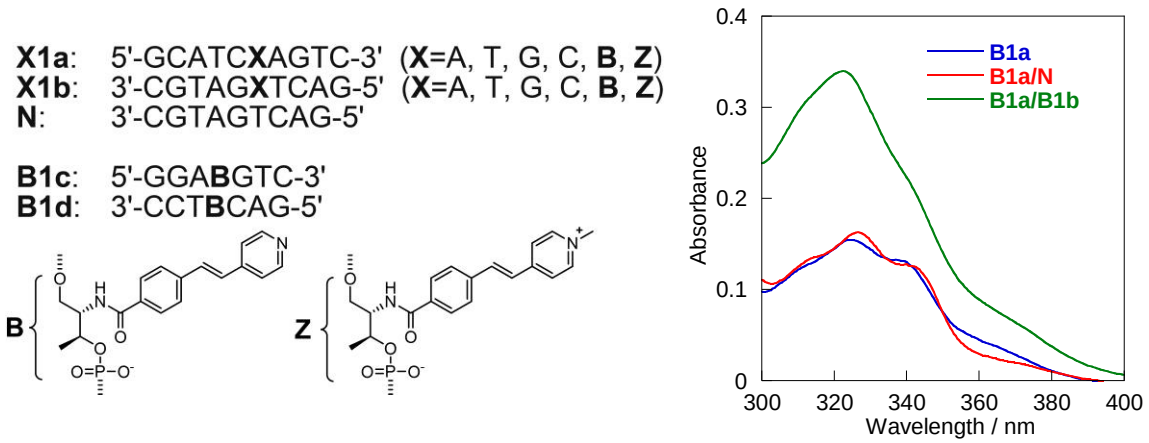

Fig. S4-1. UV-VIS spectra of **Ba**/**Bb**, **Ba/N** and single-stranded **Ba.** Conditions are as follows: [ODN] = 5.0 μM, [NaCl] = 100 mM, pH 7.0 (10 mM phosphate buffer), 20 ^{o}C.

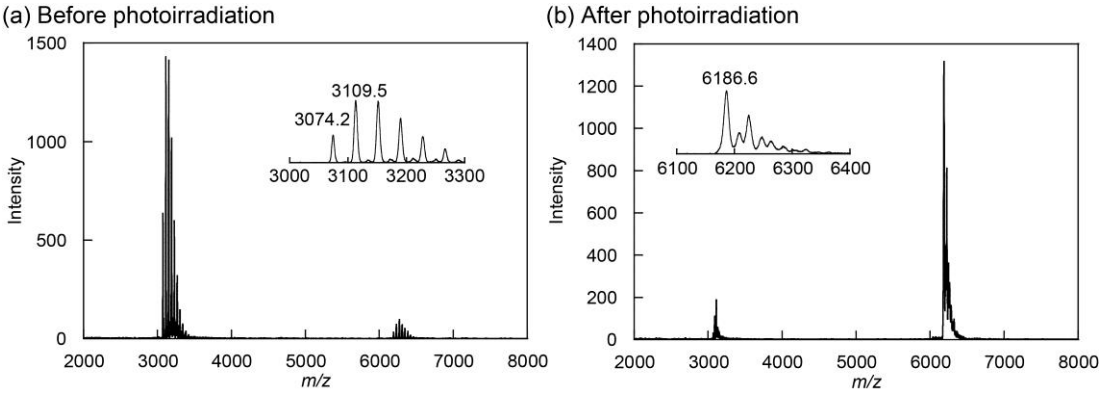

Fig. S4-2. MALDI-TOFMS data of **Ba**/**Bb** (a) before and (b) after photoirradiation. Calculated mass for [**Ba**+H^{+}]:3073, [**Bb**+H^{+}]:3113, [**Ba**/**Bb**+H^{+}]:6184.

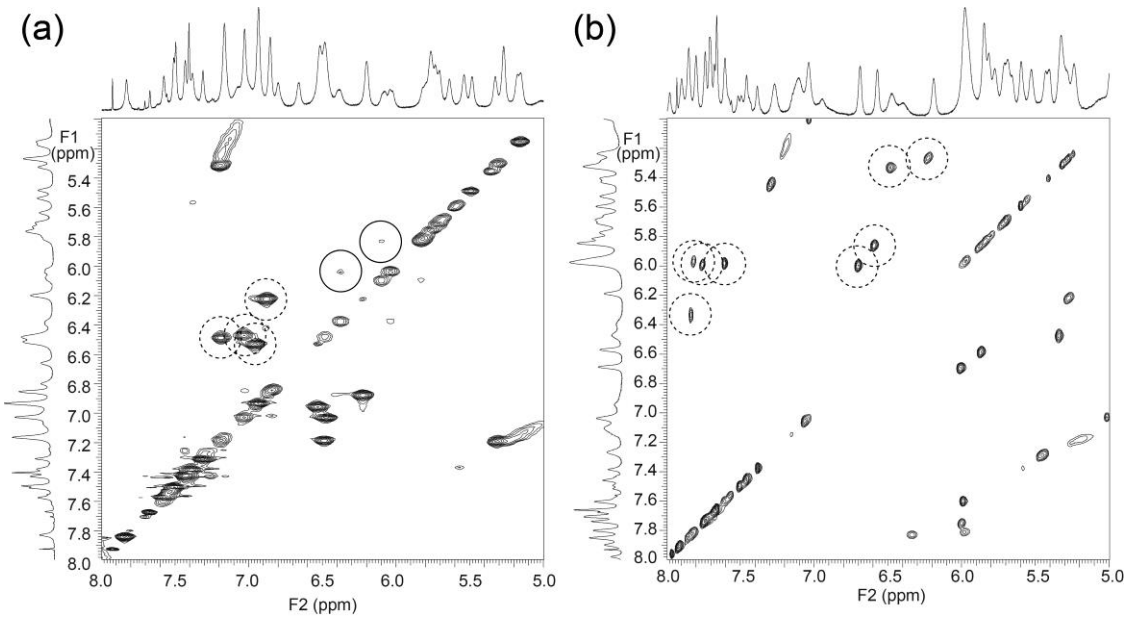

Fig. S4-3. TOCSY spectra in D_2O of **Ba**/**Bb** (a) before and (b) after photoirradiation. Signals between phenyl protons of *p*-stilbazole were marked with dotted circles whereas those between vinyl protons were marked with solid circles.

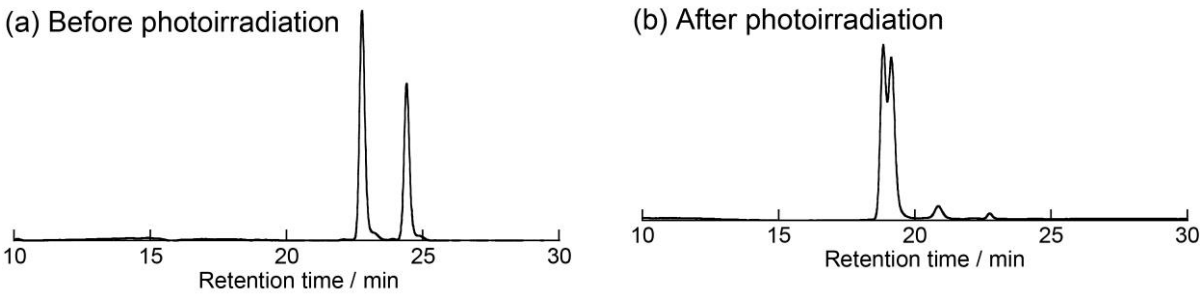

Fig. S4-4. HPLC chromatograms of **Bc**/**Bd** (a) before and (b) after photoirradiation.

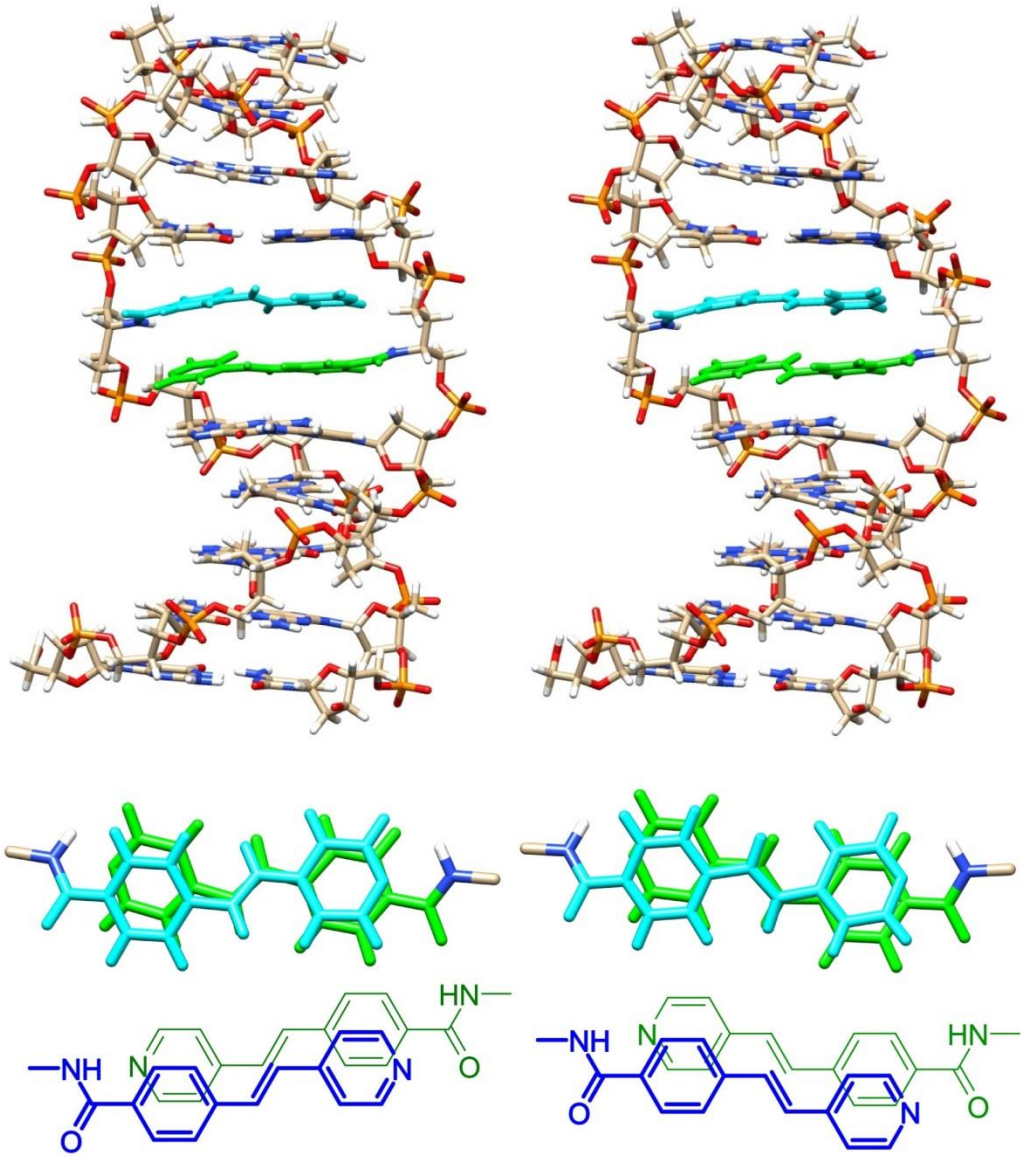

Fig. S4-5. Energy-minimized structures of two conformations of **Ba**/**Bb**, which becomes two diastereomers upon photoirradiation. Relative orientations of *p*-stilbazole moieties are shown at the bottom. The molecular dynamics simulation was conducted by using InsightII/Discover package with amber force-field.

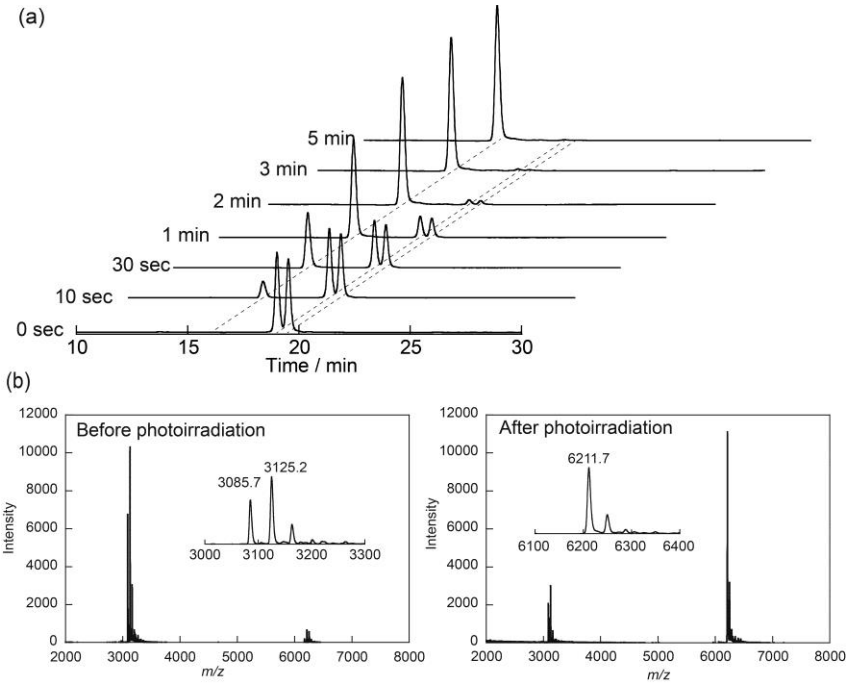

Fig. S4-6. (a) HPLC chromatograms and (b) MALDI-TOFMS charts of **Za**/**Zb** before and after photoirradiation.

(b) Calculated mass for [**Za**+H^+]:3088, [**Zb**+H^+]:3128, [**Za**/**Zb**+H^+]:6215.

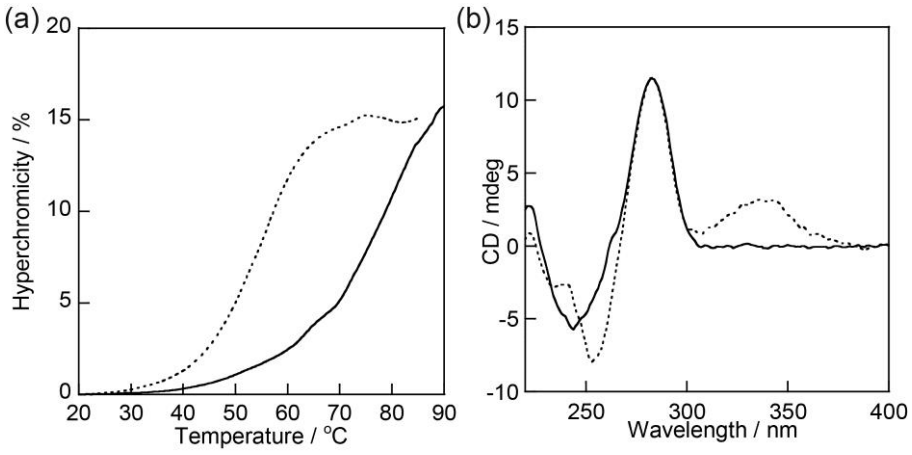

Fig. S4-7. (a) Melting curves and (b) CD spectra of **Za**/**Zb** before (dotted line) and after photoirradiation (solid line). Conditions are as follows: [ODN] = 5.0 □M, [NaCl] = 100 mM, pH 7.0 (10 mM phosphate buffer), 0 °C.

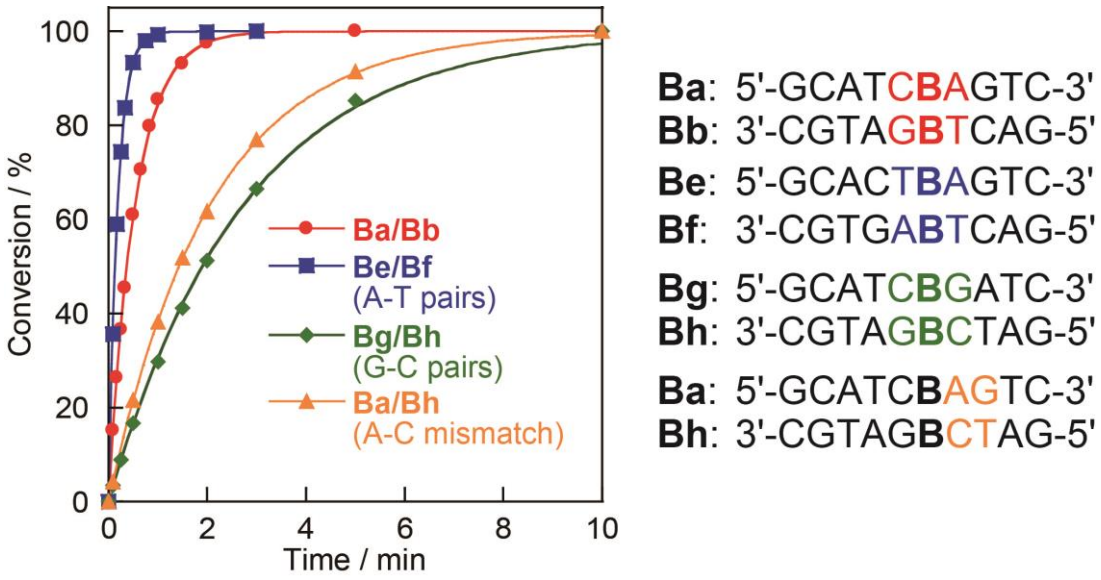

Fig. S4-8. Effects of flanking base pairs on rate constant of photocycloaddition determined from UV-VIS spectra. The first order rate constants were 1.8 (**Ba**/**Bb**), 5.2 (**Be**/**Bf**), 0.3 (**Bg**/**Bh**) and 0.4 min^{-1} (**Ba**/**Bh**). Conditions are as follows: [ODN] = 5.0 □M, [NaCl] = 100 mM, pH 7.0 (10 mM phosphate buffer), 0 ^{o}C.

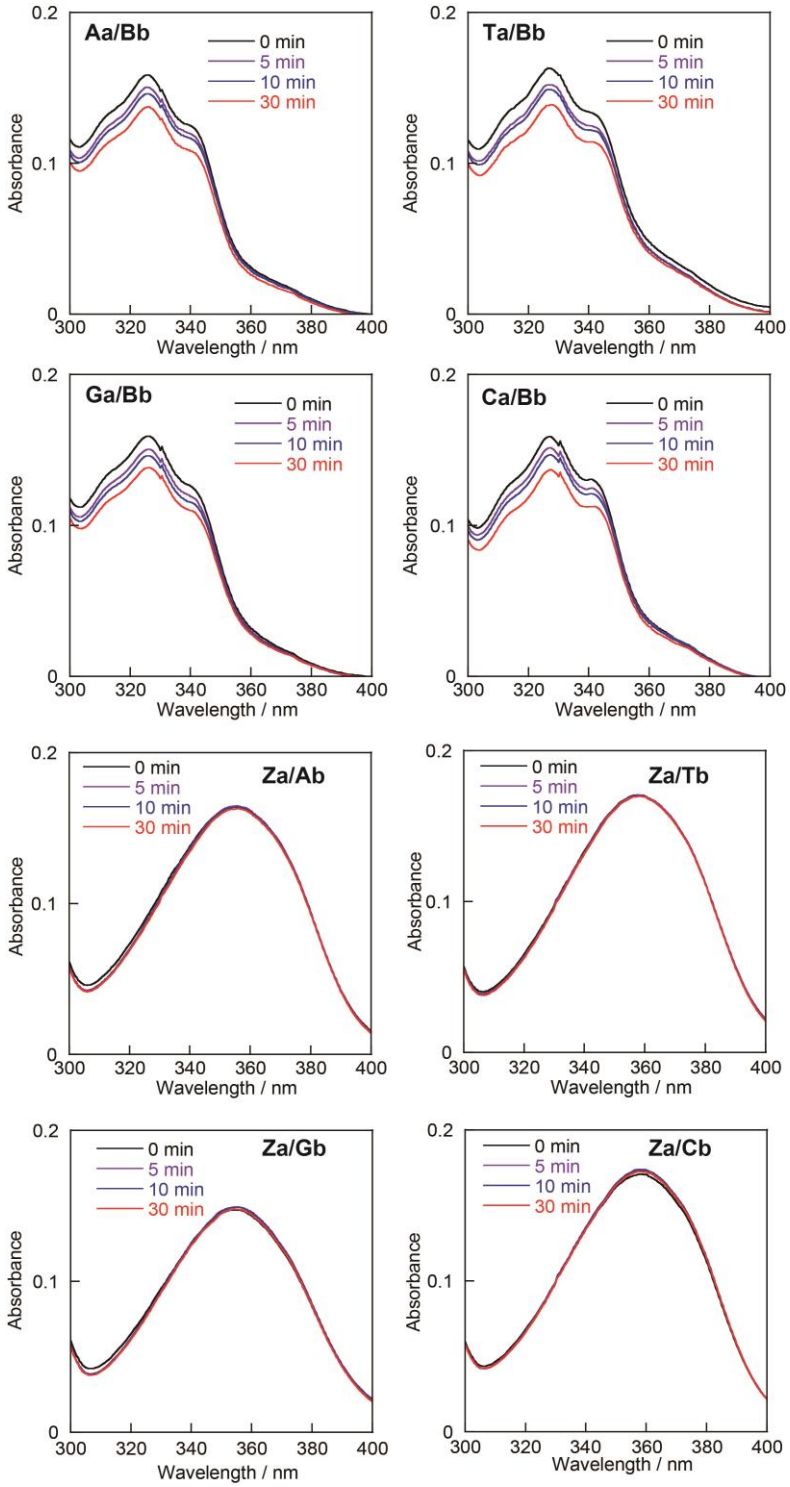

Fig. S4-9. UV-VIS spectra of **Xa**/**Bb** and **Za**/**Xb** duplexes (**X** = A, T, C or C) before and after photoirradiation. Conditions are as follows: [ODN] = 5.0 □M, [NaCl] = 100 mM, pH 7.0 (10 mM phosphate buffer), 0 ^{o}C.

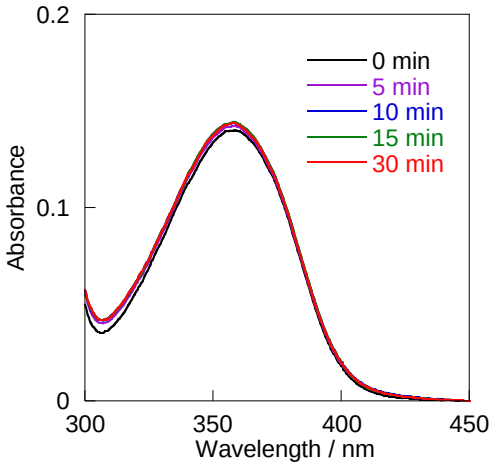

Fig. S4-10. UV-VIS spectra of **Za**/**N** before and after photoirradiation. Conditions are as follows: [ODN] = 5.0 □M, [NaCl] = 100 mM, pH 7.0 (10 mM phosphate buffer), 0 ^{o}C.

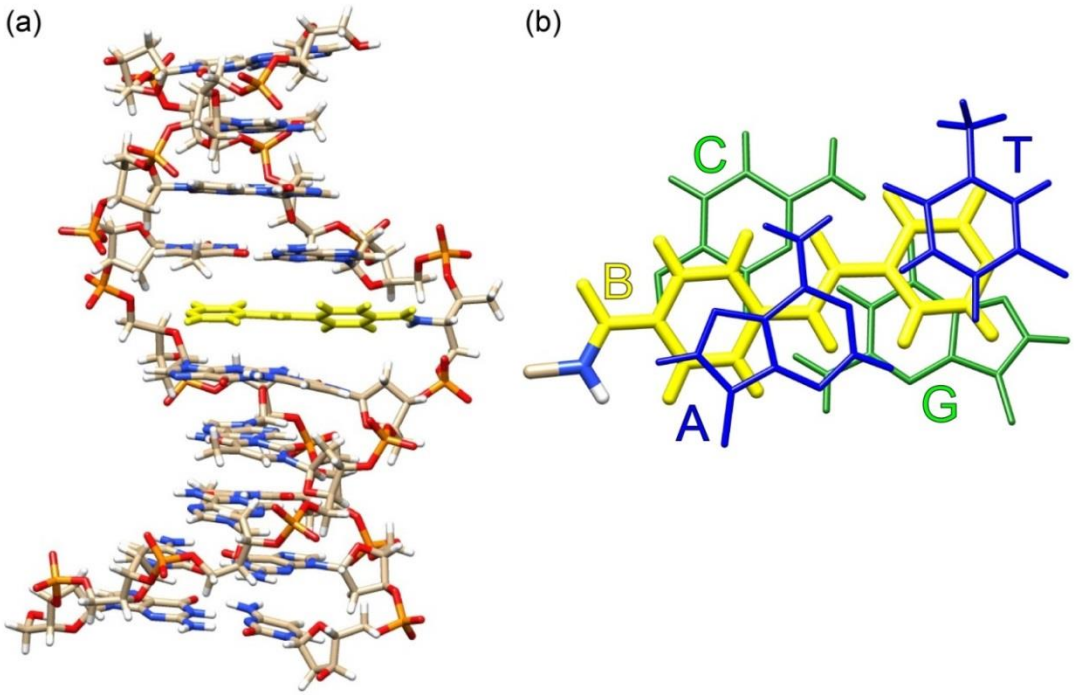

Fig. S4-11. (a) Energy-minimized structures of **Ba**/**N**. Relative orientation of *p*-stilbazole with respect to neighboring base pairs is shown in (b). Neighboring A-T and G-C pairs in (b) are colored in blue and green, respectively. The molecular dynamics simulation was conducted by using InsightII/Discover package with amber force-field.

Display Report

Analysis Info

Analysis Name	D:\Data\Asanuma_lab\sakaki\111212 p-sb mono hikarigo HPLCgo.d	Acquisition Date	12/12/2011 5:47:31 PM
Method	091215_esi_neg_wide.m	Operator	BDAL@DE
Sample Name		Instrument	micrOTOF-Q II 10233
Comment			

Acquisition Parameter

Source Type	ESI	Ion Polarity	Negative	Set Nebulizer	0.4 Bar
Focus	Active	Set Capillary	3500 V	Set Dry Heater	180 °C
Scan Begin	100 m/z	Set End Plate Offset	-500 V	Set Dry Gas	4.0 l/min
Scan End	3000 m/z	Set Collision Cell RF	620.0 Vpp	Set Divert Valve	Source

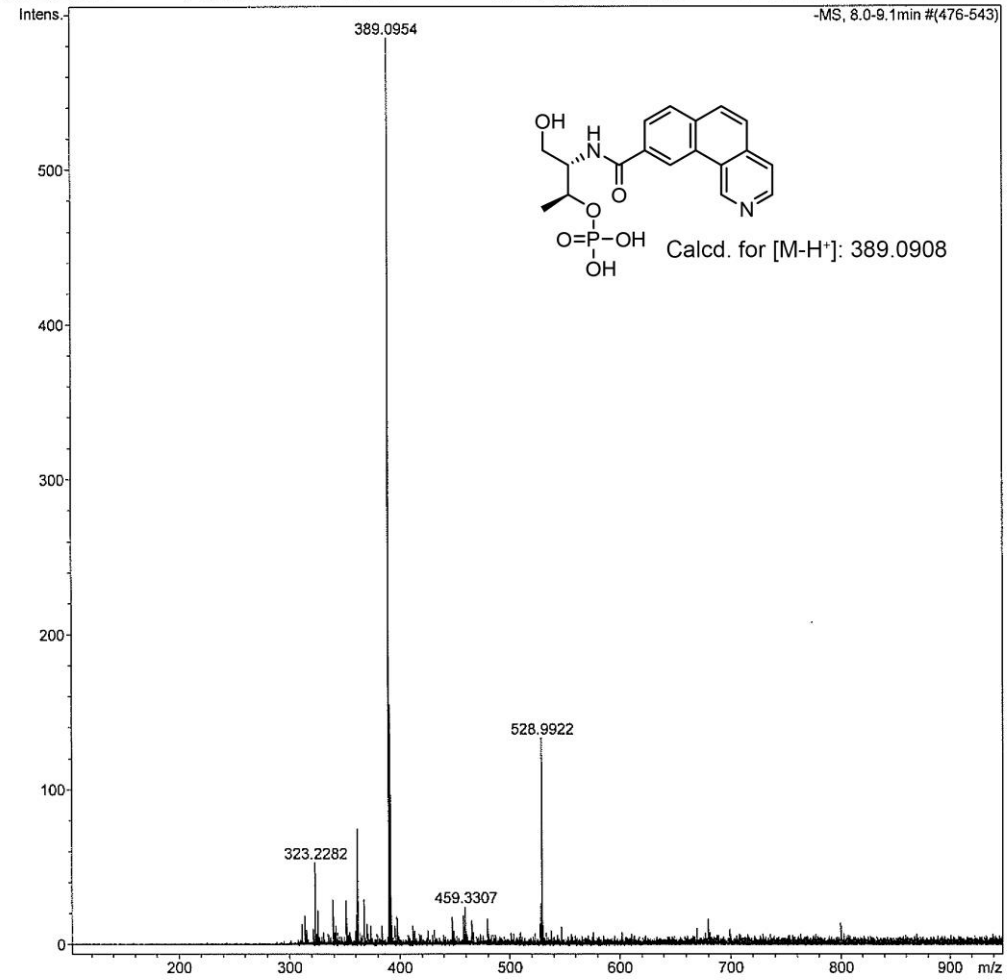

Chapter 5. Analysis of [2+2] photodimerization reactivity of various stilbenes in the context of DNA duplex

5-1 Abstract

A DNA duplex was used as a scaffold to evaluate intrinsic reactivity of [2+2] photodimerization between stilbene derivatives; the duplex pre-organizes the substrates avoiding the need for an association step. Unmodified stilbenes were first introduced at base-pairing positions on complementary DNA strands. The duplex was then irradiated with 340 nm UV light. HPLC analyses revealed that [2+2] photodimerization proceeded rapidly without side reactions. Thus, it was confirmed that the DNA duplex could be used as an ideal scaffold for [2+2] photodimerization of stilbenes. Next, we examined homo-photodimerization abilities of various stilbene derivatives. Homo-photodimerization of *p*-cyanostilbene, *p*-methylstilbazolium, and *p*-stilbazole occurred efficiently, whereas homo-photodimerization of *p*-dimethylaminostilbene and *p*-nitrostilbene did not proceed at all, probably because the reaction was quenched by dimethylamino and nitro groups.

Time-dependent density functional theory calculations revealed that excitation energy was correlated with quantum yield. We further investigated hetero-photodimerization. These reactions were made possible by use of two complementary oligodeoxyribonucleotides tethering different stilbene derivatives. Reactivities in hetero-photodimerization were highly dependent on the combination of derivatives. A high correlation was observed between the quantum yields and energy gaps of HOMO and LUMO between reactive derivatives. Unexpectedly, nitrostilbene, which was non-reactive in homo-photodimerization, cross-reacted with *p*-methylstilbazolium and *p*-stilbazole, both of which had close HOMO or LUMO with nitrostilbene. Evaluation of the intrinsic reactivity of homo- and hetero-photodimerization of stilbene derivatives was made possible by use of DNA as a scaffold.

5-2 Introduction

The [2+2] photodimerization of stilbenes has been of interest since Ciamician and Silver characterized dimerization of *E*-stilbene in 1902.[1] This photodimerization is used for the synthesis of cyclobutane derivatives, in polymer syntheses, and in

crosslinking.[2,3] The effects of concentrations[4] and solvents[5,6] on photodimerization of stilbenes have been evaluated and reactivities of several stilbene derivatives have been investigated.[7] However, since most photo-cycloadditions are conducted under conditions in which stilbene monomers are dispersed in solvent, molecules must form an aggregate (or a cluster) prior to the photoreaction. Hence, reactivities of stilbene derivatives are dependent on the ability of these derivatives to aggregate. Furthermore, monomeric stilbene also undergoes *trans*-to-*cis* photoisomerization, subsequent cyclization and irreversible phenanthrene formation via oxidation. Accordingly, it was very difficult to distinguish "intrinsic" reactivities from propensity to aggregate. Although clusters have been prepared using nanocages or via attractive interactions[8-14], reactivities remain dependent on dimer aggregate formation. Furthermore, to the best of our knowledge, it has not been possible to evaluate hetero stilbene photodimerization (i.e. cross-reaction between the two different derivatives).

Previously we developed a unique method for preparation of a dye assembly within a DNA duplex.[15,16] We utilize D-threoninol as a scaffold for the functional molecule, and this residue can be introduced at any position and in any number in

an oligodeoxyribonucleotide (ODN) or an oligoribonucleotide using standard solid-phase synthesis techniques. Introduction of the base surrogates at base-pairing positions of complementary strands allows controlled dimer aggregate formation within the duplex. Heterodimers are prepared by hybridizing two strands each of which involves a different dye. We demonstrated that azobenzene dimer formation occurs in an anti-parallel manner scaffolded by ODN duplexes using NMR structural analysis. That the duplex containing dimers or higher order aggregates were unwounded relative to an unmodified duplex was shown by circular dichroism analyses.

Here, we utilized an ODN duplex as a scaffold for systematic investigation of [2+2] photodimerization between stilbene derivatives whose photoreactivities have not yet been examined in detail. Introduction of stilbene derivatives into base-paring positions of ODNs via D-threoninol allowed us to firmly fix homo- and heterodimer aggregates before photo-irradiation. Upon 340 nm UV irradiation, the [2+2] photodimerization of stilbene derivatives occurs and duplex is crosslinked (Scheme 5-1). Recently, we examined photodimerization of *p*-stilbazole derivatives to demonstrate that the surrogate via D-threoninol can orthogonally pair with the same surrogate and serve as an artificial base pair for

photo-crosslinking of an ODN duplex.[17] We found that photodimerization proceeds very efficiently in the duplex scaffold without other side reactions such as photoisomerization and subsequent cyclization. This result strongly indicates that photodimerization of these surrogates reflects intrinsic reaction ability. In the present study, we investigated the photodimerization of six derivatives in DNA duplexes.

Their intrinsic reactivities in homo- and hetero-photodimerizations were systematically investigated to identify those factors that affect reactivity. We believe that the results reported here complement theoretical investigations[18] and will contribute to better understanding of [2+2] photo-cycloaddition reactions. This strategy will also provide new tools for photocrosslinking and photoligation that will be used in biotechnology.[19-26]

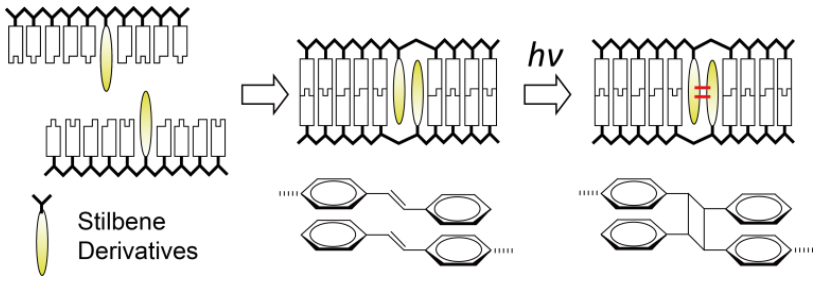

Scheme 5-1. Schematic illustration of [2+2] photodimerization inside a DNA duplex.

5-3 Results and discussions

5-3-1 Photochemical Properties of Stilbene-Modified ODN and Analysis of [2+2] Photo-dimerization of Homodimer Aggregate

Figure 5-1 show the chemical structures of the six stilbene derivatives studied. In the present study, in addition to the previously reported stilbazole derivatives, *p*-stilbazole (**B**) and *p*-methylstilbazolium (**Z**), we have newly synthesized stilbene (**S**) and *p*-cyanostilbene ($\mathbf{S_{CN}}$), the stilbene derivatives that are known to dimerize upon UV photo-irradiation. Moreover, we also synthesized *p*-nitrostilbene ($\mathbf{S_A}$) and *p*-dimethylaminostilbene ($\mathbf{S_D}$); these derivatives have not

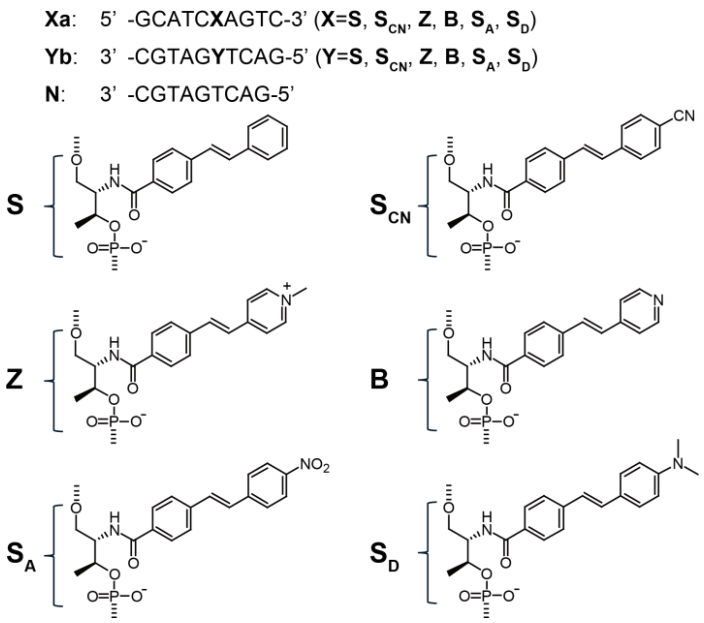

Figure 5-1. Sequences of ODNs synthesized in this study and chemical structures of stilbene derivatives.

been previously characterized. These derivatives were linked to D-threoninols and introduced into an ODN via phosphoramidite chemistry. Sequences of the ODNs are also shown in Figure 5-1. First, we prepared the homodimer aggregate of unmodified stilbene (**S**) that has been conventionally used for examining photodimerization and investigated its intrinsic reactivity. Figure 5-2a shows UV-vis spectra of the homo **Sa**/**Sb** duplex. Before photo-irradiation, **Sa**/**Sb** had an absorption maximum at 322 nm, which was 13 nm shorter than that of a duplex with a single **S** moiety (**Sa**/**N**; 335 nm). This hypsochromic shift indicates that **S** moieties in **Sa**/**Sb** form an H aggregate before photo-irradiation. Similar hypsochromic shifts were observed with all the homodimers examined in this study (Fig. S5-1), demonstrating all derivatives formed a dimer aggregate

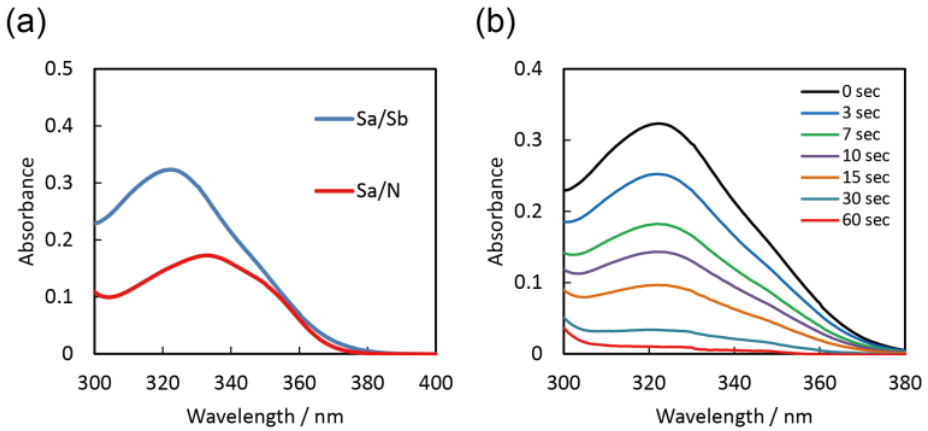

Figure 5-2. UV-vis spectra of **Sa**/**Sb** (blue) and **Sa**/**N** (red). (b) **Sa**/**Sb** before and after indicated duration of UV irradiation (340 nm). Solution conditions were 5.0 μM DNA, 100 mM NaCl, 10 mM phosphate buffer (pH 7.0), 20 ^{o}C.

scaffolded by the DNA duplex before photo-irradiation. The absorption band rapidly decreased as a function of irradiation time, and after 1 min, the absorption band of **S** had completely disappeared (Fig. 5-2b). This disappearance of the π-π* band strongly indicated that the [2+2] photodimerization occurred between the two stilbene residues.

The photodimerization reaction was further analyzed by HPLC (Fig. 5-3). Before photo-irradiation, two peaks that corresponded to the single-stranded **Sa** and **Sb** were observed. After 3 min irradiation, the two peaks completely disappeared and a new single peak appeared at a shorter retention time. MALDI-TOF MS analysis confirmed that this new peak was a crosslinked **Sa**/**Sb** duplex (Fig. S5-2). This result unambiguously demonstrates that the duplex was crosslinked via [2+2] photodimerization of **S** without any side photoreaction. The

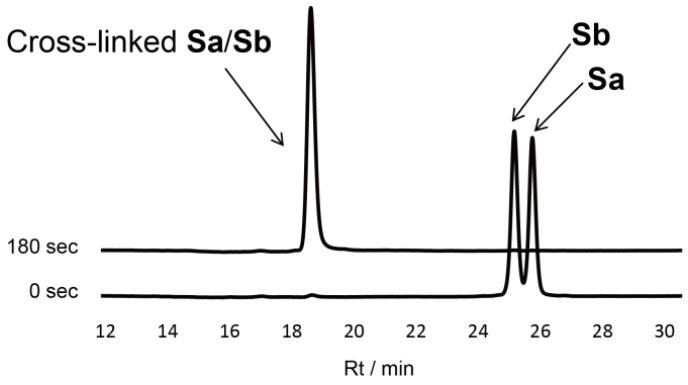

Figure 5-3. HPLC chromatograms of **Sa**/**Sb** under conditions that denature the duplex before and after 180 sec UV photo-irradiation (340 nm).

peak may involve two diastereomers, derived from rotation of stilbenes as we previously reported.[17]

We also investigated thermal stability of the DNA duplex before and after photodimerization. Before photo-irradiation, the T_m of **Sa**/**Sb** was 42.4 °C (Fig. S5-3). And after photo-irradiation, the T_m increased to more than 80 °C, confirming that the duplex is crosslinked. From these results, we concluded that [2+2] photodimerization of stilbene occurred within the ODN duplex scaffold and that *trans*-to-*cis* photoisomerization and subsequent cyclization were completely suppressed.

5-3-2 Photodimerizations of Homodimer Aggregates of *p*-Cyanostilbene and *p*-Nitrostilbene

Next, we investigated [2+2] homo-photodimerization of stilbene derivatives $\mathbf{S_{CN}}$ and $\mathbf{S_A}$ with electron-withdrawing substituents. The UV-vis spectra of the duplexes tethering these moieties, $\mathbf{S_{CN}a}$/$\mathbf{S_{CN}b}$ and $\mathbf{S_Aa}$/$\mathbf{S_Ab}$, are shown in Fig. 5-4. Before photo-irradiation, absorption maximum at 329 nm and 364 nm were observed for $\mathbf{S_{CN}}$ and $\mathbf{S_A}$, respectively. Upon photo-irradiation of $\mathbf{S_{CN}a}$/$\mathbf{S_{CN}b}$, the band at 329 nm rapidly decreased and the band completely disappeared after 5 min of irradiation (Fig. 5-4a), which indicates that

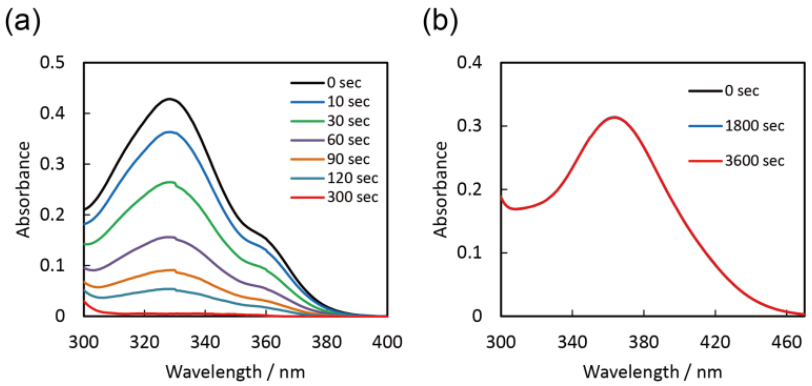

Figure 5-4. UV-vis spectra of (a) $\mathbf{S_{CN}a}$/$\mathbf{S_{CN}b}$ and (b) $\mathbf{S_Aa}$/$\mathbf{S_Ab}$ before and after indicated duration of UV irradiation (340 nm). Solution conditions were 5.0 μM DNA, 100 mM NaCl, 10 mM phosphate buffer (pH 7.0), 20 °C. Note that UV spectra in (b) after 0 sec and 1800 sec overlap with that after 3600 sec almost completely.

[2+2] photodimerization of $\mathbf{S_{CN}}$ occurred. This photodimerization was further confirmed by HPLC and MALDI-TOF (Figs. S5-4, S5-5). In contrast, photo-irradiation of $\mathbf{S_Aa}$/$\mathbf{S_Ab}$ did not cause any change in the spectrum (Fig. 5-4b), indicating that *p*-nitrostilbene did not photodimerize.

5-3-3 Photodimerization of *p*-Dimethylaminostilbene

We then investigated photodimerization of a stilbene derivative modified with an electron donating group, $\mathbf{S_D}$; the photodimerization behavior of this derivative has not been previously analyzed. The pK_a of the dimethylamino group of $\mathbf{S_D}$ is around 7; therefore, we investigated the photodimerization of $\mathbf{S_D}$ in both deprotonated (pH 9) and protonated (pH 5) states. At pH 9, the absorption

maximum appeared at 370 nm, and the peak shifted to 321 nm at pH 5 due to deconjugation resulting from protonation of the dimethylamino group. After 5 min of 340 nm irradiation of $\mathbf{S_Da}$/$\mathbf{S_Db}$ at pH 9, no change was observed in the band (Fig. 5-5a), demonstrating that *p*-dimethylaminostilbene, like *p*-nitrostilbene, did not photodimerize. In striking contrast, when the protonated $\mathbf{S_Da}$/$\mathbf{S_Db}$ duplex (pH 5) was irradiated, the band at 321 nm rapidly decreased (Fig. 5-5b). Photodimerization was also confirmed by HPLC and MALDI-TOF MS analyses; no undesired photoreaction products were observed (Figs. S5-6, S5-7). Thus, *p*-dimethylaminostilbene does not undergo [2+2] photodimerization in the deprotonated state but efficiently photodimerizes in protonated state.

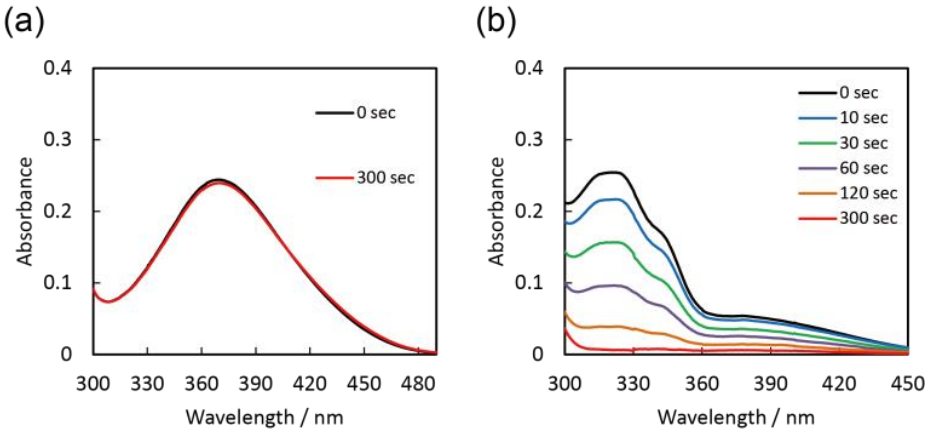

Figure 5-5. UV-vis spectra of (a) $\mathbf{S_Da}$/$\mathbf{S_Db}$ at pH 9.0 (10 mM Tris buffer) and (b) $\mathbf{S_Da}$/$\mathbf{S_Db}$ at pH 5.0 (10 mM MES buffer) before and after indicated duration of UV irradiation (340 nm). Solution conditions were 5.0 μM DNA, 100 mM NaCl, 20 ^{o}C.

5-3-4 Quantitative Comparison of the Reactivities of Homodimer Aggregates by Quantum Yield

In order to compare intrinsic reactivities of these stilbene derivatives quantitatively, we evaluated quantum yields of homo-photodimerization by using the chemical actinometry method (Table 5-1 and Fig. 5-6). Quantum yields of *p*-methylstilbazolium (**Z**) and *p*-stilbazole (**B**) are also shown. Among the six stilbene derivatives, unsubstituted stilbene showed the highest quantum yield, Φ = 0.15. This quantum yield was lower than that of stilbene monomer in benzene solution reported previously (Φ= 0.33)[4]. The lowered quantum yield in the duplex may be attributed to the difference of the solvents or to the quenching by

Table 5-1. Photochemical properties and quantum yields of homodimers of stilbene derivatives.

Sequence	$\lambda_{max}{}^{a}$/ nm	$T_m{}^{b}$/ °C	HOMO^{c}/ eV	LUMO^{c}/ eV	$\Delta E^{c,d}$/ eV	Φ ($\times 10^2$)
Sa/Sb	322	42.4	−6.05	−1.72	4.33	15
S_{CN}a/S_{CN}b	329	53.8	−6.28	−2.16	4.12	2.2
Za/Zb	342	51.5	−6.81	−2.98	3.83	1.7
Ba/Bb	322	46.4	−6.39	−1.99	4.40	2.4
S_Da/S_Db(H^+)^{e}	321	37.5	−6.33	−2.05	4.28	3.6
S_Da/S_Db^{f}	370	36.7	−5.17	−1.51	3.66	N/A
S_Aa/S_Ab	364	58.1	−6.37	−2.61	3.76	N/A

[a]Absorption maximum in UV-vis spectrum. [b]Melting temperature of duplex before photo-irradiation. [c]TD-DFT calculation values from pbe1pbe/6-31G*, solvent: water. [d]Difference in energies between LUMO and HOMO. [e]Measured at pH 5. [f]Measured at pH 9.

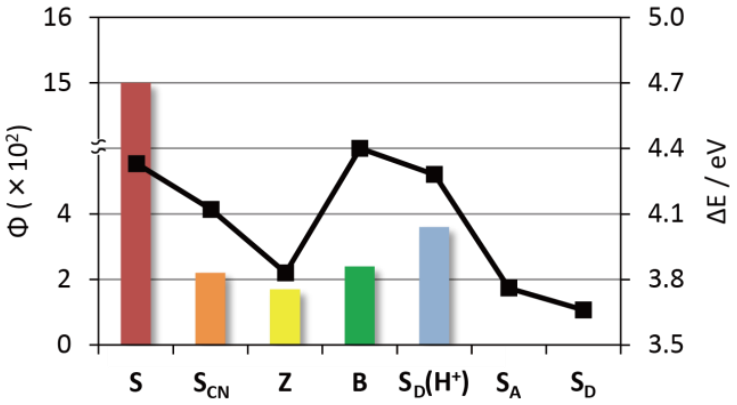

Figure 5-6. Quantum yields of homo-photodimerizations (bar graph) and calculated excitation energies (line graph). $\Delta E=E_{LUMO}-E_{HOMO}$.

adjacent nucleotides (*vide infra*). Protonated $\mathbf{S_D\,(H^+)}$ showed the second highest quantum yield (0.036); **B**, **Z**, and $\mathbf{S_{CN}}$ showed almost the same quantum yields (0.024, 0.017 and 0.022, respectively). In contrast, homodimer aggregates of both $\mathbf{S_A}$ and $\mathbf{S_D}$ did not undergo photodimerization reaction at all; their quantum yields were nil. Thus, quantum yields of homo-photodimerization are highly dependent on substituents.

In order to elucidate the factors that determine reactivities of homo-photodimerization of stilbene derivatives, we measured or calculated several photochemical properties, which are listed in Table 5-1. There was no correlation between quantum yields and T_ms of duplexes. For instance, $\mathbf{S_{CN}a/S_{CN}b}$ had a higher T_m (53.8 ˚C) than **Sa**/**Sb** (42.4 ˚C), likely due to facilitated stacking interaction by the electron-withdrawing cyano group;

however, the quantum yield of $\mathbf{S_{CN}a}$/$\mathbf{S_{CN}b}$ was far lower than that of **Sa**/**Sb**. Since the photodimerization reaction was conducted at 20 ^{o}C, T_m may not affect the reaction as all duplexes should have been stable at this temperature. Interestingly, however, we did observe a distinct correlation between quantum yield and excitation energy (ΔE = LUMO-HOMO); the derivatives with higher ΔE showed higher quantum yields, except for $\mathbf{S_A}$ and $\mathbf{S_D}$ (*vide infra*). For example, the **S** moiety, which had the highest quantum yield of derivatives evaluated, also had among the highest ΔE values. Caldwell predicted that high singlet energies are favorable for photodimerization.[18, 27] Our experimental results agree with this prediction except for derivative **B**: the quantum yield of **Ba**/**Bb** was lower than that of **Sa**/**Sb**, whereas its ΔE was higher than that of **S**. Protonation of pyridine ring of **B** at pH 7 may affect the photodimerization efficiency.[28]

As we noted above, quantum yield of photodimerization of unmodified stilbene in the duplex was lower than that in the benzene solution. We hypothesize that the lower efficiency in the duplex is due to quenching by the adjacent bases as quenching of fluorophores by electron transfer from nucleobases, especially guanine, has been previously observed.[29] In order to investigate effects of the base neighboring the stilbene derivatives, ODNs

tethering **S**, **B**, and **Z** moieties flanked by AT pairs were synthesized. The quantum yields for these modified duplexes were higher than those from duplexes with GC pairs neighboring the stilbene derivatives (Table S5-1), indicating that neighboring guanine quenched the excited state and inhibited the photodimerization. Though this quenching might affect the photochemical reaction in DNA duplex, quantum yields remained in the same order (**S** > **B** > **Z**), irrespective of neighboring nucleobase. So, we concluded that the qualitative analysis of the photoreactivities was not affected by the flanking native base pairs.

$\mathbf{S_A}$ and $\mathbf{S_D}$ did not undergo photodimerization within the DNA duplex scaffold, which can be explained by quenching of the excited state by nitro and dimethylamino substituent groups.[30] In the case of $\mathbf{S_D}$, an electron on the dimethylamino group would be intramolecularly transferred to form an intramolecular charge transfer state after photo excitation, and this would suppress the dimerization reaction. Intramolecular electron transfer quenches fluorescence of dyes substituted with the dimethylamino group.[31] Consistently, protonation of dimethylamino group ($\mathbf{S_D(H^+)}$, see Fig. 5-6) allowed

photodimerization (quantum yield increased from nil to 0.036), which strongly supports our hypothesis.

According to Rullière et al., photo-excited 4-dimethylamino-4'-nitrostilbene undergoes fast rotation of nitro group, which facilitates non-radiative decay of excited state.[32] In the case of $\mathbf{S_A}$, which has a nitro group at the *para*-position, similar fast rotation of nitro group likely resulted in non-radiative decay from an excited state and suppressed photodimerization. For other stilbene derivatives, quantum yields of photodimerization correlated strongly with ΔE values, although further theoretical investigations are required to validate the proposed mechanism.

5-3-5 Cross-photodimerizations of Heterodimer Aggregates

Next, we investigated hetero [2+2] photodimerization, that is, photodimerization between different stilbene derivatives, using the DNA duplex as a scaffold to place different derivatives in proximity (Scheme 5-2). Cross-photoreactivity between the different stilbene derivatives has not yet been reported due to the difficulty in preparing the pre-organized heterodimer aggregate. With our ODN strategy, heterodimer aggregates can be easily prepared

Scheme 5-2. Schematic illustration of hetero [2+2] photodimerization using DNA duplex as a scaffold.

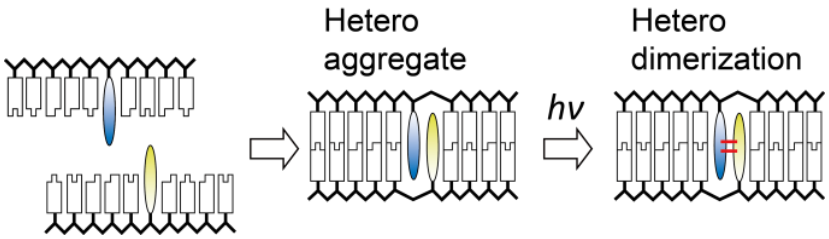

by hybridization of complementary DNA strands tethering different dyes. Here, reactivities of hetero [2+2] photodimerization of combinations of the six stilbene derivatives were systematically investigated by combining two complementary ODNs, each of which tethered a different stilbene derivative. We monitored photodimerization between different derivatives using UV-vis spectroscopy upon 340 nm UV irradiation (Figs. S5-10-S5-16); calculated quantum yields are summarized in Table 5-2.

5-3-6 Cross-photodimerization among the Reactive Derivatives

Cross-dimerization proceeded for all combinations of "reactive" derivatives (**S**, **S_{CN}**, **B**, **Z**, **S_D(H+)**), although their reactivities significantly depended on the counterpart. For instance, reactivity with **S** was in the order of **S/S** > **S/S_{CN}**> **S/$S_D(H^+)$** > **S/B** > **S/Z** (see first column and first row of Table 5-2). Interestingly,

Table 5-2. Photochemical properties and quantum yields of homodimers of stilbene derivatives.

Y \ X	Φ ($\times 10^2$)						
	S	**S_{CN}**	**Z**	**B**	**S_A**	**S_D**[a]	**$S_D(H^+)$**[b]
S	15	7.9	0.08	2.4	N/A	N/A	6.0
S_{CN}	8.9	2.2	0.89	2.0	N/A	N/A	2.8
Z	N/A	0.14	1.7	1.4	0.02	N/A	0.18
B	2.8	1.3	1.6	2.4	0.01	N/A	0.28
S_A	N/A	N/A	0.08	0.04	N/A	N/A	N/A
S_D[a]	N/A	N/A	N/A	N/A	N/A	N/A	—
$S_D(H^+)$[b]	4.5	1.1	0.36	0.31	N/A	—	3.6

[a]Absorption maximum in UV-vis spectrum. [b]Melting temperature of duplex before photo-irradiation. [c]TD-DFT calculation values from pbe1pbe/6-31G*, solvent: water. [d]Difference in energies between LUMO and HOMO. [e]Measured at pH 5. [f]Measured at pH 9.

the order was completely different in the series of **Z** combination: The order of reactivity was **Z/Z** > **Z/B** > **Z/S_{CN}** > **Z/$S_D(H^+)$** > **Z/S**. This tendency was entirely different from the reactivities in homo combinations, in which **S/S** showed the highest reactivity (Table 5-2). The reactivity order of photodimerizaton was highly correlated with the energy gap of the frontier orbitals between the derivatives but was not correlated with T_ms (Table S5-2). Figure 5-7a shows the quantum yields of photodimerizations and energy gaps of frontier molecular orbitals between **S** and each derivative (ΔHOMO or ΔLUMO). There were significant correlations between the quantum yields and ΔHOMO and ΔLUMO. The **S/S** homo combination with no energy gap showed the highest quantum yield,

whereas the **S**/**Z** pair with the largest energy gap showed the smallest quantum yield. Similar trends were also observed in the reactivities of $\mathbf{S_{CN}}$ combination as shown in Fig. 5-7b. Except for the $\mathbf{S_{CN}}$/**S** combination, lower energy gaps were correlated with higher cross-reactivities. The relatively high reactivity of **S** may result from a high excitation energy of **S** or from less electron transfer from native nucleobases to this derivative.

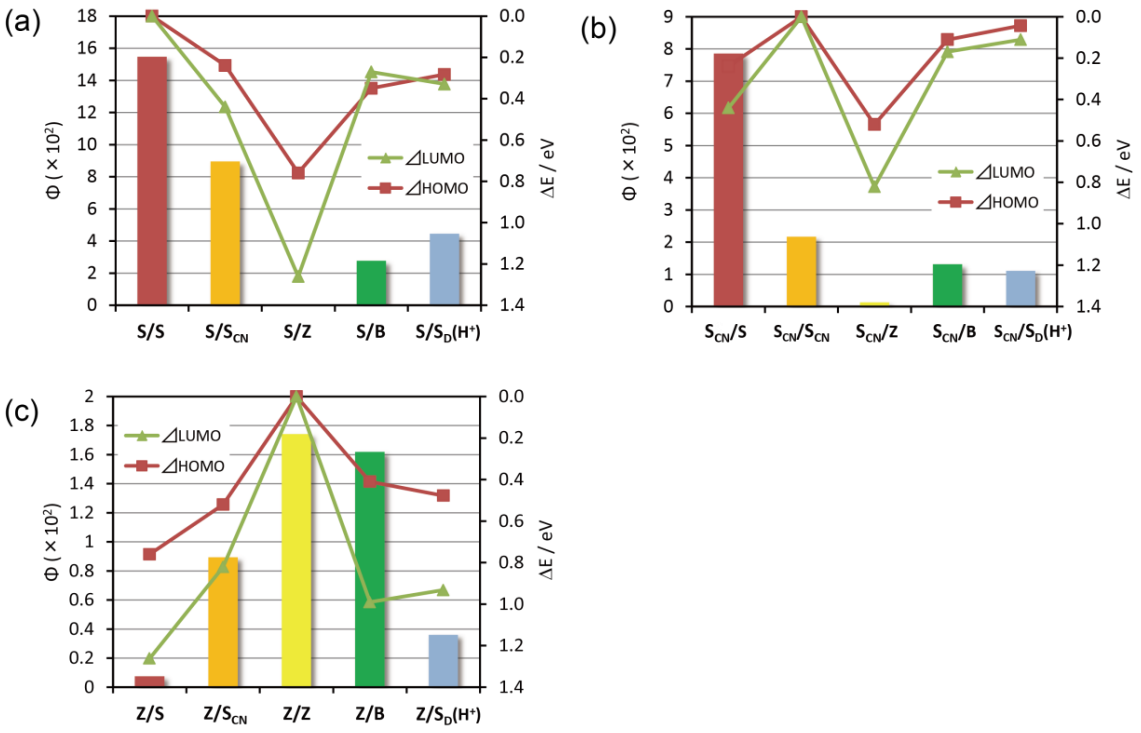

Figure 5-7. Quantum yields of photodimerizations of (a) **Sa**/**Yb**, (b) $\mathbf{S_{CN}}$**a**/**Yb**, (c) **Za**/**Yb** (**X, Y=S**, **Z**, $\mathbf{S_{CN}}$ **B**, $\mathbf{S_D(H^+)}$) duplexes (bar graphs) and energy gaps of HOMO or LUMO (line graphs). The energy gaps are displayed in absolute value and the axis is inverted.

In striking contrast to **S** and $\mathbf{S_{CN}}$, **Z** showed the lowest quantum yield with **S**, although **S** showed the highest reactivity among homo combinations (Figure 5-7c). **Z** showed the highest quantum yield with **Z** in complementary strand. The reactivities of **Z** also correlated with energy gaps. Derivatives **B** and $\mathbf{S_D(H+)}$ showed similar correlations between quantum yields and energy gaps (Figs. S5-17, S5-18). These results strongly indicate that the energy gap between the two stilbene derivatives is an important factor determining reactivity of heterodimerizations. Small energy gap is favorable for effective photodimerization, and *vice versa*. Contributions of these frontier orbitals to the reactivity of photodimerization seem reasonable, because both HOMO and LUMO of each stilbene may interact intermolecularly for [2+2] photodimerizations.[33]

5-3-7 Cross-reactivity of Non-reactive Nitro- or Dimethylaminostilbenes with Other Reactive Derivatives

Neither $\mathbf{S_A}$ nor $\mathbf{S_D}$ underwent homo-photodimerizaiton. Surprisingly, however, both **B** and **Z** cross-reacted with inactive $\mathbf{S_A}$ (Fig. 5-8), although the quantum

yield was below 10^{-3} and very small amounts of side products were observed by HPLC (Figs. S5-19, S5-20). In contrast, $\mathbf{S_D}$ did not cross-react with any of the

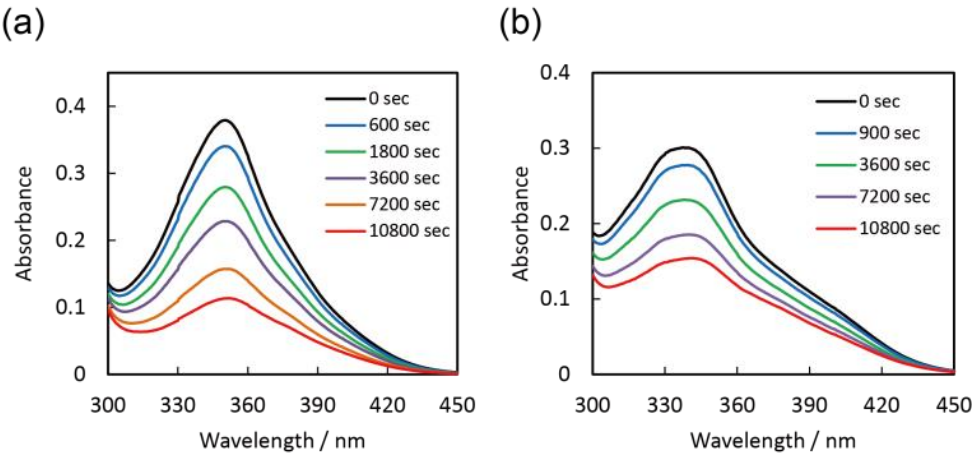

Figure 5-8. UV-vis spectra of (a) $\mathbf{S_A}$**a**/**Zb** and (b) $\mathbf{S_A}$**a**/**Bb** before and after indicated duration of UV irradiation (340 nm) time. Solution conditions were 5.0 μM DNA, 100 mM NaCl, 10 mM phosphate buffer (pH 7.0), 20 °C.

stilbene derivatives. These cross-reactivities cannot be explained simply by the energy gap of HOMO or LUMO.

Irradiation with 340 nm light excites the stilbene derivative either in strand "a" or "b" in the heterodimer aggregate because all the derivatives absorb at 340 nm. For example, irradiation of **X**/$\mathbf{S_D}$ excites either **X** or $\mathbf{S_D}$, but not both simultaneously, to afford either **X***/$\mathbf{S_D}$ or **X**/$\mathbf{S_D}$*. In both cases, the excited state should be quenched by inter- or intra-molecular charge transfer from dimethylamino group. Accordingly, the heterodimer aggregate with $\mathbf{S_D}$ does not undergo photodimerization irrespective of the energy gap of HOMO or LUMO.

But in the case of a $\mathbf{S_A}$ heterodimer aggregate, the decay path of $\mathbf{X^*/S_A}$ is different from that of $\mathbf{X/S_A^*}$. In the $\mathbf{X/S_A^*}$ state, $\mathbf{S_A}$* should non-radiatively decay in the same manner as it would in a $\mathbf{S_A}$ homodimer aggregate; fast rotation of the nitro group will result in non-radiative decay from an excited state and suppressed photodimerization. However, excited **X*** in $\mathbf{X^*/S_A}$ cannot be quenched by the fast rotation of nitro group. Resonance energy transfer (i.e. the energy transfer from the excited species to the unexcited one) might facilitate rapid migration between $\mathbf{X^*/S_A}$ and $\mathbf{X/S_A^*}$, and some of $\mathbf{X^*/S_A}$ may be decayed non-radiatively via conversion to $\mathbf{X/S_A^*}$. In the $\mathbf{X^*/S_A}$ state, however, formation of the cyclobutane ring can occur. **Z** and **B** were both reactive with $\mathbf{S_A}$ because either HOMO or LUMO levels were close; ΔHOMO of $\mathbf{B/S_A}$ and ΔLUMO of $\mathbf{Z/S_A}$ were 0.02 and 0.37 eV, respectively. Accordingly, **B** and **Z** cross-photodimerized with $\mathbf{S_A}$ although their intrinsic reactivities were far smaller than that of **S**.

At present, we cannot propose a clear intermediate or pathway for the photodimerization reactions of these stilbene derivatives. The intermediate electronic state of the radical ion pair as depicted in Fig. S5-21 is also possible.

[34,35] Theoretical calculations and ultrafast spectroscopic measurements will provide important clues to understanding these interesting phenomena.

5-4 Conclusions

We have successfully developed a new methodology to evaluate the [2+2] photodimerization reactivities of various stilbene derivatives by using a DNA duplex as a scaffold. When a duplex tethering a stilbene pair at its center was irradiated with 340 nm UV light, photodimerization occurred rapidly. UV-vis and HPLC analyses revealed that photodimerization proceeded selectively and no side reactions occurred. Protonated *p*-dimethylaminostilbene and *p*-cyanostilbene also dimerized upon photo-irradiation, whereas *p*-nitrostilbene and deprotonated *p*-dimethylaminostilbene were inactive. Time-dependent density functional theory calculations indicated that excitation energy is correlated with efficient homo-photodimerization. Homo-photodimerization of *p*-dimethylaminostilbene and *p*-nitrostilbene probably did not proceed due to quenching by dimethylamino and nitro groups, respectively. We also investigated the reactivity of hetero-dimerization controlled by hybridizing DNA strands tethering different derivatives. The quantum yields of hetero-dimerization showed excellent correlation with the energy gaps of frontier molecular orbitals. Furthermore, we have unexpectedly found that non-reactive nitrostilbene could photodimerize with stilbazole or methylstilbazolium. This observation will lead to further

experimental and theoretical mechanistic studies and this strategy should prove useful for photocrosslinking and photoligation in biotechnology applications. Although photocycloadditions are extensively applied in biological fields such as crosslinking of nucleic acids[36,37], their detailed reactivities between nucleobases and crosslinkers are still not known. Our results on hetero-photodimerization might illustrate their reactivities by focusing on energy gaps of HOMO or LUMO between nucleobases and crosslinkers.

5-5 Experimental section

Materials

All conventional phosphoramidite monomers, CPG columns, and reagents for DNA synthesis were purchased from Glen Research. Other reagents for the syntheses of phosphoramidite monomers were purchased from Tokyo Chemical Industry, Wako, and Aldrich. Unmodified ODNs were purchased from Integrated DNA Technologies.

Synthesis of ODNs

All the modified ODNs were synthesized on an automated DNA synthesizer (H-8-SE, Gene World) by using phosphoramidite monomers bearing **S**, $\mathbf{S_{CN}}$, **Z**, **B**, $\mathbf{S_A}$, or $\mathbf{S_D}$. Syntheses of phosphoramidite monomers **B** and **Z** were reported previously.[17] **S**, $\mathbf{S_{CN}}$, $\mathbf{S_A}$, and $\mathbf{S_D}$ were synthesized as described in the Appendix Information. Samples were handled under dark to avoid photoreaction in ambient light. After workup, ODNs were purified by reversed phase HPLC and characterized using a matrix-assisted laser desorption ionization time-of-flight mass spectrometer (MALDI-TOF; Autoflex II, Bruker Daltonics). MALDI-TOF MS data for the synthesized ODNs: **Sa**, obsd 3071 (calcd for [**Sa** + H^+], 3072); **Sb**, obsd 3111 (calcd for [**Sb** + H^+], 3111); $\mathbf{S_{CN}a}$, obsd 3098 (calcd for [$\mathbf{S_{CN}a}$ + H^+], 3097); $\mathbf{S_{CN}b}$, obsd 3137 (calcd for [$\mathbf{S_{CN}b}$ + H^+], 3136); $\mathbf{S_Aa}$, obsd 3117 (calcd for [$\mathbf{S_Aa}$ + H^+], 3116); $\mathbf{S_Ab}$, obsd 3157 (calcd for [$\mathbf{S_Ab}$ + H^+], 3157); $\mathbf{S_Da}$, obsd 3114 (calcd for [$\mathbf{S_Da}$ + H^+], 3115); $\mathbf{S_Db}$, obsd 3155 (calcd for [$\mathbf{S_Db}$ + H^+], 3155).

Spectroscopic Measurements

UV-vis spectra were measured on a JASCO model V-560 equipped with a programmable temperature controller; 10-mm quartz cells were used.

Measurement of the Melting Temperature

The melting curves were obtained with a Shimadzu UV-1800 by measuring the change in absorbance at 260 nm versus temperature. The melting temperature (T_m) was determined from the maximum in the first derivative of the melting curve. Both the heating and the cooling curves were measured, and the calculated T_ms from these curves agreed to within 2.0 °C. The temperature ramp was 0.5 °C min^{-1}.

Chemical Actinometry

Quantum yields were determined by using 3,4-dimethoxynitrobenzene actinometry as reported by Zhang et al.[38] Conversion rate was calculated from the UV-vis spectra at each irradiation time, and the quantum yields were determined by calculating the ratio between initial slope and absorbed photons determined by actinometry.

UV Irradiation

A xenon light source (MAX-301, Asahi Spectra) equipped with interference filters centered at 340.0 nm (half bandwidth 10 nm, power density 0.15 mW/cm^2) was used for photoreaction. The sample solution was added to a cuvette, and the temperature of light irradiation was controlled using a programmable temperature controller. Photo-irradiation was conducted at 20 °C.

HPLC Analyses

A Merck LiChrospher 100 RP-18(e) column heated to 50 °C was used for HPLC analyses. The flow rate was 0.5 mL/min. A solution of 50 mM ammonium formate (solution A) and a mixture of 50 mM ammonium formate and acetonitrile (50/50, v/v; solution B) were used as mobile phases. A linear gradient of 5−35% solution B over 30 min was employed. HPLC chromatograms were monitored at 260 nm.

5-6 References

(1) Ciamician, G.; Silber, P. *Chem. Ber.* **1902**, *35*, 4128.

(2) Schraub, M.; Gray, H.; Hampp, N. *Macromolecules* **2011**, *44*, 8755.

(3) Goodall, G. W.; Hayes, W. *Chem. Soc. Rev.* **2006**, *35*, 280.

(4) Lewis, F. D.; Johnson, D. E. *J. Photochem.* **1977**, *7*, 421.

(5) Syamala, M. S.; Ramamurthy, V. *J. Org. Chem.* **1986**, *51*, 3712.

(6) Ito, Y.; Kajita, T.; Kunimoto, K.; Matsuura, T. *J. Org. Chem.* **1989**, *54*, 587.

(7) Ulrich, H.; Rao, D. V.; Stuber, F. A.; Sayigh, A. A. R. *J. Org. Chem.* **1970**, *35*, 1121.

(8) Yamada, S.; Uematsu, N.; Yamashita, K. *J. Am. Chem. Soc.* **2007**, *129*, 12100.

(9) Papagni, A.; Buttero, P. D.; Bertarelli, C.; Miozzo, L.; Moret, M.; Pryce, M. T.; Rizzato, S. *New J. Chem.* **2010**, *34*, 2612.

(10) Herrmann, W.; Wehrle, S.; Wenz, G. *Chem. Commun.* **1997**, 1709.

(11) Rao, K. S. S. P.; Hubig, S. M.; Moorthy, J. N.; Kochi, J. K. *J. Org. Chem.* **1999**, *64*, 8098.

(12) Kaliappan, R.; Kaanumalle, L. S.; Natarajan, A.; Ramamurthy, V. *Photochem. Photobiol. Sci.* **2006**, *5*, 925.

(13) Pattabiraman, M.; Natarajan, A.; Kaliappan, R.; Mague, J. T.; Ramamurthy, V. *Chem. Commun.* **2005**, 4542.

(14) Maddipatla, M. V. S. N.; Kaanumalle, L. S.; Natarajan, A.; Pattabiraman, M.; Ramamurthy, V. *Langmuir* **2007**, *23*, 7545.

(15) Kashida, H.; Fujii, T.; Asanuma, H. *Org. Biomol. Chem.* **2008**, *6*, 2892.

(16) Fujii, T.; Kashida, H.; Asanuma, H. *Chem. Eur. J.* **2009**, *15*, 10092.

(17) Kashida, H.; Doi, T.; Sakakibara, T.; Hayashi, T.; Asanuma, H. *J. Am. Chem. Soc.* **2013**, *135*, 7960.

(18) Caldwell, R. A. *J. Am. Chem. Soc.* **1980**, *102*, 4004.

(19) Lewis, F. D.; Wu, T.; Burch, E. L.; Bassani, D. M.; Yang, J.-S.; Schneider, S.; Jaeger, W.; Letsinger, R. L. *J. Am. Chem. Soc.* **1995**, *117*, 8785.

(20) Fujimoto, K.; Matsuda, S.; Takahashi, N.; Saito, I. *J. Am. Chem. Soc.* **2000**, *122*, 5646.

(21) Ogasawara, S.; Fujimoto, K. *Angew. Chem. Int. Ed.* **2006**, *45*, 4512.

(22) Ihara, T.; Fujii, T.; Mukae, M.; Kitamura, Y.; Jyo, A. *J. Am. Chem. Soc.* **2004**, *126*, 8880.

(23) Manchester, J.; Bassani, D. M.; Duprey, J.-L. H. A.; Giordano, L.; Vyle, J. S.; Zhao, Z.; Tucker, J. H. R. *J. Am. Chem. Soc.* **2012**, *134*, 10791.

(24) Mukae, M.; Ihara, T.; Tabara, M.; Jyo, A. *Org. Biomol. Chem.* **2009**, *7*, 1349.

(25) Pasternak, K.; Pasternak, A.; Gupta, P.; Veedu, R. N.; Wengel, J. *Bioorg. Med. Chem.* **2011**, *19*, 7407.

(26) Fujimoto, K.; Yamada, A.; Yoshimura, Y.; Tsukaguchi, T.; Sakamoto, T. *J. Am. Chem. Soc.* **2013**, *135*, 16161.

(27) We also investigated the correlation between the energy level of HOMO or LUMO. See Fig.S5-8 for details. It also showed a good correlation and we could not determine critical factor determining the reactivities in homo combination.

(28) We also measured the photodimerization of **B** at pH 9. As shown in Fig.S5-9, the reactivity was enhanced which indicates that the protonation has suppressed the reaction.

(29) Torimura, M.; Kurata, S.; Yamada, K.; Yokomaku, T.; Kamagata, Y.; Kanagawa, T.; Kurane, R. *Anal. Sci.* **2001**, *17*, 155.

(30) Orientation of double bond should affect the reactivities. In UV-VIS spectra, all derivatives showed hypsochromic shift, demonstrating they formed H-type aggregate in DNA duplexes. In addition, no correlation was observed between melting temperatures and quantum yields, indicating strength of stacking interaction did not significantly affect the reactivities. Hence, we believe effects of the difference of the orientation on the photodimerization reactivities are marginal.

(31) de Silva, A. P.; Gunaratne, H. Q. N.; Gunnlaugsson, T.; Huxley, A. J. M.; McCoy, C. P.; Rademacher, J. T.; Rice, T. E. *Chem. Rev.* **1997**, *97*, 1515.

(32) Oberlé, J.; Abraham, E.; Jonusauskas, G.; Rullière, C. *J. Raman Spectrosc.* **2000**, *31*, 311.

(33) Fleming, I. *Frontier Orbitals and Organic Chemical Reactions*; Wiley: NewYork, 1976.

(34) Peters, K. S.; Freilich, S. C.; Lee, J. *J. Phys. Chem.* **1993**, *97*, 5482.

(35) Peters, K. S.; Lee, J. *J. Phys. Chem.* **1992**, *96*, 8941.

(36) Shigeno, A.; Sakamoto, T.; Yoshimura, Y.; Fujimoto, K. *Org. Biomol. Chem.* **2012**, *10*, 7820.

(37) Grigoriev, M.; Praseuth, D.; Guieysse, A. L.; Robin, P.; Thuong, N. T.; Hélène, C.; Harel-Bellan, A. *Proc. Natl. Acad. Sci. USA* **1993**, *90*, 3501.

(38) Zhang, J.-Y.; Esrom, H.; Boyd, I. W. *Appl. Surf. Sci.* **1999**, *138–139*, 315.

5-7 Appendixes

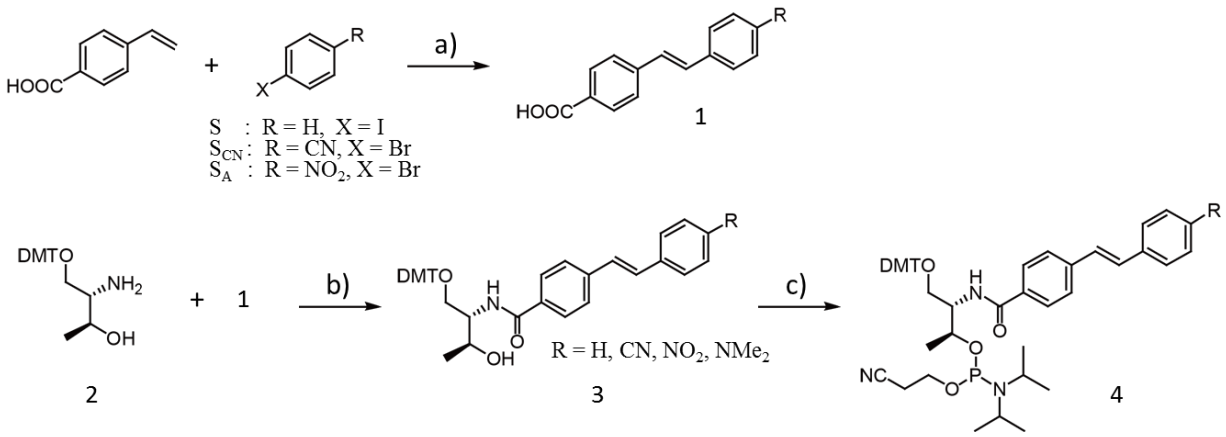

Scheme S5-1. Synthesis of phosphoramidite monomers tethering stilbene, *p*-cyanostilbene, *p*-nitrostilbene, and *p*-dimethylaminostilbene. Reagents and conditions: a) $Pd(OAc)_2$, PPh_3, NMe_3, DMF, 100 ^oC, overnight, **S**: 52.2%, $\mathbf{S_{CN}}$: 52.2%, $\mathbf{S_A}$: 72.6%. b) EDC, HOBt, NEt_3, DMF, r.t., overnight, **S**: 69.2%, $\mathbf{S_{CN}}$: 92.5%, $\mathbf{S_A}$: 53.6%, $\mathbf{S_D}$: 57.5%. c) $(iPr)_2NP(Cl)(OCH_2CH_2CN)$, NEt_3, THF, 0 ^oC, 20 min, **S**: 92.3%, $\mathbf{S_{CN}}$: 68.5%, $\mathbf{S_A}$: 77.8%, $\mathbf{S_D}$: 65.2 %.

Compound **1** (R = NMe_2) and compound **2** were synthesized according to the previous reports.[1, 2] The phosphoramidite monomers tethering stilbene (**S**), *p*-cyanostilbene ($\mathbf{S_{CN}}$), *p*-nitrostilbene ($\mathbf{S_A}$), and *p*-dimethylaminostilbene ($\mathbf{S_D}$) were synthesized as follows:

General Procedure for Synthesis of Compound 1 (except for R = NMe_2)

To a stirred solution of iodobenzene (2.04 g, 10 mmol), 4-bromobenzonitrile (1.82 g, 10 mmol), or 4-bromonitrobenzene (2.02 g, 10 mmol) in DMF (30 mL) was added 4-vinylbenzoic acid (1.48 g, 10 mmol), palladium(II) acetate (22.4 mg, 1 mol%), triphenylphosphine (52.5 mg, 2 mol%) and triethylamine (15 mL). After the reaction mixture was heated at 100 ^oC overnight, the solvent was removed by evaporation and filtered with ethyl acetate. The obtained residue was used in the next reaction without further purification. **S**: (Yield: 52.2%) ^{1}H-NMR [DMSO-d_6, 500 MHz] δ=7.97 (d, J = 8.5 Hz, 2H, aromatic protons), 7.76 (d, J = 8.5 Hz, 2H, aromatic protons), 7.68 (d, J =

8.5 Hz, 2H, aromatic protons), 7.40 (m, 5H, aromatic protons and vinyl protons). ^{13}C-NMR [DMSO-d_6, 125 MHz] δ = 168.6, 142.9, 138.1, 132.4, 131.2, 131.0, 130.3, 129.7, 128.9, 128.3, 127.9. HRMS(FAB) (*m*/*z*): $[M]^+$ Calcd for $C_{15}H_{12}O_2$ 224.0832; found 224.0838. **S_{CN}**: (Yield: 52.2%) ^{1}H-NMR [DMSO-d_6, 500 MHz] δ=8.00 (d, *J* = 8.5 Hz, 2H, aromatic protons), 7.90 (d, *J* = 8.5 Hz, 2H, aromatic protons), 7.87 (d, *J* = 8.5 Hz, 2H, aromatic protons), 7.80 (d, *J* = 8.5 Hz, 2H, aromatic protons), 7.61 (d, *J* = 17 Hz, 1H, vinyl proton), 7.53 (d, *J* = 17 Hz, 1H, vinyl proton). ^{13}C-NMR [DMSO-d_6, 125 MHz] δ = 168.5, 142.9, 142.1, 135.6, 134.2, 132.6, 131.7, 131.3, 131.1, 130.7, 128.9, 128.5, 127.7, 120.4, 111.5. HRMS(FAB) (*m*/*z*): $[M]^+$ Calcd for $C_{16}H_{11}NO_2$ 249.0784; found 249.0760. **S_A**: (Yield: 72.6%) ^{1}H NMR [DMSO-d_6, 500MHz] δ=8.30 (d, *J* = 8.5 Hz, 2H, aromatic protons), 8.01 (d, *J* = 8.5 Hz, 2H, aromatic protons), 7.95 (d, *J* = 8.5 Hz, 2H, aromatic protons), 7.82 (d, *J* = 8.5 Hz, 2H, aromatic protons), 7.66 (d, *J* = 17 Hz, 1H, vinyl proton), 7.61 (d, *J* = 17 Hz, 1H, vinyl proton). ^{13}C-NMR [DMSO-d_6, 125 MHz] δ = 168.5, 148.0, 145.0, 142.0, 133.6, 132.1, 131.3, 131.1, 130.2, 129.5, 129.2, 128.6, 127.7, 125.5. HRMS(FAB) (*m*/*z*): $[M]^+$ Calcd for $C_{15}H_{11}NO_4$ 269.0683; found 269.0585.

General Procedure for Synthesis of Compound 3

To a stirred solution of 1 (1.0 equiv) and triethylamine (2.8 equiv) in DMF was added HOBt (1.6 equiv), EDC (1.6 equiv) and **2** (1.2 equiv), and the mixture was stirred overnight. Ethyl acetate was added, and the organic layer was washed with saturated aqueous solution of $NaHCO_3$ and NaCl. After drying over $MgSO_4$, the solvent was removed by evaporation, followed by silica gel column chromatography using hexane and ethyl acetate as eluent (3% triethylamine was added). **S**: (Yield: 69.2%) ^{1}H-NMR [DMSO-d_6, 500 MHz] δ=8.06 (d, *J* = 9.0 Hz, 1H, -N*H*CO-), 7.96 (d, *J* = 8.5 Hz, 2H, aromatic protons of stilbene), 7.76 (d, *J* = 8.5 Hz, 2H, aromatic protons of stilbene), 7.68 (d, *J* = 8.5 Hz, 2H, aromatic protons of stilbene), 7.46-7.23 (m, 14H, aromatic protons of DMT and stilbene and vinyl protons), 6.88 (m, 4H, aromatic protons of DMT), 4.63 (d, *J* = 6.0 Hz, 1H, -O*H*), 4.18 (m, 1H, -CH_2-C*H*(NH-)-$CH(CH_3)$), 4.08 (m, 1H, -C*H*(CH_3)-OH), 3.76 (s, 6H, -C_6H_4-OC*H*$_3$), 3.26, 3.01 (m, each 1H, -C*H*$_2$-ODMT), 1.06 (d, *J* = 6.5 Hz, 3H, -CH(C*H*$_3$)-OH). ^{13}C-NMR [DMSO-d_6, 125 MHz] δ = 167.6,

159.4, 146.6, 141.2, 138.2, 137.4, 137.3, 134.9, 131.6, 131.2, 130.2, 129.5, 129.3, 129.2, 129.0, 128.1, 128.0, 127.6, 114.5, 86.6, 66.7, 64.5, 56.7, 56.4, 21.8. HRMS(FAB) (*m*/*z*): $[M]^+$ Calcd for $C_{40}H_{39}NO_5$ 613.2823; found 613.2801. **S_{CN}**: (Yield: 92.5%) ^{1}H-NMR [DMSO-d_6, 500 MHz] δ=8.10 (d, *J* = 9.0 Hz, 1H, -N*H*CO-), 7.99 (d, *J* = 8.0 Hz, 2H, aromatic protons of *p*-cyanostilbene), 7.90 (d, *J* = 8.5 Hz, 2H, aromatic protons of *p*-cyanostilbene), 7.87 (d, *J* = 8.5 Hz, 2H, aromatic protons of *p*-cyanostilbene), 7.81 (d, *J* = 8.5 Hz, 2H, aromatic protons of *p*-cyanostilbene), 7.59 (d, *J* = 16.5 Hz, 1H, vinyl proton), 7.47 (d, *J* = 16.5 Hz, 1H, vinyl proton), 7.44-7.26 (m, 9H, aromatic protons of DMT), 6.88 (m, 4H, aromatic protons of DMT), 4.64 (d, *J* = 6.0 Hz, 1H, -O*H*), 4.18 (m, 1H, -CH_2-C*H*(NH-)-CH(CH_3)), 4.07 (m, 1H, -C*H*(CH_3)-OH), 3.76 (s, 6H, -C_6H_4-OCH_3), 3.27, 3.01 (m, each 1H, -CH_2-ODMT), 1.06 (d, *J* = 6.5 Hz, 3H, -CH(CH_3)-OH). ^{13}C-NMR [DMSO-d_6, 125 MHz] δ = 167.5, 159.4, 146.6, 143.0, 140.5, 137.3, 137.2, 135.7, 134.1, 132.8, 131.2, 129.9, 129.4, 129.2, 129.1, 128.8, 128.7, 128.2, 128.0, 114.5, 111.3, 86.6, 66.7, 64.5, 56.7, 56.4, 21.8. HRMS(FAB) (*m*/*z*): $[M]^+$ Calcd for $C_{41}H_{38}N_2O_5$ 638.2775; found 638.2799. **S_A**: (Yield: 53.6%) ^{1}H NMR [DMSO-d_6, 500 MHz] δ=8.30 (d, *J* = 9.0 Hz, 2H, aromatic protons of *p*-nitrostilbene), 8.11 (d, *J* = 8.5 Hz, 1H, -N*H*CO-), 8.00 (d, *J* = 8.5 Hz, 2H, aromatic protons of *p*-nitrostilbene), 7.95 (d, *J* = 8.5 Hz, 2H, aromatic protons of *p*-nitrostilbene), 7.83 (d, *J* = 8.5 Hz, 2H, aromatic protons of *p*-nitrostilbene), 7.65 (d, *J*=17 Hz, 1H, vinyl protones), 7.60 (d, *J*=17 Hz, 1H, vinyl protones), 7.45-7.22 (m, 9 H, aromatic protons of DMT), 6.87 (m, 4 H, aromatic protons of DMT), 4.64 (d, *J*=6.0 Hz, 1H, -O*H*), 4.18 (m, 1H, -CH_2-C*H*(NH-)-CH(CH_3)), 4.08 (m, 1H, -C*H*(CH_3)-OH), 3.76 (s, 6H, -C_6H_4-OCH_3), 3.27, 3.02 (m, each 1H, -CH_2--ODMT), 1.07 (d, *J*=6.0 Hz, 3H, -CH(CH_3)-OH). ^{13}C-NMR [DMSO-d_6, 125 MHz] δ = 167.5, 159.4, 147.9, 146.6, 145.2, 140.4, 137.4, 137.2, 135.8, 133.8, 131.2, 129.5, 129.4, 129.2, 129.0, 128.3, 128.0, 125.5, 114.5, 86.6, 66.7, 64.5, 56.7, 56.4, 21.8. HRMS(FAB) (*m*/*z*): $[M]^+$ Calcd for $C_{40}H_{38}N_2O_7$ 658.2674; found 658.2675. **S_D**: (Yield: 57.5%) ^{1}H NMR [DMSO-d_6, 500 MHz] δ=7.99 (d, 1H, *J*=8.5 Hz, -N*H*CO-), 7.92 (d, 2H, *J*=8.5 Hz, aromatic protons of *p*-dimethylaminostilbene), 7.67 (d, 2H, *J*=8.5 Hz, aromatic protons of *p*-dimethylaminostilbene), 7.51 (d, 2H, *J*=9.0 Hz, aromatic protons of *p*-dimethylaminostilbene), 7.44-7.22 (m, 10 H, aromatic protons of DMT and vinyl proton), 7.01 (d, 1H, *J*=16.5 Hz, vinyl proton), 6.88 (m, 4 H, aromatic protons of DMT),

6.77 (d, 2H, *J*=9.0 Hz, aromatic protons of *p*-dimethylaminostilbene), 4.62 (d, 1H, *J*=6.5 Hz, -O*H*), 4.17 (m, 1H, -CH_2-C*H*(NH-)-CH(CH_3)), 4.08 (m, 1H, -C*H*(CH_3)-OH), 3.76 (s, 6H, -C_6H_4-OCH_3), 3.26, 3.02 (m, 1H, -CH_2-ODMT), 2.99 (s, 6H, -C_6H_4-N(CH_3)$_2$), 1.06 (d, 3H, *J*=6.0 Hz, -CH(CH_3)-OH). ^{13}C-NMR [DMSO-d_6, 125 MHz] δ = 167.6, 159.6, 159.5, 159.4, 151.7, 146.6, 142.1, 137.3, 133.8, 132.0, 131.1, 129.3, 129.2, 129.1, 128.0, 126.9, 126.0, 124.0, 114.7, 114.5, 113.6, 87.0, 86.6, 76.4, 66.7, 64.5, 59.4, 56.6, 56.5, 56.4, 21.8. HRMS(FAB) (*m*/*z*): $[M]^+$ Calcd for $C_{42}H_{44}N_2O_5$ 656.3245; found 656.3246.

General Procedure for Synthesis of Compound 4

Triethylamine (5.0 equiv) and 2-cyanoethyl N,N-diisopropylchlorophosphoramidite (2.0 equiv) were added to a solution of compound **3** (1.0 equiv) in THF at 0 ^{o}C. After 20 min of vigorous stirring on ice, an excess of ethyl acetate was added to the reaction mixture, and the mixture was washed with saturated aqueous solution of $NaHCO_3$ and with NaCl. After drying over $MgSO_4$, the solvent was removed by evaporation, followed by silica gel column chromatography using hexane and ethyl acetate as eluent (3% triethylamine was added). **S**: (Yield: 92.3%) ^{31}P NMR [DMSO-d_6, 121 MHz] δ=147.9, 147.7 ppm. $\mathbf{S_{CN}}$: (Yield: 68.5%) ^{31}P NMR [DMSO-d_6, 121 MHz] δ=147.9, 147.7 ppm. $\mathbf{S_A}$: (Yield: 77.8%) ^{31}P NMR [DMSO-d_6, 121 MHz] δ=147.9, 147.7. $\mathbf{S_D}$: (Yield: 65.2%) ^{31}P NMR [DMSO-d_6, 121 MHz] δ=147.9, 147.7.

References

1. Clement, B.; Weide, M.; Ziegler, D. M. *Chem. Res. Toxicol.* **1996**, *9*, 599-604.

2. Hara, Y.; Fujii, T.; Kashida, H.; Sekiguchi, K.; Liang, X.G.; Yoshida, Y.; Asanuma, H. *Angew. Chem. Int. Ed.* **2010**, *49*, 5502 –5506.

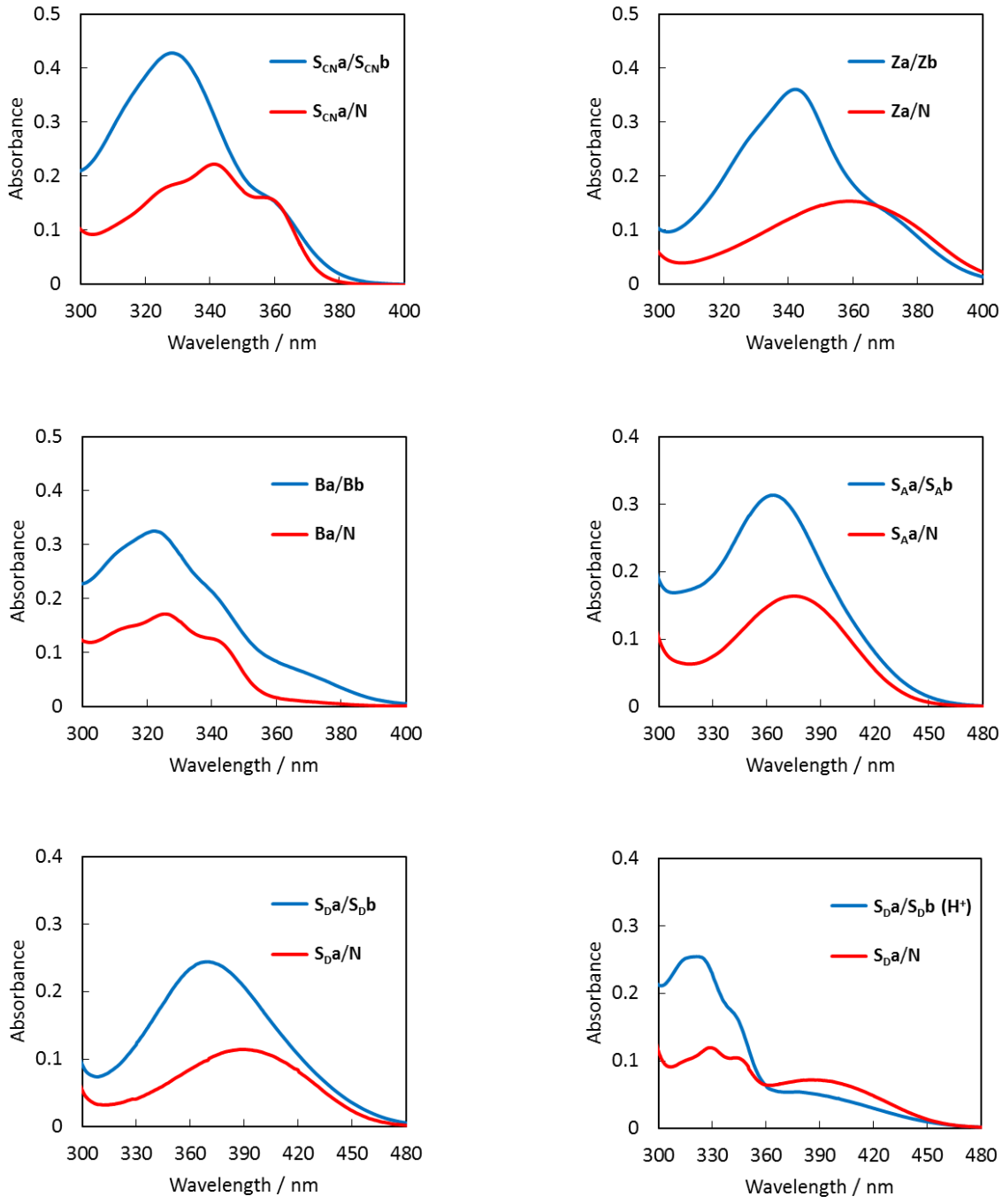

Fig. S5-1. UV-vis spectra of **Xa**/**Yb** and **Xa**/**N** duplexes (**X, Y** = $\mathbf{S_{CN}}$, **Z**, **B**, $\mathbf{S_A}$ or $\mathbf{S_D}$). Conditions are as follows: [ODN] = 5.0 μM, [NaCl] = 100 mM, pH 7.0 (10 mM phosphate buffer), pH 9.0 (10 mM Tris buffer) for $\mathbf{S_D}$, pH 5.0 (10 mM MES buffer) for $\mathbf{S_D(H^+)}$, 20 °C.

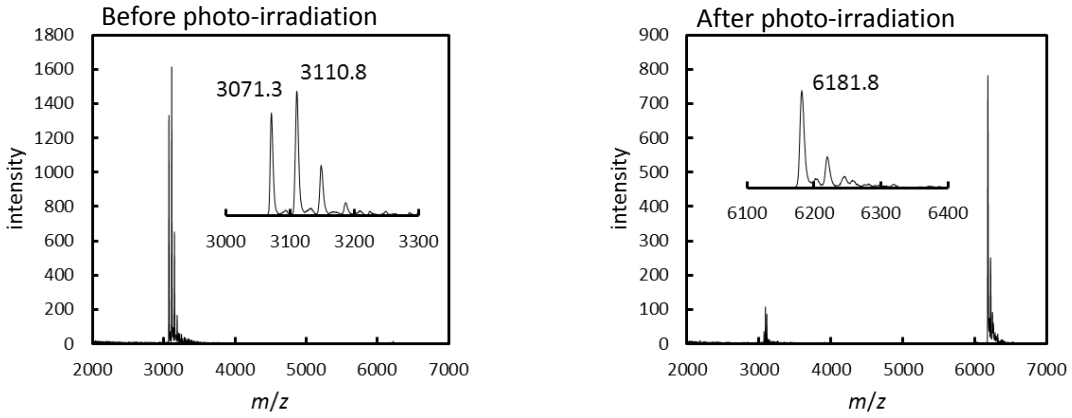

Fig. S5-2. MALDI-TOF MS charts of **Sa**/**Sb** before and after 180 sec UV irradiation (340 nm). Calculated mass for [**Sa**+H^+]:3072, [**Sb**+H^+]:3112, [**Sa**/**Sb**+H^+]:6182.

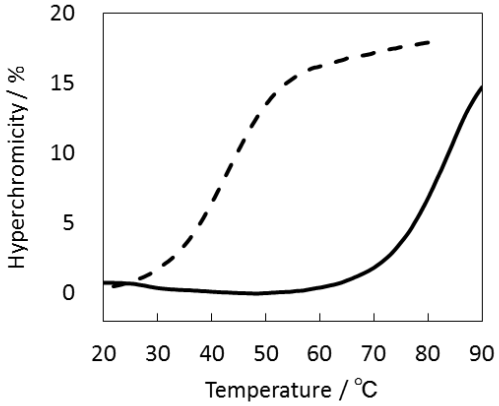

Fig. S5-3. Melting curves of **Sa**/**Sb** before (broken line) and after 340 nm UV irradiation for 180 sec (solid line). Conditions are as follows: [ODN] = 5.0 μM, [NaCl] = 100 mM, pH 7.0 (10 mM phosphate buffer).

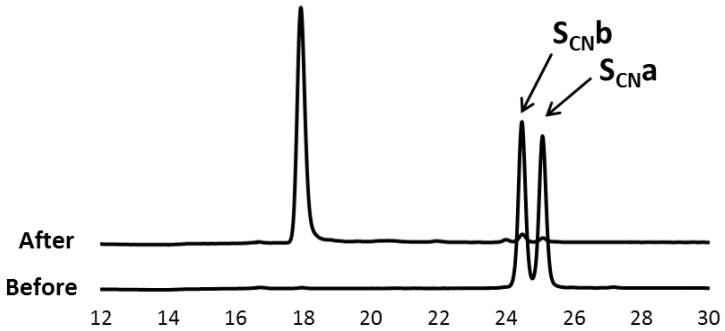

Fig. S5-4. HPLC chromatograms of $\mathbf{S_{CN}a}$/$\mathbf{S_{CN}b}$ before and after 300 sec UV irradiation (340 nm).

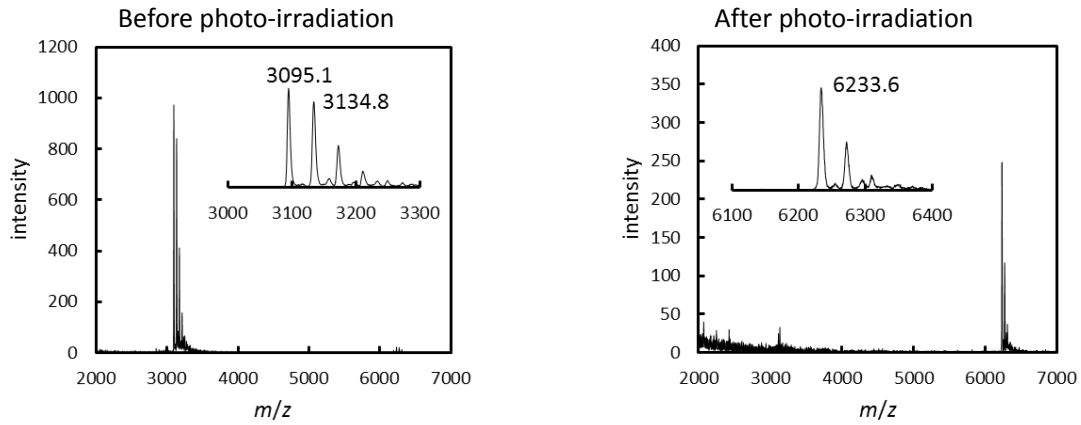

Fig. S5-5. MALDI-TOFMS charts of $\mathbf{S_{CN}a}$/$\mathbf{S_{CN}b}$ before and after 300 sec UV irradiation (340 nm). Calculated mass for [$\mathbf{S_{CN}a}$+H^+]:3097, [$\mathbf{S_{CN}b}$+H^+]:3137, [$\mathbf{S_{CN}a}$/$\mathbf{S_{CN}b}$+H^+]:6232.

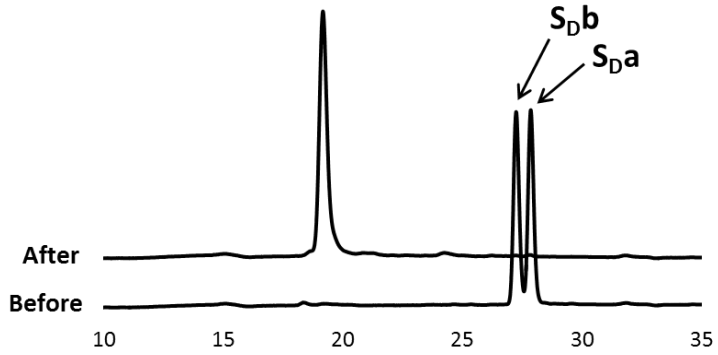

Fig. S5-6. HPLC chromatograms of $\mathbf{S_Da}$/$\mathbf{S_Db}$ **(H^+)** before and after 300 sec UV irradiation (340 nm) at pH5.

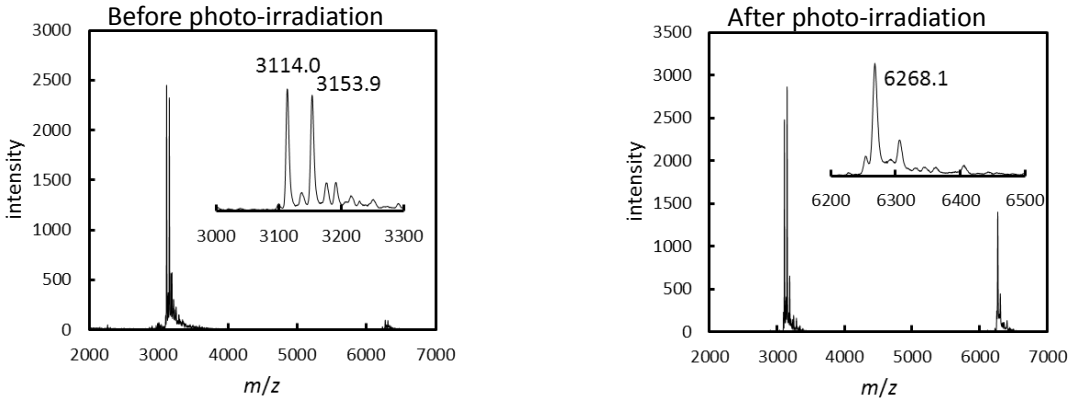

Fig. S5-7. MALDI-TOFMS charts of $\mathbf{S_Da}$/$\mathbf{S_Db}$ **(H^+)** before and after 300 sec UV irradiation (340 nm). Calculated mass for [$\mathbf{S_Da}$+H^+]:3115, [$\mathbf{S_Db}$+H^+]:3155, [$\mathbf{S_Da}$/$\mathbf{S_Db}$+H^+]:6268.

Table S5-1. Neighboring base pair dependence of quantum yields of **S**, **Z** and **B**.

	Φ (×10²)		
	S	**Z**	**B**
Xa/Yb	15	1.7	2.4
Xc/Yd	23	6.9	10
Xe/Yf	12	0.56	0.77

Xa: 5'-GCATC **X** AGTC-3'

Yb: 3'-CGTAG **Y** TCAG-5'

Xc: 5'-GCACT **X** AGTC-3'

Yd: 3'-CGTGA **Y** TCAG-5'

Xe: 5'-GCATC **X** GATC-3'

Yf: 3'-CGTAG **Y** CTAG-5'

(**X, Y** = **S**, **Z**, **B**)

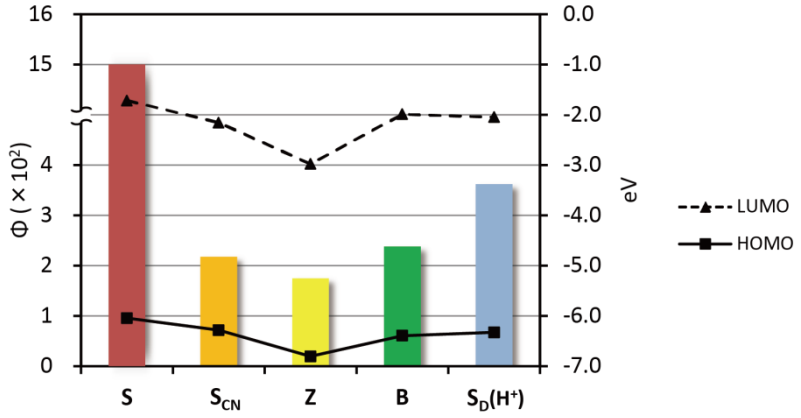

Fig. S5-8. Quantum yields of homo-photodimerizations (bar graph) and calculated energy level of LUMO and HOMO.

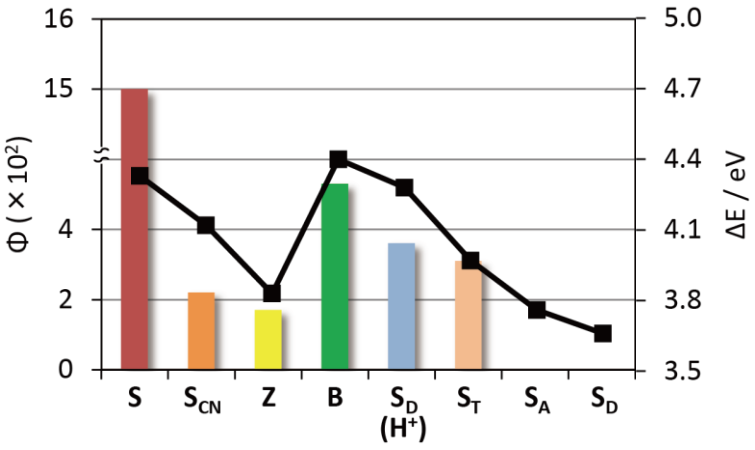

Fig. S5-9. Quantum yields of homo-photodimerizations (bar graph) and calculated excitation energies (line graph). $\Delta E=E_{LUMO}-E_{HOMO}$. **B** was measured at pH 9. The quantum yield of **B** at pH9 was 5.3.

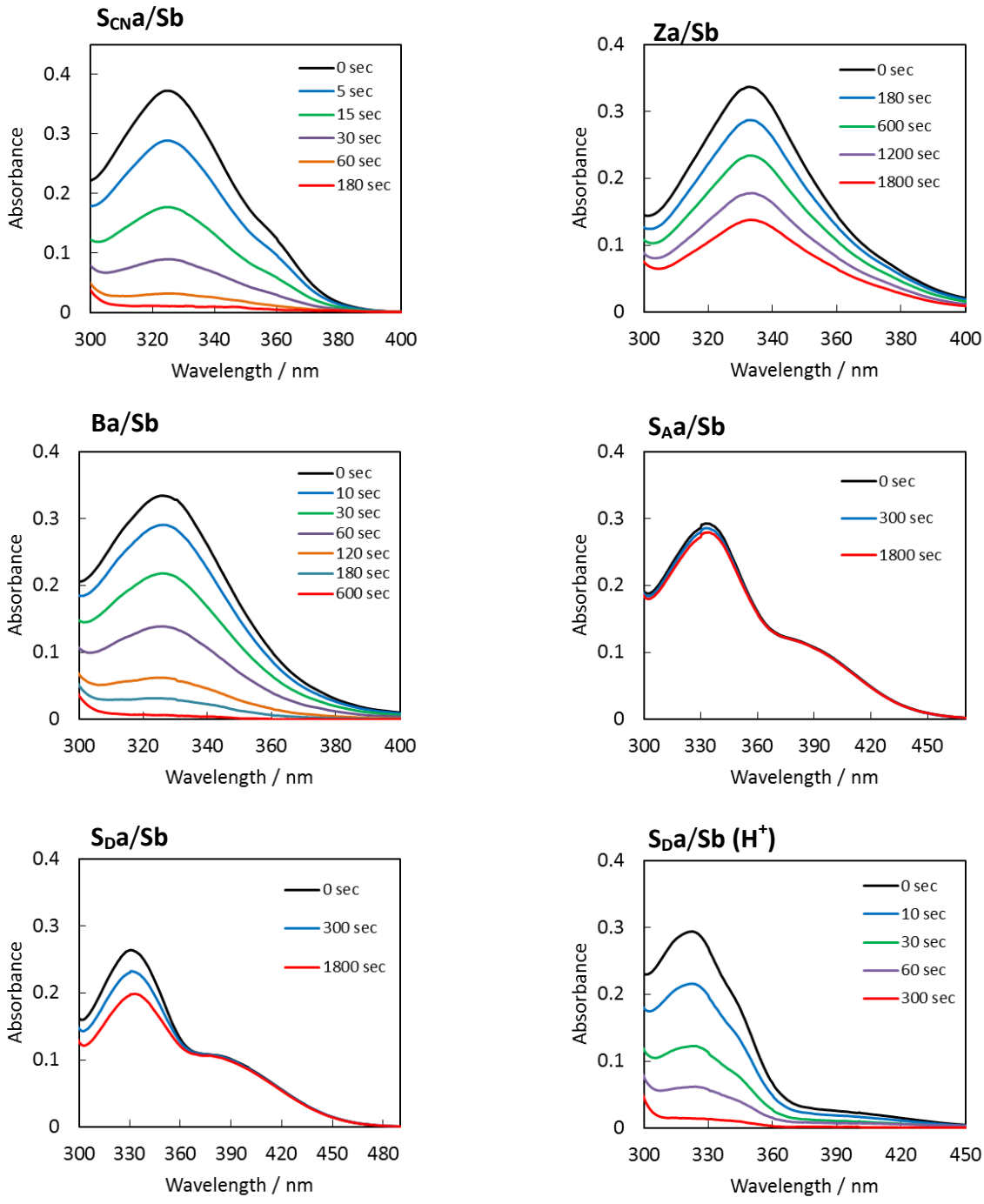

Fig. S5-10. UV- vis spectra of **Xa**/**Sb** duplexes (**X** = $\mathbf{S_{CN}}$, **Z**, **B**, $\mathbf{S_A}$ or $\mathbf{S_D}$) before and after indicated duration of UV irradiation (340 nm). Conditions are as follows: [ODN] = 5.0 µM, [NaCl] = 100 mM, pH 7.0 (10 mM phosphate buffer), pH 9.0 (10 mM Tris buffer) for $\mathbf{S_D}$, pH 5.0 (10 mM MES buffer) for $\mathbf{S_D(H^+)}$, 20 ^{o}C.

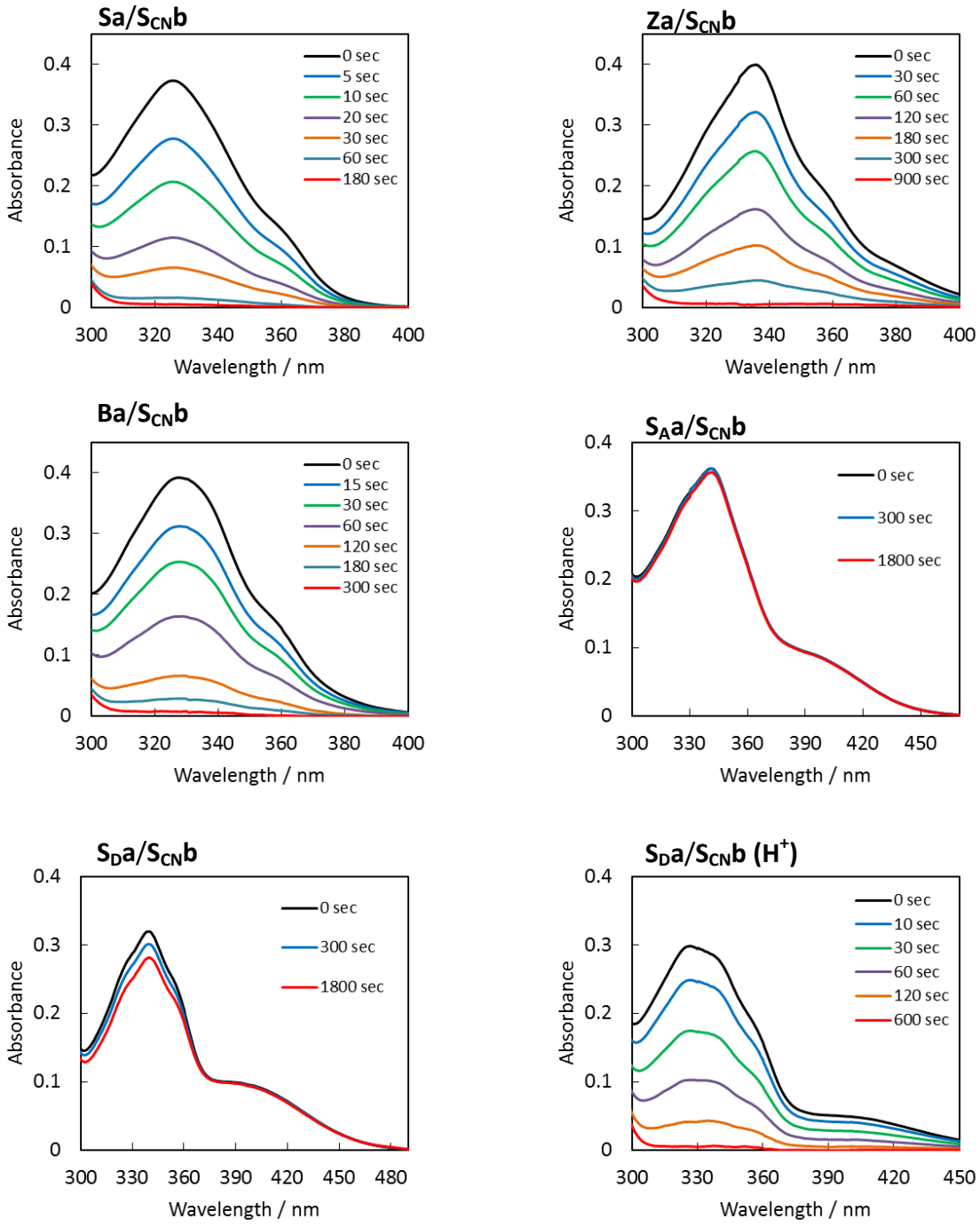

Fig. S5-11. UV- vis spectra of **Xa/S$_{CN}$b** duplexes (**X** = **S**, **Z**, **B**, **S$_A$** or **S$_D$**) before and after indicated duration of UV irradiation (340 nm). Conditions are as follows: [ODN] = 5.0 µM, [NaCl] = 100 mM, pH 7.0 (10 mM phosphate buffer), pH 9.0 (10 mM Tris buffer) for **S$_D$**, pH 5.0 (10 mM MES buffer) for **S$_D$(H$^+$)**, 20 ^{o}C.

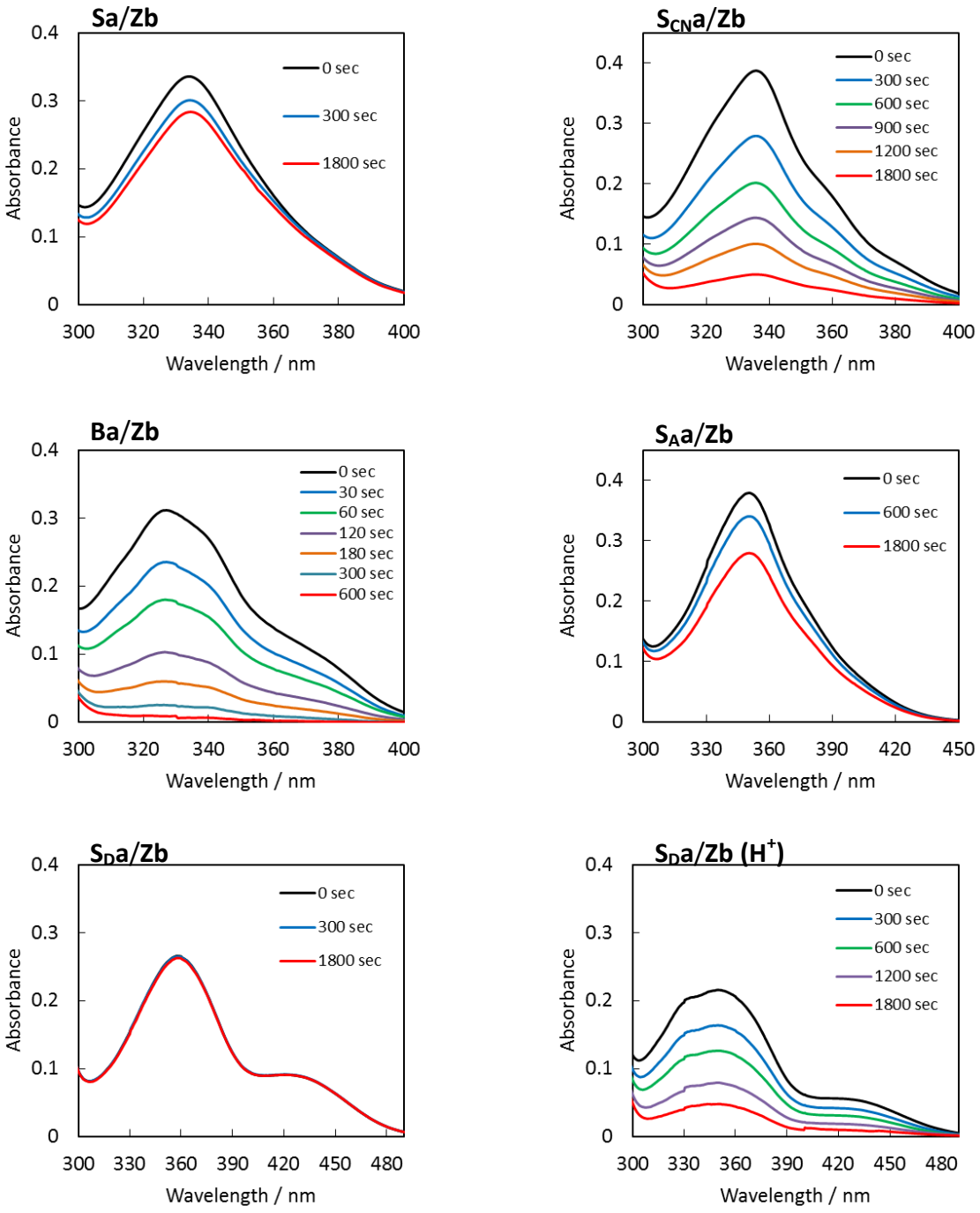

Fig. S5-12. UV- vis spectra of **Xa**/**Zb** duplexes (**X** = **S**, $\mathbf{S_{CN}}$, **B**, $\mathbf{S_A}$ or $\mathbf{S_D}$) before and after indicated duration of UV irradiation (340 nm). Conditions are as follows: [ODN] = 5.0 μM, [NaCl] = 100 mM, pH 7.0 (10 mM phosphate buffer), pH 9.0 (10 mM Tris buffer) for $\mathbf{S_D}$, pH 5.0 (10 mM MES buffer) for $\mathbf{S_D(H^+)}$, 20 ^{o}C.

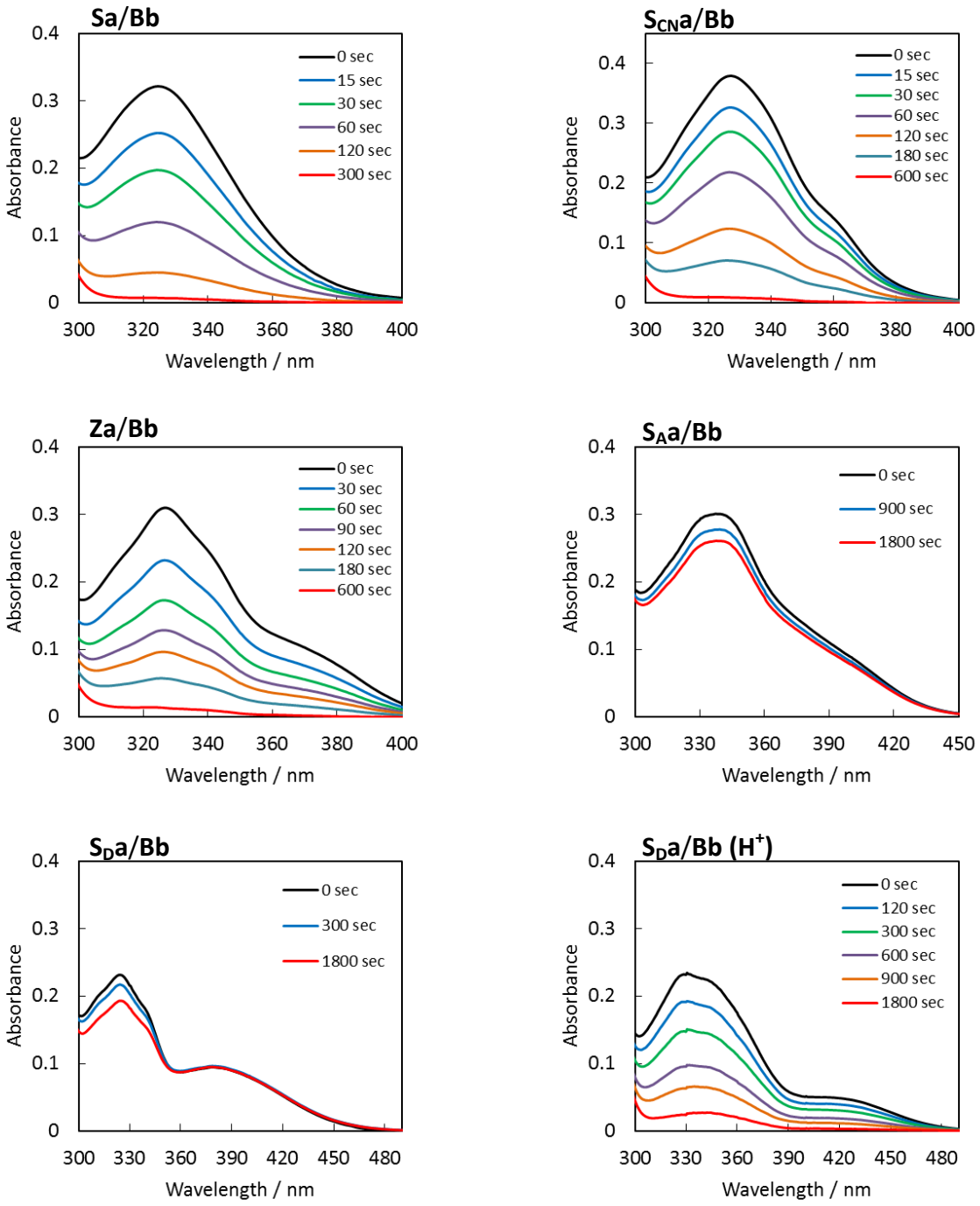

Fig. S5-13. UV- vis spectra of **Xa**/**Bb** duplexes (**X** = **S**, $\mathbf{S_{CN}}$, **Z**, $\mathbf{S_A}$ or $\mathbf{S_D}$) before and after indicated duration of UV irradiation (340 nm). Conditions are as follows: [ODN] = 5.0 μM, [NaCl] = 100 mM, pH 7.0 (10 mM phosphate buffer), pH 9.0 (10 mM Tris buffer) for $\mathbf{S_D}$, pH 5.0 (10 mM MES buffer) for $\mathbf{S_D(H^+)}$, 20 °C.

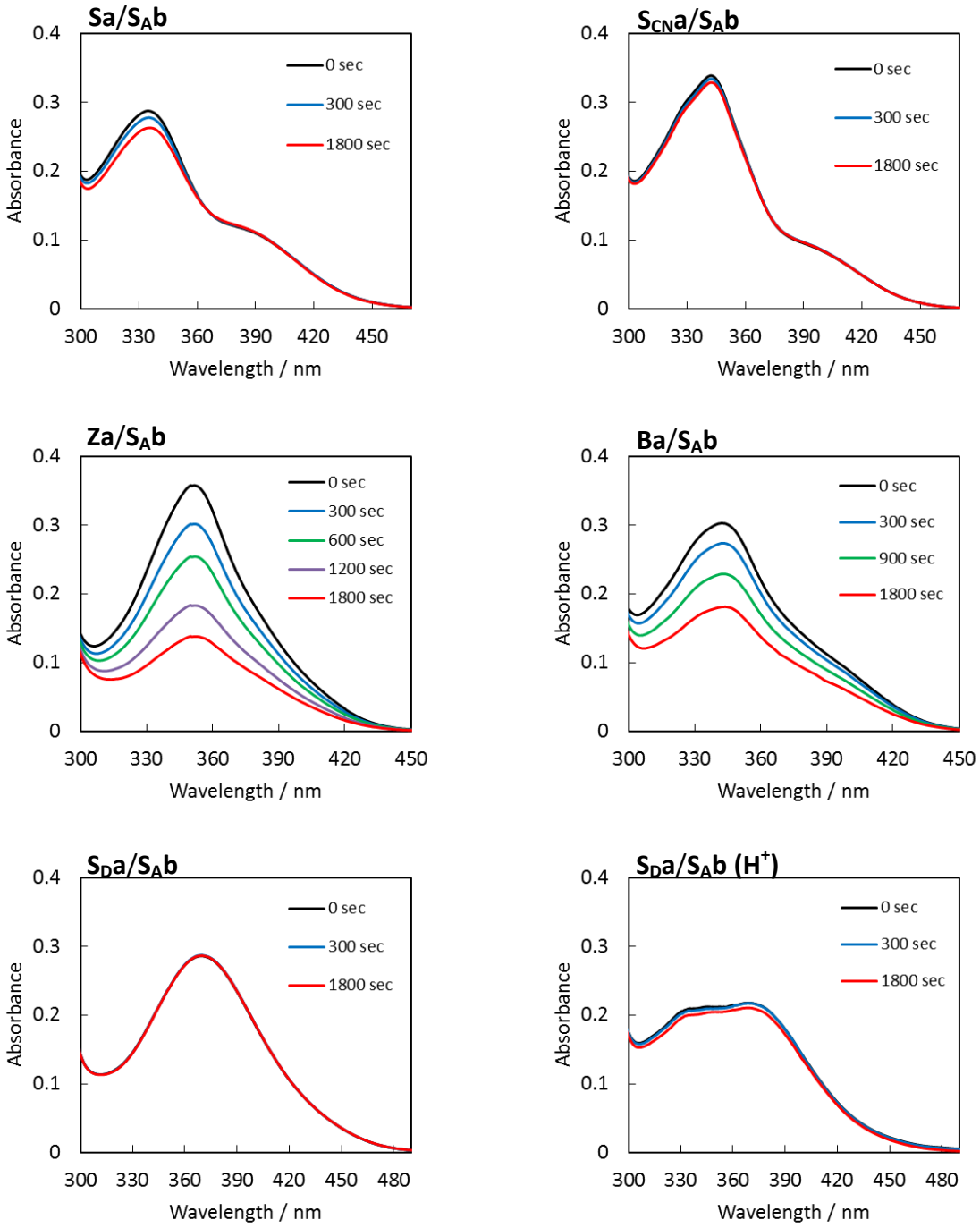

Fig. S5-14. UV- vis spectra of **Xa/S$_A$b** duplexes (**X** = **S**, **S$_{CN}$**, **Z**, **B** or **S$_D$**) before and after indicated duration of UV irradiation (340 nm). Conditions are as follows: [ODN] = 5.0 μM, [NaCl] = 100 mM, pH 7.0 (10 mM phosphate buffer), pH 9.0 (10 mM Tris buffer) for **S$_D$**, pH 5.0 (10 mM MES buffer) for **S$_D$(H$^+$)**, 20 ^{o}C.

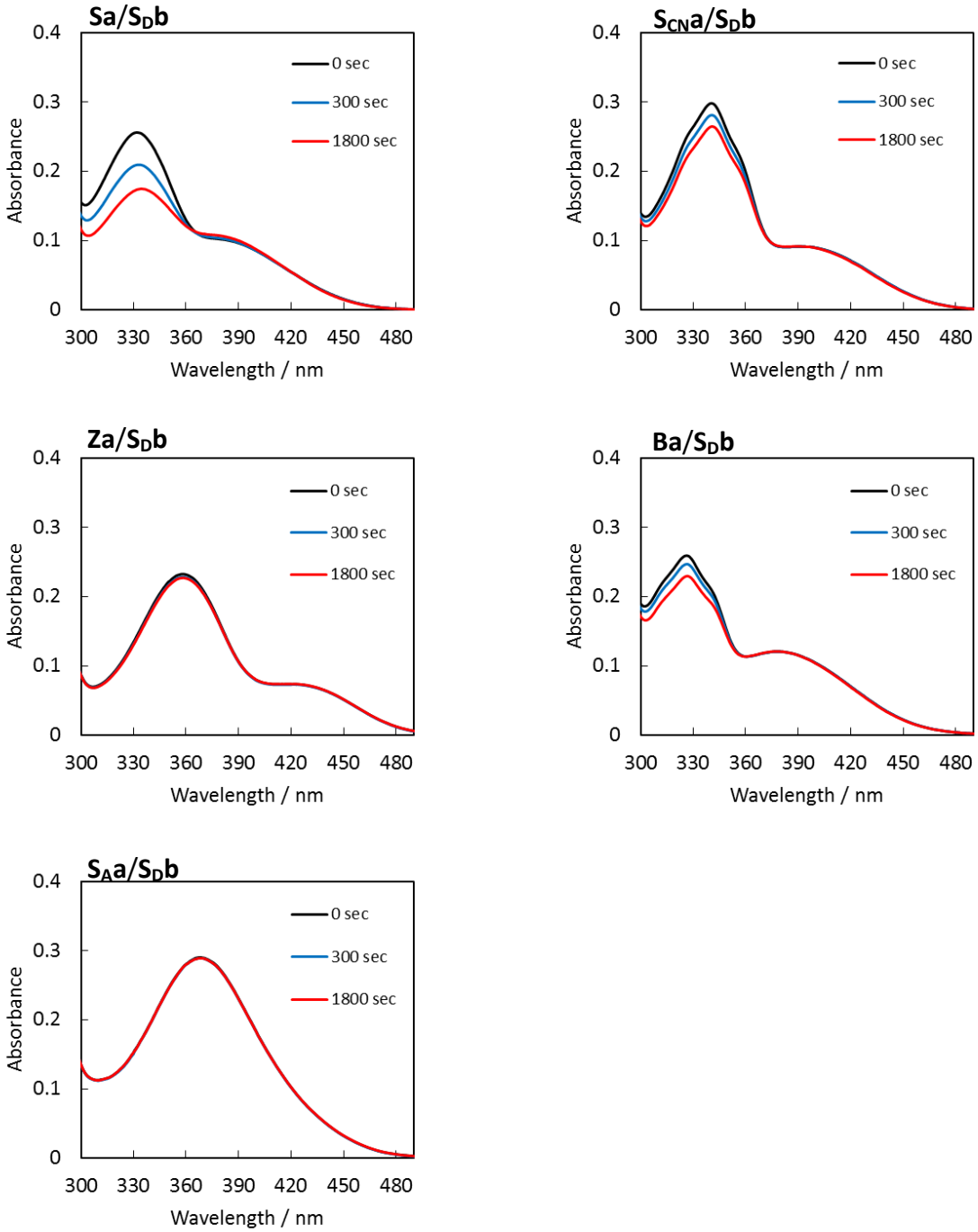

Fig. S5-15. UV- vis spectra of **Xa/S$_D$b** duplexes (**X** = **S**, **S$_{CN}$**, **Z**, **B** or **S$_A$**) before and after indicated duration of UV irradiation (340 nm). Conditions are as follows: [ODN] = 5.0 μM, [NaCl] = 100 mM, pH 9.0 (10 mM Tris buffer), 20 ^{o}C.

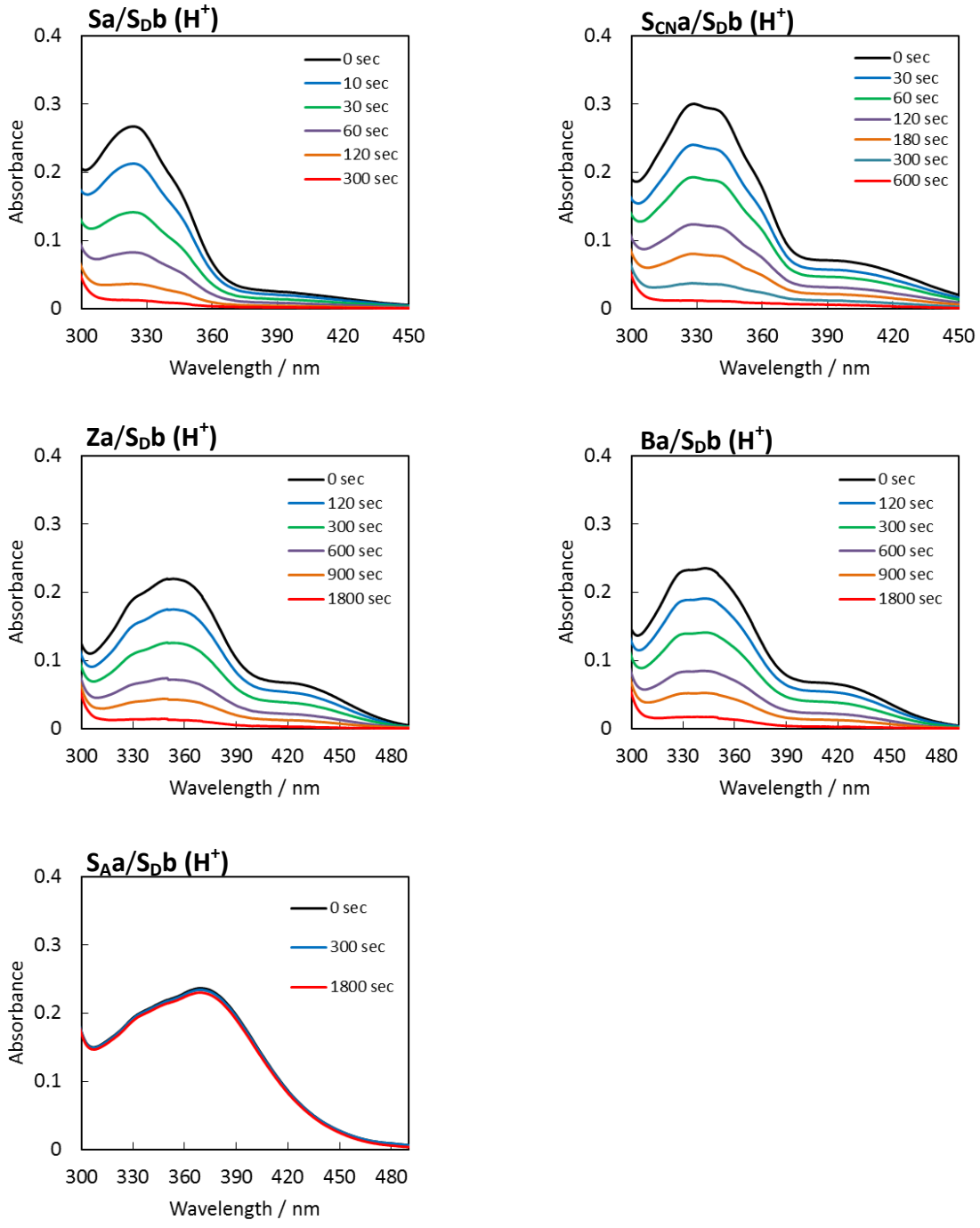

Fig. S5-16. UV- vis spectra of **Xa/S$_D$b (H$^+$)** duplexes (**X** = **S**, **S$_{CN}$**, **Z**, **B** or **S$_A$**) before and after indicated duration of UV irradiation (340 nm). Conditions are as follows: [ODN] = 5.0 µM, [NaCl] = 100 mM, pH 5.0 (10 mM MES buffer), 20 ^{o}C.

Table S5-2. Melting temperatures of duplexes in homo and hetero combinations.

	T_m / °C[a]						
	Sa	**S_{CN}a**	**Za**	**Ba**	**S_Aa**	**S_Da**[b]	**S_Da(H^+)**[c]
Sb	42.4	46.5	51.1	45.3	48.6	39.4	36.0
S_{CN}b	46.0	53.8	55.4	49.0	56.3	47.7	40.5
Zb	49.7	54.4	53.6	50.4	56.2	47.5	42.2
Bb	44.9	49.5	52.0	46.1	51.3	41.2	42.3
S_Ab	47.9	56.4	57.2	51.3	58.1	47.4	41.4
S_Db[b]	39.6	47.6	48.8	41.4	48.1	37.5	-
S_Db(H^+)[c]	35.0	39.8	44.7	44.2	42.5	-	36.7

[a]Conditions: 5.0 μM DNA, 100 mM NaCl, pH 7.0 (10 mM phosphate buffer). [b]Measured at pH 9 (Tris buffer). [b]Measured at pH 5 (MES buffer).

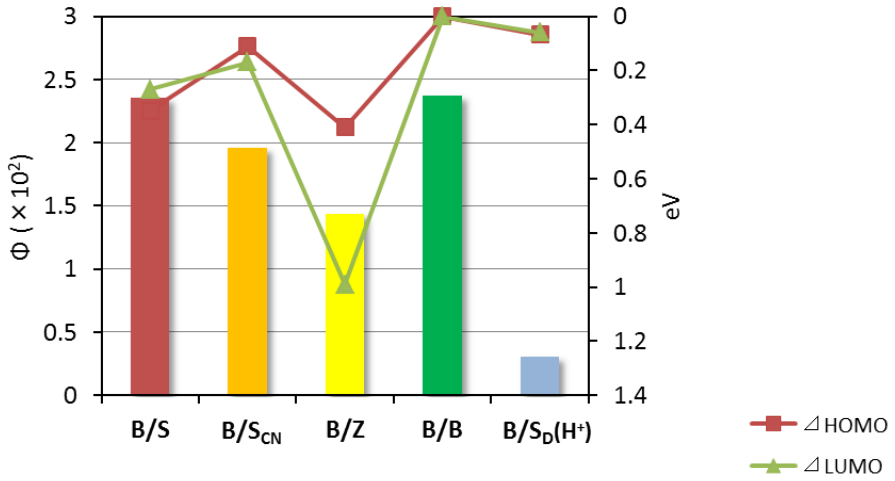

Fig. S5-17. Quantum yields of photodimerizations of **Ba**/**Yb** duplexes (bar graph) and energy gaps of HOMO or LUMO (line graphs). The energy gaps are displayed in absolute value and the axis is inverted. Note that, **B** should be protonated at pH 5 and hence, **Ba**/**S_Db (H^+)** showed similar reactivity with **Za**/**S_Db (H^+)**.

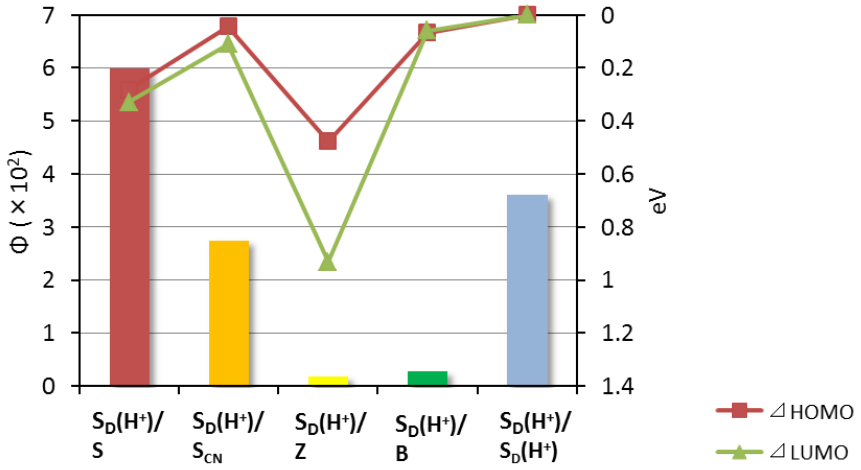

Fig. S5-18. Quantum yields of photodimerizations of **S_Da/Yb (H^+)** duplexes (bar graph) and energy gaps of HOMO or LUMO (line graphs). The energy gaps are displayed in absolute value and the axis is inverted. Note that, **B** should be protonated at pH 5 and hence, **S_Da/Bb (H^+)** showed similar reactivity with **S_Da/Zb (H^+)**.

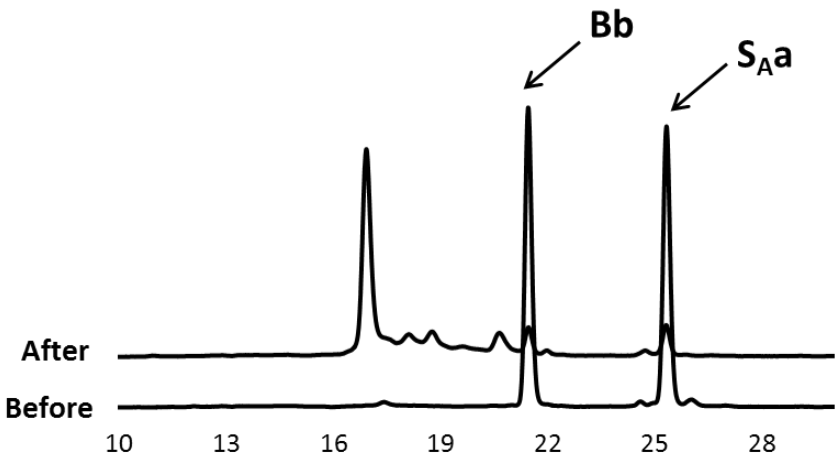

Fig. S5-19. HPLC chromatograms of **S_Aa/Bb** before and after 300 min photo-irradiation (340 nm).

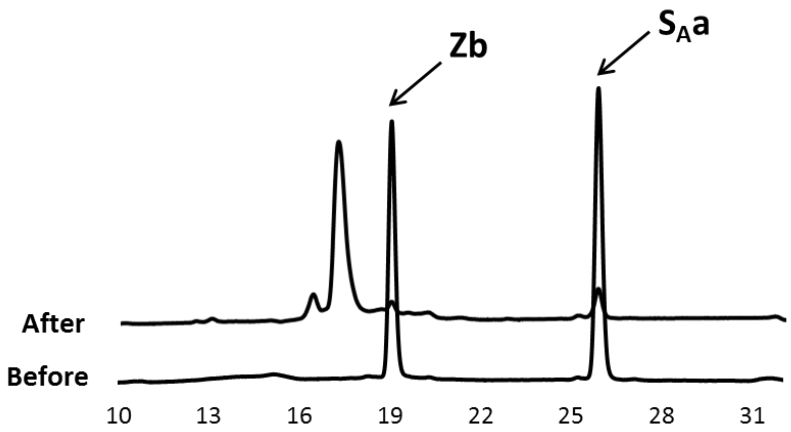

Fig. S5-20. HPLC chromatograms of **S_Aa**/**Zb** before and after 180 min UV irradiation (340 nm).

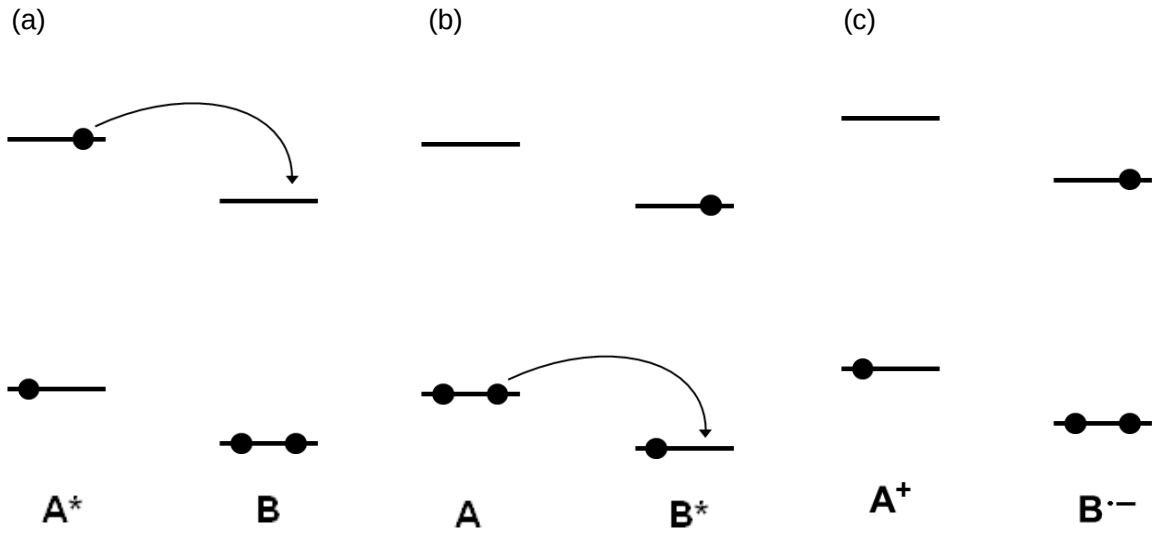

Fig. S5-21. Schematic energy diagram of the (a) **A** excited state and (b) **B** excited state in **A**/**B** hetero dimer aggregate. (c) Electron transfer from **A** (higher energy level) to **B** (lower energy level) may result the same radical ion pair state.

List of Publications

Journal Articles

1) "*p*-Stilbazole Moieties As Artificial Base Pairs for Photo-Cross-Linking of DNA Duplex" Hiromu Kashida, Tetsuya Doi, Takumi Sakakibara, Takamitsu Hayashi, Hiroyuki Asanuma, *J. Am. Chem. Soc.*, **2013**, *135*, 7960-7966.

2) "Efficiency of [2+2] photodimerization of various stilbene derivatives within the DNA duplex scaffold" Tetsuya Doi, Hiromu Kashida, Hiroyuki Asanuma, *Org. Biomol. Chem.*, **2015**, *13*, 4430-4437.

3) "Hetero-Selective DNA-like Duplex Stabilized by Donor-Acceptor Interaction" Tetsuya Doi, Takumi Sakakibara, Hiromu Kashida, Yasuyuki Araki, Takehiko Wada, Hiroyuki Asanuma, *Chem. Eur. J.*, **2015**, *21*, 15974-15980.

List of Presentations

International Conference

1) "Photocrosslinking of DNA through photodimerization of *p*-methylstilbazole" Tetsuya Doi, Takamitsu Hayashi, Taiga Fujii, Takumi Sakakibara, Hiromu Kashida, Hiroyuki Asanuma, The 38th International Symposium on Nucleic Acids Chemistry, November 9-11, Sapporo (Japan), pp. 360-361 (2011).

2) "Crosslinking of DNA throughphotodimerization of stilbene derivatives" Tetsuya Doi, Takamitsu Hayashi, Taiga Fujii, Takumi Sakakibara, Hiromu Kashida, Hiroyuki Asanuma, The 39th International Symposium on Nucleic Acids Chemistry, November 15-17, Nagoya (Japan), pp. 292-293 (2012).

3) "Crosslinking of DNA duplex through photodimerization of stilbazole derivatives" Tetsuya Doi, Takamitsu Hayashi, Takumi Sakakibara, Hiromu Kashida, Hiroyuki Asanuma, 26th International Conference on Photochemistry, July 21-26, Leuven (Belgium), p. 380 (2013).

4) "Photodimerization reactivity evaluation of stilbene derivatives by using DNA duplex as a scaffold" Tetsuya Doi, Takumi Sakakibara, Hiromu Kashida, Hiroyuki Asanuma, The 41th International Symposium on Nucleic Acids Chemistry, November 5-7, Kitakyushu (Japan), pp. 350-351 (2014).

5) "Hetero-selective artificial duplex stabilized by charge-transfer interaction of Pyrene/Anthraquinone residues" Tetsuya Doi, Takumi Sakakibara, Hiromu Kashida, Yasuyuki Araki, Takehiko Wada, Hiroyuki Asanuma, The 42th International Symposium on Nucleic Acids Chemistry, September 23-25, Himeji (Japan), pp. 148-149 (2015).

6) "Development of hetero-selective pseudo base pair stabilized by charge-transfer interaction, and its hetero-duplex formation" Tetsuya Doi, Takumi Sakakibara, Hiromu Kashida, Hiroyuki Asanuma, 2015 International Chemical Congress of Pacific Basin Societies, December 15-20, Honolulu (USA), p. MTLS807 (2015).

Internal Conference

19 presentations. Omitted.

List of Awards

1) 第 42 回中部化学関係学協会支部連合秋季大会高分子学会東海支部優秀学生発表賞　2011 年 11 月

2) 日本化学会東海支部長賞　2013 年 3 月

3) 光化学討論会　優秀学生発表賞(口頭)　2013 年 7 月

4) ICP2013 Poster award in the category Biology　2013 年 9 月

5) IGER Annual Meeting 2013 Poster Award　2014 年 1 月

6) 日本化学会第 95 春季年会　学生講演賞　2015 年 3 月

Acknowledgements

The present article is a thesis for application of doctoral degree at the Department of Molecular Design and Engineering, Graduate School of Engineering, Nagoya University. All the study work was carried out under direction of Professor Hiroyuki Asanuma from April 2010 to March 2016.

I would like to express my sincere gratitude to Prof. Hiroyuki Asanuma and Associate Professor Hiromu Kashida who provided a number of helpful comments and valuable suggestions which were necessary for improvement of this study. I also especially thank Prof. Xingguo Liang who provided a lot of comments for my investigation.

I would also like to thank my coworkers Dr. Taiga Fujii, Dr. Keiji Murayama, Mr. Takamitsu Hayashi, Mr. Takumi Sakakibara and other members of Asanuma Laboratory for their contribution to this study. Especially, I would thank Mr. Takumi Sakakibara for providing me his valuable data in Chapter 3.

I am also greatly indebted to “Japan Society for the Promotion of Science Fellows” and “Integrative Graduate Education and Research Program in Green Natural Science” for their financial support.

Finally, I would like to give special thanks to Professor Takahiro Seki and Professor Hideo Kishida for giving helpful comments and suggestion on this thesis.